Harald Kren

About the Continuous Growth of the Solid Electrolyte Interphase in Lithium Ion Batteries

Doctoral Thesis

Submitted in fulfilment for doctors degree of technical science

at

Graz University of Technology

Institute for Chemistry and Technology of Materials

Graz University of Technology

2011

Deutsche Fassung:

Beschluss der Curricula-Kommission für Bachelor-, Master- und Diplomstudien vom 10.11.2008

Genehmigung des Senates am 1.12.2008

EIDESSTATTLICHE ERKLÄRUNG

Ich erkläre an Eides statt, dass ich die vorliegende Arbeit selbstständig verfasst, andere als die angegebenen Quellen/Hilfsmittel nicht benutzt, und die den benutzten Quellen wörtlich und inhaltlich entnommene Stellen als solche kenntlich gemacht habe.

Graz, am …… ……..

(Unterschrift)

Englische Fassung:

STATUTORY DECLARATION

I declare that I have authored this thesis independently, that I have not used other than the declared sources / resources, and that I have explicitly marked all material which has been quoted either literally or by content from the used sources.

…… ……..

date (signature)

Acknowledgement

I feel deeply grateful to my supervisor, the head of the Institute for Chemistry and Technology of Materials, Prof. Dipl.-Ing. Dr. techn. Franz Stelzer, whose encouragement, guidance and support from the initial to the final level enabled me to develop an understanding of the subject.

I would like to express my very great appreciation to the financial supporters of this thesis:

On the one hand I would like to express my deep gratitude to the VARTA Micro Innovation GmbH. Special thanks has to be given to Dipl.-Ing. Dr. techn. Stefan Koller for his willingness to give his time so generously, for his enthusiastic encouragement and useful critiques of this research work.

On the other hand I am particularly grateful to the "Modelling, Validation and Test of Lithium-Ion-Batteries for Hybrid Vehicles" -project. This project was part of the Virtual Vehicle Competence Center and was supported by the State of Austria's FFG competence center program COMET. Within this project I would like to thank the following companies and institutes for their assistance:

AVL List GmbH, Continental AG, GAIA Akkumulatorenwerke GmbH, Volkswagen AG, Institute of Electrical Measurement and Measurement Signal Processing; TU Graz and the Institute of Physical Chemistry; WWU Münster

My special thanks are extended to Dipl.-Ing. Dr. techn. Martin Cifrain and my co-workers Dipl.-Ing. Dr. techn. Daniel Hrach and Dipl.-Ing. Martin Sommer. In addition I would like to thank Ing. Stefan Theuerkauf (GAIA Akkumulatorenwerke GmbH), who provided me with very valuable informations.

I would like to thank Prof. Dipl.-Ing. Dr.techn. Ferdinand Hofer and the staff of the Austrian Centre for Electron Microscopy and Nanoanalysis FELMI-ZFE for giving me the opportunity to perform Microtome cuts and EDX mapping measurements, as well as, for their support and helpful discussions.

Furthermore I am particularly grateful for the assistance given by my working colleagues Andrea Droisner, Dipl.-Ing. Bernd Fuchsbichler, Dipl.-Ing. Christoph Stangl, Dipl.-Ing. Colin God, Dipl.-Ing. Cornelia Bayer, Dipl.-Ing. BSc Laura Kaltenböck, Dipl.-Ing. Dr. Martin Schmuck, Dipl.-Ing. BSc Michaela Scharfegger and Dipl.-Ing. Roland Hohl. I am very grateful for their support and the friendly working environment during the last three years.

I would also like to extend my thanks to the technicians and non scientific staff of the ICTM; TU Graz for the valuable assistance, that has been very much appreciated.

I wish to express my special thanks to Dipl.-Ing. Dr. techn. Ute Daschiel for her support and encouragement throughout my study.

Finally, I feel deeply grateful to my parents, who gave me the opportunity to study and supported me unconditional all over the years.

Abstract

In recent years the lithium ion battery was able to consolidate its outstanding position within electronic industries. Furthermore the demands on solutions for secure, sustainable and environmentally friendly energy sources are continuously rising due to decreasing oil reserves and low-carbon policies.

Beyond the intensive research on novel materials in order to achieve higher specific energies and energy densities within lithium ion cells, it is actual purpose, to model battery characteristics during prolonged cycling and to study ageing processes in lithium ion batteries. These research activities are strongly supported due to the demands on more energy efficient and environmentally friendly transportation technologies by automotive industries.

The present work focuses on the estimation of cell parameters of lithium ion batteries by the use of embedded reference electrodes in commercial lithium ion cells. These reference electrodes allowed the study of the anode and cathode potential next to the cell voltage. By the use of this technique the major influence of the loss of “mobile lithium” on the capacity fading of the cell could be observed. By the use of a novel analysis method, this thesis presents a possibility to estimate the loss of mobile lithium contributed to the continuous growth of the solid electrolyte interphase.

Furthermore this method is especially capable to display the immense influence of the lithium ion batteries operating temperatures on the loss of mobile lithium.

Finally approaches to overcome this major ageing effect are introduced.

Kurzfassung

Die Lithium Ionen Batterie konnte innerhalb der letzten Jahre ihre herausragende Rolle im Sektor der Elektronikindustrie festigen. Die Nachfrage an Lösungen für sichere, nachhaltige und umweltfreundliche Energiespeicher steigt allerdings aufgrund der Abnahme der weltweiten Ölreserven und der Vereinbarung von CO_2-Minderungszielen zunehmend.

Neben der intensiven Forschung an neuen Elektrodenmaterialien, welche höhere spezifische Energien und Energiedichten in Lithium Ionen Batterien ermöglichen sollen, gewinnt die Modellierung von diesen Batterien in Abhängigkeit von Langzeitzyklisierungen, sowie die Erforschung von Alterungsphänomenen zunehmende Bedeutung. Diese Forschungsaktivitäten werden vor allem durch die Nachfrage an energieeffizienten und umweltfreundlichen Transporttechnologien im Automobilsektor angetrieben.

Der vorliegenden Arbeit liegt die Aufgabe zugrunde, die Zellparameter von Lithium Ionen Batterien mit Hilfe von implementierten Referenzelektroden aufzuklären. Neben der Zellspannung ermöglichen implementierte Referenzelektroden die Untersuchung der Anoden und Kathoden Potentiale. Im Zuge dieser Arbeiten konnte der starke Einfluss des „Verlustes an mobilem Lithium“ auf die Kapazitätsabnahme der Zellen nachgewiesen werden. Innerhalb der vorliegenden Arbeit wurde eine neue Analysenmethode gefunden, welche die Bestimmung des Verlustes an mobilem Lithium ermöglichte. Dieser Verlust kann dem kontinuierlichen Anwachsen der Deckschicht aus Elektrolytzersetzungsprodukten an der Anode zugeordnet werden.

Des Weiteren ermöglicht diese Methode die Abbildung des starken Einflusses der Betriebstemperatur von Lithium Ionen Batterien auf diesen Verlustes an mobilem Lithium.

Abschließend werden in dieser Arbeit Möglichkeiten vorgestellt, diesen dominanten Alterungeffekt unterdrücken.

1 Introduction

In recent years the lithium ion battery was able to consolidate its outstanding position within electronic industries. This battery type is widely used for mobile phones, laptop computers and digital cameras. In addition, lithium ion batteries are also extensively used for power tools and larger energy storage devices.

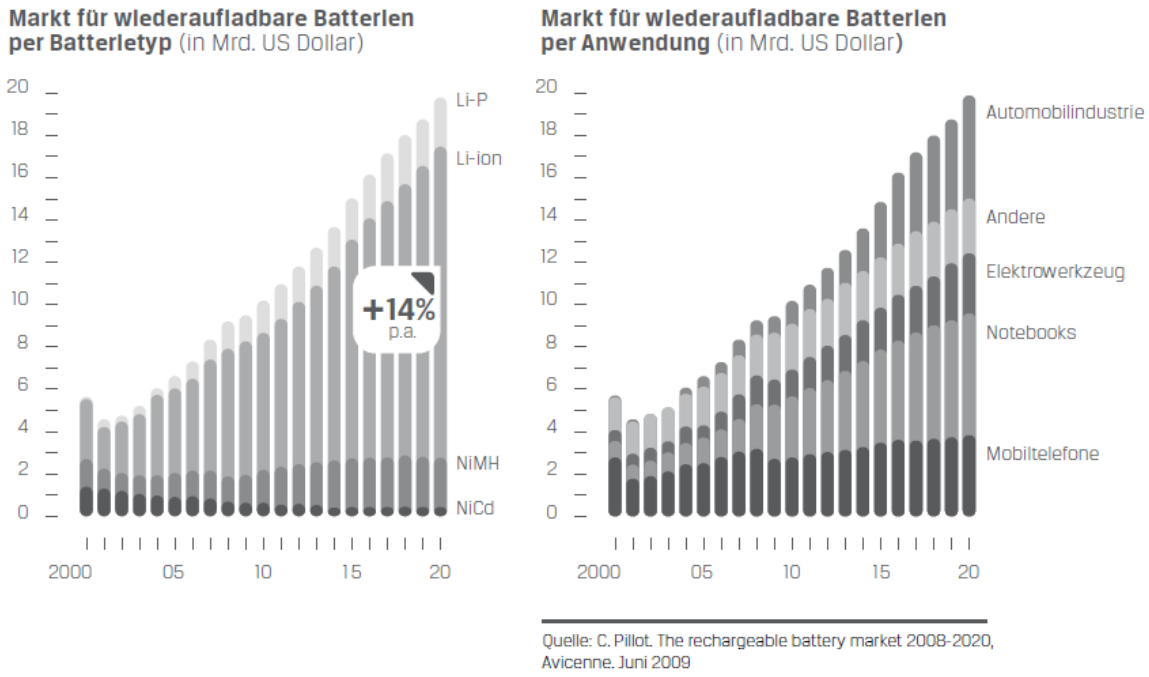

Figure 1: Battery Market Prospective (1)

The demands on solutions for secure, sustainable and environmentally friendly energy sources are continuously rising due to decreasing oil reserves and the related price increases. Agreements on low-carbon policies reinforce these demands furthermore.

Lithium ion batteries provide the technical and economic potential to enlarge the application fields of photovoltaic and wind-power technologies and therefore, they provide the potential to define new branches of industry as well. One of these branches is represented by the automotive industry, which is developing hybrid and fully electric vehicles in order to fulfil upcoming consumer demands regarding to “green” mobility.

Next to the development of advanced lithium ion batteries, life time modelling and the study of ageing effects of these cells becomes more and more research key role.

The present work focuses on the estimation of cell parameters. With the help of the established data a validation of a model developed within the “COMET K2 Forschungsförderungsprogramm” of the Virtual Vehicle will be enabled.

Special focus will be contributed to the realisation of investigation methods with negligible influence on the cell chemistry.

During this work a major ageing mechanism of lithium ion batteries will be displayed evidently. The large influence of the loss of “mobile lithium” on the capacity fading of the cell will be observed.

In order to estimate this loss of mobile lithium - or the growth of the solid electrolyte interphase in other words – a novel analysis method will be introduced. This method is especially capable to display the immense influence of the operating temperatures on the loss of mobile lithium. Furthermore, this novel investigation method will be validated by the use of electrochemical measurements.

Finally the author will introduce approaches to overcome ageing effects caused by this growth of the SEI and the connected loss of mobile lithium. Measurement data will prove the benefits on cell ageing by the use of these approaches.

2 Theoretical Aspects

2.1 Electrochemical Fundamentals

A battery is a device that converts chemical energy stored in its active materials directly into electric energy by means of an electrochemical oxidation-reduction (redox) reaction (2). Although the term battery is often used, the basic unit being referred to is the electrochemical cell. Depending on the desired output voltage and capacity a battery consists of one or more of this electrochemical cells, connected in series or/and parallel. The distinguished feature of an electrochemical cell is the generation of an electric current by the electrochemical processes taking place at the electrodes. This electric current is the result of the movement of electrons in the external circuit, which is counterbalanced by the move of ions between the negative and positive electrode within the electrolyte.

An electrochemical cell consists of three major components (2).

- The negative electrode or anode is oxidized during the electrochemical reaction and gives electrons to the external circuit as a consequence of that.
- The positive electrode or cathode accepts electrons from the external circuit and is reduced within the electrochemical reaction.
- The electrolyte ensures the transfer of electrons between the anode and the cathode. This electrolyte must not be electrically conductive but should provide good ionic conductivity. The anode and cathode electrodes are electronically isolated in the cell to prevent internal short-circuiting, which is guaranteed by the use of a separator in practical cells (2). In order to ensure ionic conductivity the separator is permeable to the electrolyte.

In addition the general galvanic cell system and its reactions should be made clear by the well known Daniell Element shown in Figure 2. This electrochemical system consists of a zinc anode (negative electrode) and a copper cathode (positive electrode) and their corresponding ion sulphates as aqueous electrolyte. Due to the fact that the electrolytes are different, these two half cells ($Zn \mid Zn^{2+}$ as well as $Cu \mid Cu^{2+}$) may be joined by a salt bridge (3). This salt bridge serves as an ion conducting connection between the two compartments. The charge exchange by the migration of sulphate-ions through the salt bridge ensures the charge equilibration (4).

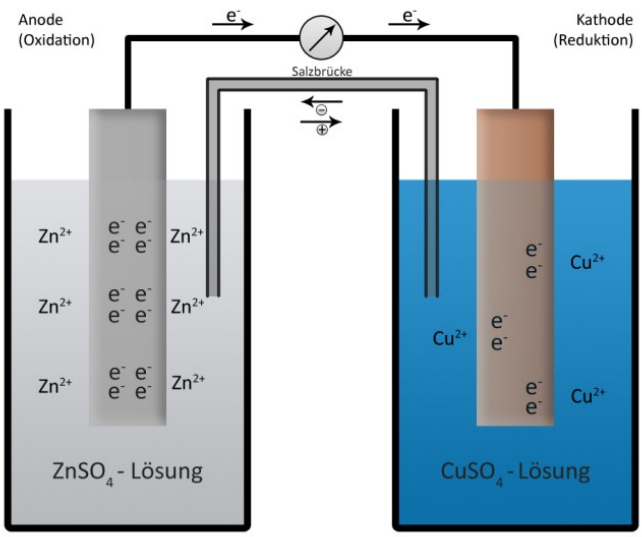

Figure 2: Daniell Element (5)

The potential of metals in their 1 mol·L^{-1} salt solutions are related to the normal hydrogen electrode (NHE), measured by combining a hydrogen half-cell with another half-cell to form a galvanic cell (4). The measured voltage is called the normal or standard electrode potential (Figure 3).

Electrode		Electrode reaction	E^0/V
Au	Gold	$Au^{3+} + 3e^- \rightleftharpoons Au$	+1.43
Ag	Silver	$Ag^+ + e^- \rightleftharpoons Ag$	+0.80
Cu	Copper	$Cu^{2+} + 2e^- \rightleftharpoons Cu$	+0.34
H	Hydrogen	$H^+ + e^- \rightleftharpoons H$	0
Pb	Lead	$Pb^{2+} + 2e^- \rightleftharpoons Pb$	−0.13
Sn	Tin	$Sn^{2+} + 2e^- \rightleftharpoons Sn$	−0.14
Ni	Nickel	$Ni^{2+} + 2e^- \rightleftharpoons Ni$	−0.25
Cd	Cadmium	$Cd^{2+} + 2e^- \rightleftharpoons Cd$	−0.40
Fe	Iron	$Fe^{2+} + 2e^- \rightleftharpoons Fe$	−0.44
Zn	Zinc	$Zn^{2+} + 2e^- \rightleftharpoons Zn$	−0.76
Ti	Titanium	$Ti^{2+} + 2e^- \rightleftharpoons Ti$	−1.63
Al	Aluminium	$Al^{3+} + 3e^- \rightleftharpoons Al$	−1.66
Mg	Magnesium	$Mg^{2+} + 2e^- \rightleftharpoons Mg$	−2.37
Na	Sodium	$Na^+ + e^- \rightleftharpoons Na$	−2.71
K	Potassium	$K^+ + e^- \rightleftharpoons K$	−2.93
Li	Lithium	$Li^+ + e^- \rightleftharpoons Li$	−3.05

Figure 3: Electrochemical series of metals, their electrode reaction and their standard potentials measured against NHE (V) (6)

For the Daniell Element in Figure 2 a terminal voltage of the cell is obtained according to Figure 3 and Eq. 1.

$$\Delta\varepsilon_{00} = E^0(Cu/Cu^{2+}) - E^0(Zn/Zn^{2+})$$

$\Delta\varepsilon_{00}$ ... potential difference between two materials
E^0 ... standard electrode potential

Eq. 1

In addition, Figure 4 explains the two half cell reactions for the discharge process of the Daniell Element. After closing the external circuit the oxidation reaction starts with the dissolution of the zinc electrode and the formation of zinc ions in the half cell. At the same time copper ions are reduced and metallic copper is deposited in the second half cell.

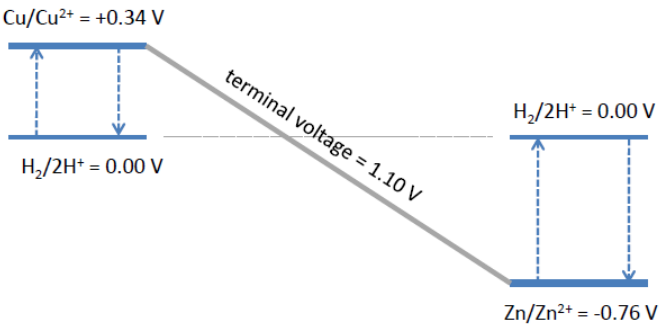

Reduction (Cathode): $Cu^{2+} + 2\ e^- \rightarrow Cu^0$

Oxidation (Anode): $Zn^0 \rightarrow Zn^{2+} + 2\ e^-$

Figure 4: Daniell Element; terminal cell voltage according to the equilibrium conditions; half cell reactions

When electrons are released from the anode during discharging and the active material is oxidized, a relationship exists between electronic current *I* and the mass *m* of the electron donating substance. This relationship is described in Eq. 2 and is well known as Faraday´s first law.

$$m = \frac{M}{zF} \cdot It$$

m ... active mass
M ... molar mass
z ... number of exchanged electrons
F ... Faraday constant = 96485 C mol^{-1} (4)
I ... current
t ... time

Eq. 2

Faraday´s first law applies for cathodic processes as well, and in addition Faraday recognized that for different electrode reactions and the same amount of charge, the ratio of the reacting masses is equal to the ratio of the equivalent masses (see Eq. 3) (4).

$$\frac{m_A}{m_B} = \frac{M_A|z_B|}{M_B|z_A|}$$

Eq. 3

2.2 Thermodynamic Fundamentals

Within electrochemical cell reactions the utilizable electrochemical energy corresponds to the reaction free energy *ΔG*. The reaction enthalpy *ΔH* represents the theoretical available energy, which is increased or reduced by an amount *TΔS*.

The amount *TΔS* describes the reversibly consumed or released heat during the reaction (4). The fundamental equation describing this is called the Gibbs-Helmholtz relation, shown in Eq. 4 (7).

$$\Delta G = \Delta H - T\Delta S$$

ΔG … reaction free energy
ΔH … reaction enthalpy
T … temperature
ΔS … reaction entropy

Eq. 4

Eq. 5 describes the definition of the Faraday constant.

$$F = \frac{It}{n} = \frac{Q}{n} = N_A e$$

Q ... quantity of electricity (electric charge)
N_A ... Avogadro constant = 6.023 x 10^{23} mol^{-1}
e ... elementary charge = 1.602 x 10^{-19} C

Eq. 5

Using the equation for a one formular conversion, the amount of charge for the cell reaction is defined according to Eq. 6, while the quantity of charge results in electrical energy, according to Eq. 7.

$$Q = It = nF$$

Eq. 6

$$\Delta\ \varepsilon_{00} \cdot Q = \Delta\ \varepsilon_{00} \cdot F$$

Eq. 7

Thermodynamic considerations require reversible cell reactions during the formula conversion, which actually means that all partial processes in a cell remain in equilibrium. The current has to be kept infinitely small in order to fulfill that the equilibrium cell voltage $\Delta\varepsilon_{00}$ is equal to the cell voltage $\Delta\varepsilon_{0}$. If additionally concentration gradients in the electrolyte can be ruled out, it is possible to estimate the reaction free energy ΔG, using Eq. 8 (4).

$$\Delta\ G = -zF\varepsilon_{00}$$

Eq. 8

According to the example used before, the cell voltage of the Daniell Element can be estimated.

$$Zn + CuSO_4 \rightarrow ZnSO_4 + Cu$$

For the reaction enthalpy ΔH the value of -210.1 kJ·mol^{-1} and for the reaction entropy ΔS the value of -7.2 J·K^{-1}mol^{-1} were estimated (4). According to Eq. 4 a reaction free energy of -208 kJ·mol^{-1} can be calculated under standard conditions (T=298K). Due to the fact that two electrons are exchanged, rearranging of Eq. 8 produces a cell voltage of 1.1 V.

In order to describe the concentration dependence of the equilibrium potential the Nernst equation is used (Eq. 9) (8).

$$\Delta\varepsilon_0 = \Delta\varepsilon_{00} + \frac{RT}{zF} * \sum v_i * lnc_i$$

$\Delta\varepsilon_0$ ... cell voltage
v_i ... stoichiometric factors (components i)
c_i ... concentrations (components i)
R ... universal gas constant = 8.3 J·mol^{-1}K^{-1}

Eq. 9

In addition the Nernst equation for metal-ion electrodes is given by Eq. 10:

$$\Delta\varepsilon_0 = \Delta\varepsilon_{00} + \frac{RT}{zF} * ln\left(\frac{c_{Me2+}}{c_{Me}}\right)$$

c_{Me2+} ... concentration of metal ions
c_{Me} ... concentration of the metal

Eq. 10

Partial differentiation of Eq. 8 at constant cell pressure gives the temperature dependence of the cell voltage $\Delta\varepsilon_0$.

$$\left(\frac{\partial \Delta\varepsilon_0}{\partial T}\right)_p = -\frac{1}{zF}\left(\frac{\partial \Delta G}{\partial T}\right)_p$$

T ... temperature
p ... pressure

Eq. 11

The temperature coefficient of the reaction free energy follows by the partial differentiation of Eq. 4, through thermodynamic relationships (8).

$$\left(\frac{\partial \Delta G}{\partial T}\right)_p = -\Delta S$$

Eq. 12

If the reaction takes place between solid phases and liquid phases, the cell voltage is nearly independent of the pressure, because of the negligible volume changes. The pressure dependence of the equilibrium cell voltage has to be considered in reactions involving the evaluation or disappearance of gases due to volume changes (9).

$$\left(\frac{\partial \Delta\varepsilon_0}{\partial p}\right)_T = -\frac{RT}{nF} \cdot \frac{1}{p}$$

Eq. 13

In equilibrium of a single galvanic cell the current in anodic and cathodic directions are equal and the potential of the electrode surface can be determined by the Nernst equation Eq. 9. If the currents are related to the electrode area, they are called exchange current densities i_0 in A·cm^{-2}. Current flow, for instance while discharging a battery, causes a measurable shift in the potential of the single half cell. This shift in the potential is called over-potential η (10). Due to this effect the real potential $\Delta\varepsilon_{real}$ has to be calculated following Eq. 14 (4).

$$\Delta\varepsilon_{\mathrm{real}} = \Delta\varepsilon_0 - \sum|\eta|$$

$\Delta\varepsilon_{real}$ ... real potential
η ... over-potential

Eq. 14

The over-potential of an electrochemical cell has to be considered as the sum of various types of over-potentials, depending on their origin. According to this, the most reasonable over-potentials are subsequently mentioned:

Charge-transfer over-potential: Dependent on the nature of the reacting substances, the electrolyte conditions as well as the characteristics of the electrode, the speed of charge transfer through the phase-boundary electrode/electrolyte differs. This form of over-potential is described by the Butler-Volmer equation (Eq. 15) as well as the Tafel equation (4). If the electrode reaction is controlled by the electrical charge transfer at the electrode the Butler-Volmer equation is valid. In case that the electrode reaction is controlled by the mass transfer to/ from the electrode surface from/to the bulk electrolyte the Butler-Volmer equation is not valid and has to be expanded to Eq. 16 (11).

$$I = A \cdot i_0 \cdot \left\{ exp\left[\frac{(1-\alpha)\cdot zF}{RT}\cdot(E-E_0)\right] - exp\left[-\frac{\alpha\cdot zF}{RT} * (E-E_0)\right]\right\}$$

i_0 ... exchange current density, A·m^{-2}
A ... electrochemical reactive surface area, m^2
α ... symmetry factor, dimensionless

Eq. 15

$$i = i_0 \cdot \left\{ -\frac{C_0(0,t)}{C_0^*} exp\left[\frac{(1-\alpha)\cdot zF}{RT}\eta\right] + \frac{C_r(0,t)}{C_r^*} exp\left[-\frac{\alpha\cdot zF}{RT}\eta\right]\right\}$$

i ... current density, A·m^{-2}
C_0 ... concentration of the oxidized form
C_r ... concentration of the reduced form
$C_0(0,t)$ ... time dependent concentration at the distance zero from the surface of the oxidized form
$C_r(0,t)$ ... time dependent concentration at the distance zero from the surface of the reduced form

Eq. 16

In addition the Butler-Volmer equation (see Eq. 15) is limited in two further cases: In low over-potential regions the Butler-Volmer equation can be simplified to Eq. 17, because in that case the equilibrium potential is approximately the same as the cell potential. In contrast, the Butler-Volmer equitation is replaced by the Tafel equation at high over-potential regions (2).

$$i = i_0 \frac{zF}{RT} \cdot \left(E - E_{eq}\right)$$

E_{eq} ... equilibrium potential

Eq. 17

The Tafel equation is described by Eq. 18 for cathodic reactions, when $E << E_{eq}$. For anodic reactions ($E >> E_{eq}$) the Tafel equation is described by Eq. 19. The Tafel equations assume that the reverse reaction is negligible in comparison to the forward reaction rate.

$$\eta = a - b \log i$$

a,b ... Tafel equation constants (for a given temperature and reaction)

Eq. 18

$$\eta = a + b \log i$$

Eq. 19

Diffusion over-potential: This kind of over-potential occurs due to the effect of an impoverishment of the reacting substances at the electrodes, caused by high current densities *i*. In this case reaction kinetics are only determined by the diffusion processes through the so called Nernst layer zone. The diffusion over-potential can be described according to Eq. 20.

$$\eta_{diff} = \left| \frac{RT}{zF} \ln\left(1 - \frac{i}{i_{limit}}\right) \right|$$

η_{diff} ... diffusion potential
i_{limit} ... maximum current density

Eq. 20

Reaction over-potentials occur when adsorption and desorption processes within the electrolyte or during electrode processes are the speed-limiting factors. Typically, the charge-transfer over-potential and the diffusion over-potential mentioned above are of higher importance (4).

Crystallization over-potentials represent fundamental processes in secondary batteries and occur, when the intercalation of metal ions into their lattice is inhibited. Especially for the charging process of secondary batteries this effect is of great importance. This effect results in a shift of the overall cell voltage and moreover an increasing cell temperature is observed (4).

As described in Eq. 21 and Eq. 22 heat losses W_J, thermal losses W_K (related to over-potentials) are besides the Joule-effect the reason for this phenomenon (4).

$$W_J = I^2 R_i t$$

W_J ... heat loss
R_i ... internal resistance (electrolyte, contact to the electrodes, etc.)

Eq. 21

$$W_K = I \sum \eta_i t$$

W_K... heat loss

Eq. 22

2.3 Assessment Criteria and Cell Characteristics for the Quality of Batteries

Depending on the field of application a variety of different battery systems in an immense number of sizes and configurations has been developed. Electrochemical cells and batteries are identified as primary and secondary cells, depending on their capability of being electrically recharged.

The terminal voltage *U* is measured between the negative and positive pole during charge and discharge. Its value can also be calculated from thermodynamic data, although the value often differs slightly due to an inhibited equilibrium state or side reactions (see chapter 2.1 and chapter 2.2) (4). According to Eq. 23, the product of the current *I* (A) and the accompanying terminal voltage *U* (V) gives the power *P* (W).

$$P = I \cdot U$$

P... power

Eq. 23

The power related to the battery weight is described by the specific power P_S ($W \cdot kg^{-1}$). The capacity (Ah), which is strongly dependent on the charge/discharge conditions, represents the achievable or loadable charge of the electrochemical cell. The discharge characteristics of a commercialized lithium ion battery (LIB) at different discharge currents are described in Figure 5.

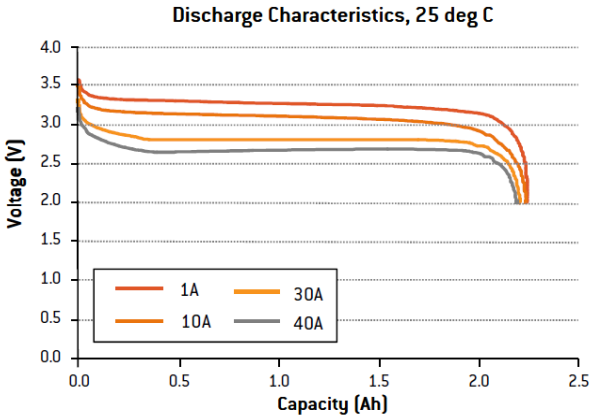

Figure 5: Discharge characteristics of a commercialized lithium ion battery indicating the power dependence of the cell on the current (28650; nominal 2.3Ah, 3.3 V) (12)

The storage capacity or capability of active materials is determined by the amount of the delivered or received electrons per mass, described by the value of specific charge ($Ah \cdot kg^{-1}$). Respectively, the amount of the delivered or received electrons per volume is given by the value of specific charge density ($Ah \cdot L^{-1}$). Desirable high values for the specific energy ($Wh \cdot kg^{-1}$) can be established by the combination of materials with high specific capacity and a large window between their oxidation and reduction potentials. The combination of materials providing high charge density, as well as a large potential difference between their oxidation and reduction potential results in electrochemical cells with high energy densities ($Wh \cdot L^{-1}$) (13). Furthermore the specific power ($W \cdot kg^{-1}$) and the specific power density ($W \cdot L^{-1}$) respectively, are characteristics for the current carrying capacity of a battery. For lithium ion batteries oxidation and reduction potentials according to the specific capacity of commonly used cathode and anode materials for LIB are displayed in Figure 6.

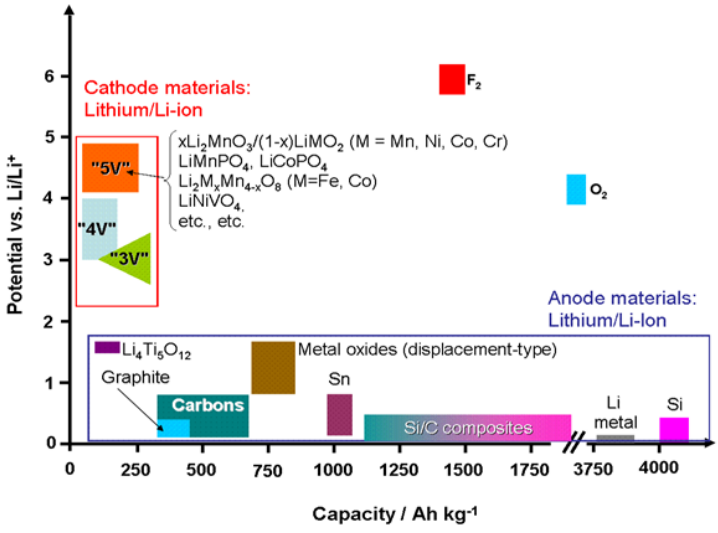

Figure 6: Oxidation / reduction potentials vs. capacity of common used electrode materials for LIB (14)

Regarding to the specific energy major distinctions can be made between today´s aqueous and nonaqueous battery systems, pointed out in Figure 7. Furthermore Figure 7 evaluates industrial lithium ion cells of various battery manufactures and illustrates nicely the complexity of lithium ion batteries. Depending on the active materials, cell and electrode design LIBs provide the opportunity to be manufactured for either high power or high energy applications.

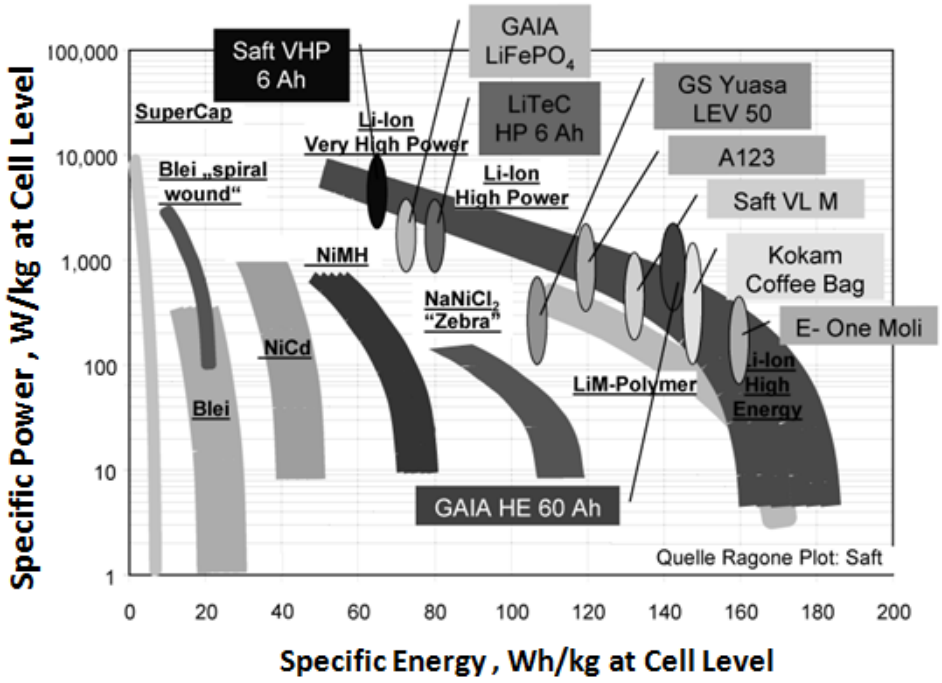

Figure 7: Ragone Plot for various battery systems in comparison to lithium ion batteries; benchmark cell characteristics of lithium ion battery manufacture 2009 (15)

2.4 The History of Electrochemical Storage Devices – from Shrugging Frog Legs to the Early Developments in Lithium Ion Batteries

The first generation of flowing electricity dates back to the Italian physician *Luigi Galvani* (1737 - 1798). Within an experiment in the year 1789 *Galvani* discovered that frog legs occur to shrug by touching them with Iron and Copper. *Galvani* concluded in his essay *De Viribus Electricitatis in Motu Musculari Commentarius* (Commentary on the Effect of Electricity on Muscular Motion) the theory of animal electricity (16).

By interpreting *Galvani's* experiment, *Alessandro Volta* (1745 – 1827) realised that the shrugging of the frog's legs were caused by the generated electricity due to the two different metals in contact with the conducting liquid of the animal tissue. Based on that knowledge he developed a device, which made history as the so called voltaic pile. This device was the first, permanent ready to operate power source of the world. The voltaic pile was constructed as a pillar of staggered copper and zinc plates, which were separated by felts drenched in sulphuric acid. However *Alessandro Volta* rejected any chemical effect of the voltaic pile and credited it´s function exclusively with the contact of the metals. In the year 1801 *Johann Wilhelm Ritter* (1776 – 1810) developed the first accumulator, called "Rittersche Säule". It was composed of a vessel filled with sodium chloride solution and staggered copper and paperboard plates.

Fauré patented the lead-acid accumulator in the year 1880, but substantial work on that battery device must also be conceded to *Gaston Planté* (1834 – 1889). Even nowadays that rechargeable battery system is still vitally important in automotive industries and developing countries. That outstanding development can be mainly contributed to economic reasons, availability of resources and the ability to supply high surge currents, despite to the very low energy to weight ration and low energy to volume ratio, provided by this accumulator system. In the charged state the electrochemical cell contains electrodes of elemental lead (Pb) as negative electrode, lead(IV)oxide (PbO_2) as positive electrode and approximately 33.5 % sulphuric acid as electrolyte. During discharging both electrodes turn into lead(II)sulphate ($PbSO_4$), while the electrolyte loses the dissolved sulphuric acid and becomes primarily water.

The desire for more powerful electrochemical storage devices appeared due to the development of first mobile electronic devices. The first NiCd-battery was created by *Waldemar Junger* and *Thomas*

Alva Edison (1847 – 1931) in 1899. Anyhow, commercial production started not until the 1940`s, because at that time a gas tight cell system was developed. A fully charged NiCd-cell contains a nickel(III)oxide-hydroxide (NiOOH) positive electrode plate, a cadmium negative electrode plate and a separator containing a 20% aqueous solution of potassium hydroxide (KOH) as electrolyte. During discharging, on the negative electrode cadmium is oxidized to cadmium(II)-hydroxide ($Cd(OH)_2$), while on the positive electrode the resulting electrons reduce nickel(III)oxide-hydroxide to nickel(II)-hydroxide ($Ni(OH)_2$). During charging the reactions take place in the opposite direction. At the end of the charging process the cell voltage increases up to 1.6 V, and for that reason the decomposition voltage of water is exceeded. In order to prevent the dangerous gas evolution a excess of cadmium(II)-hydroxide is used. This leads to the generation of oxygen during overcharging at the positive electrode, while the reduction of cadmium(II)-hydroxide is still going on at the negative electrode. The emerging oxygen reacts with cadmium to cadmium(II)-hydroxide and is consumed directly (4).

Due to even higher energy demands and in order to avoid environmental problems caused by the use of cadmium the NiCd-accumulator was replaced during the 90´s of the last century by the nickel-metal hydride accumulator (NiMH). The replacement of the NiCd-accumulator by NiMH-accumulator and lithium ion batteries was even enforced by a law passing the European parliament in 2006, which prohibited the use of more than 0,002 % cadmium in battery systems.

The first consumer grade NiMH-accumulator appeared on the market at the beginning of the 90´s of the last century. Within the NiMH battery, for the negative electrode, cadmium was substituted by a hydrogen absorbing alloy, while the positive electrode remained a nickel(III)oxide-hydroxide electrode, as in NiCd-accumulators (17) (4). During charging, protons (H^+) are reduced to hydrogen (H_2), which is reversibly bond by the metal alloy and stored as metal hydride, while the metal hydride is oxidized to the metal and protons during discharging. Furthermore the protons react with the hydroxide-ions (OH^-) of the potassium hydroxide containing electrolyte to water. In order to prevent the oxidation of the metal instead of the hydrogen at the end of the discharging process, the negative electrode is much larger than the positive electrode.

From the electrochemical point of view lithium has the lightest weight, the most reductive potential and the greatest energy density combined with a small ion radius (18). First work on lithium batteries started by *Harris* back in the year 1958, resulting in the development and commercialization of a variety of primary lithium cells during the 1970s (18). The most prominent primary lithium cells included for example lithium-sulfurdioxide (Li/SO_2), lithium-thionylchloride ($Li/SOCl_2$), lithium-

polycarbon monofluoride ($Li/(CF_x)_n$) and lithium-manganese dioxide (Li/MnO_2). Unfortunate events pertaining to safety casted a damning light on primary lithium cells. The main reason for these events was correctly attributed to the reactivity of metallic lithium in combination with a flammable non-aqueous electrolyte.

During the late 1970s and 1980s rechargeable lithium batteries using lithium insertion compounds as positive electrodes were developed. Exxon and Moli Energy tried to commercialize the Li/TiS_2 and Li/MoS_2 systems. Later on, rechargeable lithium batteries containing positive electrodes of V_2O_5, V_6O_{13} and MnO_2, all in combination with metallic lithium, were tried to be commercialized (18). But the commercial application was strongly limited by the safety problems due to the metallic lithium electrodes.

After the era of transition metal chalcogenides the UK Atomic Energy Authority demonstrated in the year 1971 within their patent the reversible intercalation of alkaline metals (A_x) into compounds $A_xM_yO_2$, where M_y is a transition metal (19). The patent was used by Sony in 1990 to produce first lithium ion batteries in cell sizes 14500, where 14 refers to the diameter and 50 to the length in mm, and 20500 for their cellular phones. Due to the fact that the higher voltage oxides serve as lithium source, they can be combined with insertion host compounds on the negative electrode. The cells by Sony had an open circuit voltage of 4.2 V and an operating voltage of 3.6 V (18). Respectively, the capacities of the 14500 and 20500 model were only 350 mAh and 900 mAh, but the naming of the "lithium-ion rechargeable battery" was a marketing success (18) (20).

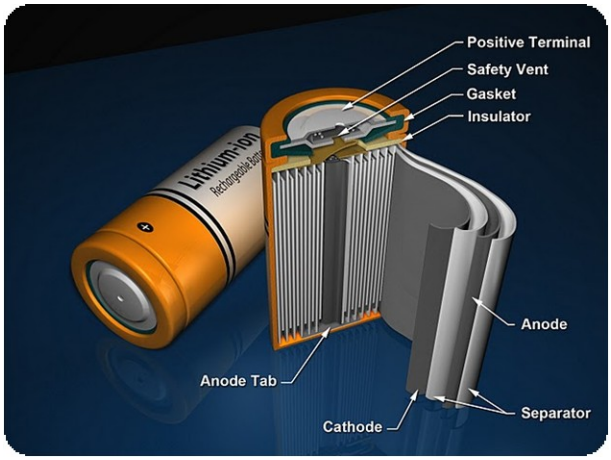

Figure 8: Inside structure of a commercial lithium ion battery (21)

3 Theoretical Background on Lithium Ion Batteries

3.1 Build up

Although the definition of battery actually describes at least two galvanic cells connected in series, the term of battery for single galvanic cells is increasingly expanding. During the discharge process of galvanic cells the stored chemical energy is converted to electrical energy. This conversion consists of two separated, but nevertheless coupled partial reactions.

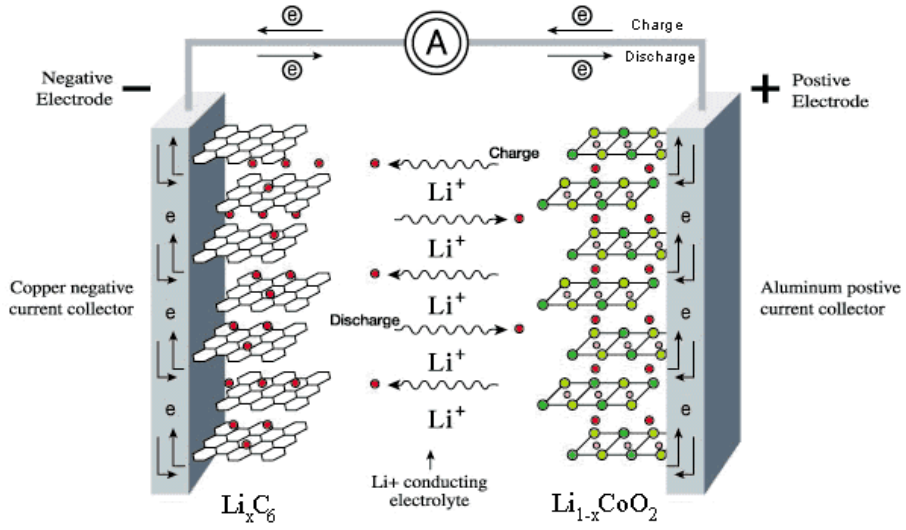

Figure 9: Schematic drawing of the lithium ion battery working principle during charge/discharging (22)

Rechargeable lithium ion batteries involve a reversible insertion / extraction of lithium ions (guest species) into / from the anode and cathode host species during the charge / discharge process. The insertion / extraction process occurring due to a flow of lithium ions within the electrolyte is accomplished by a reduction / oxidation reaction of the host species. This reaction is accompanied with a flow of electrons through the external circuit (23).

At the negative electrode the partial reaction at the lower redox potential takes place, while the redox reaction at higher oxidation potential proceeds at the positive electrode. Presently a large number of lithium ion cells contain a $LiCoO_2$ cathode host material and carbon anode host material, as shown in Figure 9. Within this specific and commonly used anode active material the lithium ions are coordinated to six carbon atoms during charging, resulting in a reductive potential similar to

metallic lithium, whereby the accommodation of the negative charge is done by the host material. Measurements using NMR revealed that parts of the lithium exist as ion (24).

For a lithium ion battery containing carbon host material the partial redox reaction on the anode side can be described as follows:

$$LiC_6 \underset{\text{charge}}{\overset{\text{discharge}}{\rightleftharpoons}} Li^+ + C_6 + e^-$$

Eq. 24

At the positive electrode lithium ions are coordinated within the host structure resulting in a strongly oxidising compound. For lithium ion cells containing $LiCoO_2$ (Figure 9) or other lithium transition metal oxides, lithium insertion / deinsertion is accompanied with a change of the transition metal oxidation state (25).

Accordingly the partial redox reaction on the cathode side for a lithium ion battery containing $LiCoO_2$ host material can be described as follows:

$$0.5\ Li^+ + 0.5\ e^- + Li_{0.5}CoO_2 \underset{\text{charge}}{\overset{\text{discharge}}{\rightleftharpoons}} LiCoO_2$$

Eq. 25

Regarding to the partial redox reactions described in Eq. 24 and Eq. 25 the overall cell reaction can be formulated according to Eq. 26:

$$LiC_6 + 2\ Li_{0.5}CoO_2 \underset{\text{charge}}{\overset{\text{discharge}}{\rightleftharpoons}} 2\ LiCoO_2 + C_6$$

Eq. 26

3.2 Anode Host Materials

3.2.1 Carbonaceous Materials

At the present mainly carbonaceous materials are used as the negative electrode material in commercial lithium ion batteries. This is due to the fact, that carbonaceous materials exhibit high specific charges and a strong negative redox potential, next to excellent cycling performance caused by their dimensional stability (13).

The insertion of lithium into carbon, also named intercalation, strongly depends on the crystallinity, the microstructure and the micromorphology of the carbonaceous material (26) (27). Carbons that are capable to intercalate lithium ions reversibly, can be roughly classified as graphitic and disordered (non graphitic) carbons.

The term graphite is only applicable to carbons having a layered lattice structure with a perfect stacking order, either the common AB structure (hexagonal graphite) or the less common ABC (rombohedral graphite), although perfectly stacked graphite crystals are not readily available due to the small transformation energy of AB to ABC structure (13). The term graphite is used for all ordered carbons, neglecting the stacking order of the graphene layers.

The preparation of graphite particles is done either by milling and graphitisation of natural graphite or by decomposition and graphitisation of suitable precursors.

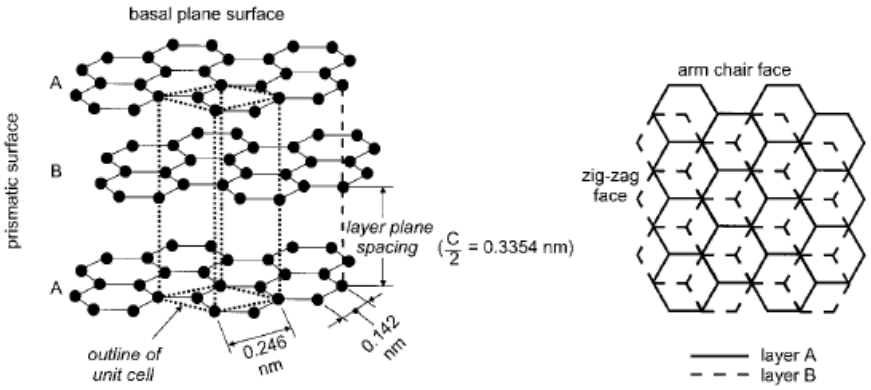

Figure 10: Left: schematic drawing of the crystal structure of hexagonal graphite (AB stacking layer); Right: perpendicular view to the basal plane of hexagonal graphite. (13)

The carbon within non graphitic carbonaceous materials is mainly arranged in a hexagonal network, but without a far-reaching crystallographic order in c-direction. These materials are characterized by

amorphous areas embedding and crosslinking more graphitic areas (28). Depending on precursor material and manufacturing temperature the number and size of the amorphous areas vary. Preparation of non graphitic carbonaceous materials is done by pyrolysis of organic polymers and hydrocarbons at temperatures below 1800 K.

By heat treatment of most non graphitic carbons at temperatures up to 3300 K two different types of carbon can be distinguished. The so called graphitizing carbon develops graphite structure during the heating process. This is due to the fact, that crosslinking between the carbon layers is weak and therefore, the layers are mobile enough to form graphite like crystallites.

On the opposite non graphitizing carbon develops no graphite structure when heated to 2500 K or even 3300 K (13) (29). Non graphitizing carbons are mechanically harder and therefore named hard carbons, while graphitizing carbons are called soft carbons (29).

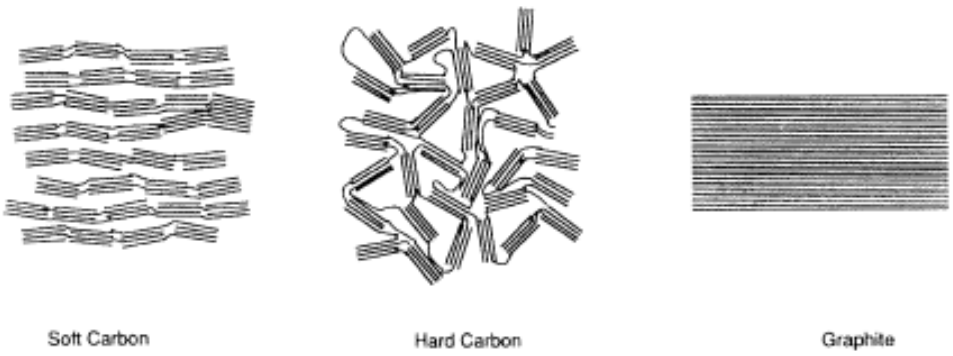

Figure 11: Structural differences of carbonaceous materials (29)

The synthesis of lithium graphite intercalation compounds has been known since the mid 1950s (30) (31). At ambient pressure and for highly orientated graphite the maximum possible lithium content is one lithium atom per six carbon host atoms (13).

The intercalation reaction is limited to the prismatic surface (arm-chair and zig-zag faces; see Figure 10, right) and does not occur through the basal planes, if no defect sides are provided (32).

During the intercalation of lithium into graphite the stacking order of carbon (graphene) layers shifts to AA, which is attributed to a good coordination of the p-orbitals of the graphene layer (Figure 12). According to that, the interlayer distance between the graphene layers increases for about 10% (33) (34).

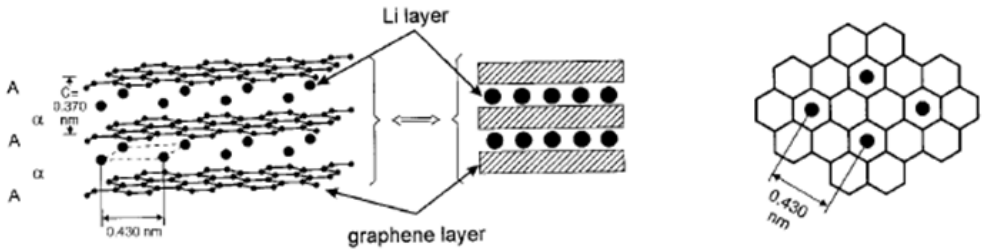

Figure 12: Left: structure and schematic drawing of the AA Layer stacking sequence in LiC_6; Right: Perpendicular view to the base plane of LiC_6 (13)

The intercalation of lithium into the graphitic host structure proceeds stepwise. This phenomenon is called stage formation and is affected by thermodynamic reasons (35) (31) (36).

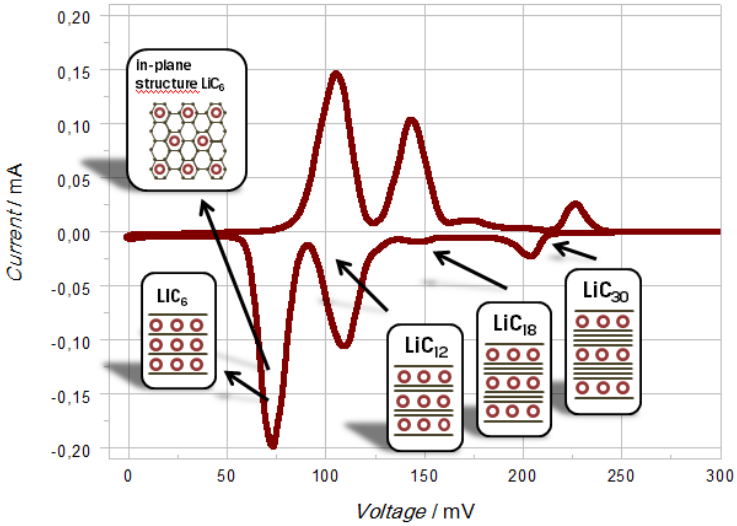

a.) edited Kren H.
b.) measurement provided by Koller S.

Figure 13: Stepwise intercalation of lithium into highly crystalline graphite; linear potential sweep voltammetry measurement: scan rate 10 µV•s^{-1}, Electrolyte EC:DEC = 3:7, v:v, 1 M $LiPF_6$

The phenomenon can be explained by the energy required to enlarge the space between the planes in order to overcome the van der Waals forces between two graphene layers, as well as the repulsive interactions between guest species (37). The stepwise intercalation of lithium within the graphitic host structure can be identified by current peaks within linear potential sweep voltammetry. The electrochemical reduction of graphite within suitable organic electrolytes containing lithium salts reflects the four intercalation compounds (LiC_{30}, LiC_{18}, LiC_{12} and LiC_6). Next to electrochemical measurements the stepwise intercalation of lithium within the graphitic host structure was also confirmed by X-ray diffraction (38) (39) and Raman spectroscopy (40).

Theoretically, the intercalation and deintercalation of lithium ions from an organic electrolyte is completely reversible, showing a theoretical capacity of 372 $mAh \cdot g^{-1}$, if the LiC_6 compound is formed (13) (29) (18).

In practice, unfortunately, the consumed charge during the first intercalation cycle exceeds the theoretical specific capacity, while the subsequent deintercalation of lithium ions recovers only about 80 to 95% of the consumed charge. Within the following charging/discharging cycles the charge recovery is close to desirable 100% (see Figure 14) (13).

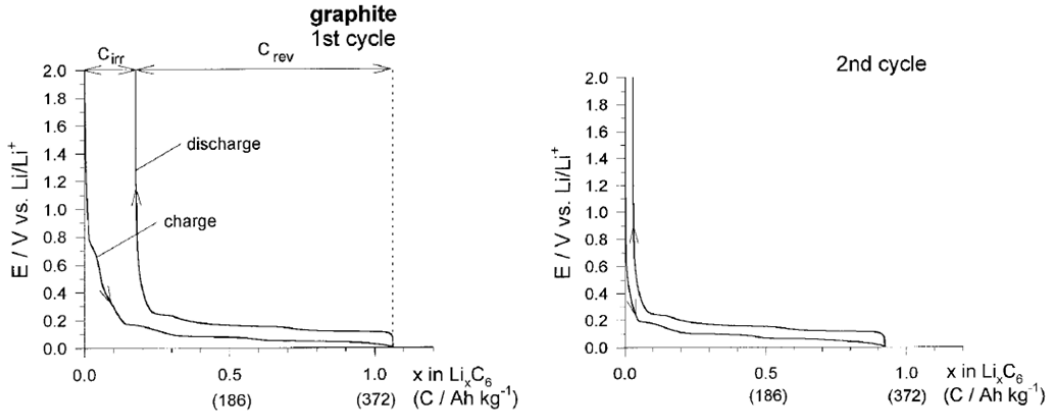

Figure 14: Constant current charge/discharge curves (Left: 1st and Right: 2nd cycle) of the graphite Timrex KS 44; electrolyte $LiN(SO_2CF_3)^2$/EC/DMC (C_{irr} is the irreversible specific capacity, C_{rev} the reversible specific capacity) (13)

This excess charge consumed during the first cycle is ascribed to the so called Solid Electrolyte Interphase (SEI) formation, as well as corrosion like reactions of Li_xC_6 (41) (42). The intercalation of lithium into carbon is in all known electrolytes thermodynamically unstable due to the reductive potential of the lithium intercalation. This is close to the potential of metallic lithium itself (13). The formed protecting layer prevents the electrolyte from further reductive decomposition. A narrow description of this passivation layer, first described by *Peled* in 1979 (43), will be given within chapter 3.5.

3.2.2 Intermetallic Anode Materials and Alloys

The demand for high specific energy batteries gives reason to believe that battery materials, anodes or cathodes, have to provide high specific and/or high volumetric capacities. Regarding to this, scientists considered the usage of metallic lithium as negative electrode material within rechargeable lithium ion batteries. Unfortunately, lithium typically deposits as dendritic and highly reactive metal particles (44) (45) (46).

These dendrites are covered with SEI, tend to break and disconnect from the electrode and are leading to immense, continuous electrolyte decomposition. Moreover, the dendrites may form filaments that locally short-circuit the cell (13).

However, lithium alloys (Li_xM) are able to provide same or even higher lithium packaging densities than metallic lithium, due to the fact that within lithium alloys lithium ions are incorporated instead of metallic lithium. Accordingly lithium alloys, like for example $Li_{22}Si_5$, can provide high specific (4200 $mAh \cdot g^{-1}$) and volumetric capacities (2400 $mAh \cdot ml^{-1}$). Further metal host materials that electrochemically form lithium alloys are for example Al, Sn, Pb, In, Sb, Ag. These materials have been studied very intensively (47) (13) (48).

Metallic host materials are used in the discharged (delithiated) state, whereas, in analogy to carbonaceous materials, the formation of the Li/Me intermetallic phase and the SEI takes place during the first charging cycle (Eq. 27).

$$Me + x\,Li^+ + x\,e^- \underset{\text{discharge}}{\overset{\text{charge}}{\rightleftharpoons}} MeLi_x$$

Eq. 27

During the storage of lithium ions within the metallic host structure highly ionic $Li_x^+Me^{x-}$ - phases are formed. Unfortunately, the insertion of lithium ions into the metallic host structure is accompanied with large volume changes. The difference between the lithiated and unlithiated metal host is in the range of 100 to 300 % (4), resulting in huge mechanical stress for the host particle, as well as for the manufactured electrode. Due to the high ionic character of the formed Zintl phases they are very brittle, which results in a rapid decay of the host materials dimensional stability (4) (18) (13). The cracking of host material particles leads to their disintegration, followed by their loss of electrical contact to the electrode environment. These effects result in a large capacity fading of the active material, next to massive electrolyte decomposition due to the continuous reductive formation of

new active sides. The problem of insufficient dimensional instability, the major drawback of metal alloy electrodes, is answered by two major adoptions.

On the one hand scientists try to keep the absolute volume changes low. Therefore nano-scaled particles are used, because small particles tend to crack less. The influence of the particle size on the cycling stability of metal alloy electrodes has been described within references (49) and (50), as well as different manufacturing methods of small tin or silicon particles have been studies intensely (51).

On the other hand the dimensional stability can be improved by embedding the metal alloy host material into a stable matrix. This adoption aims at the strategy that the local volume expansion should be lowered by the inactive matrix, which buffers the expansion of the intermetallic host materials. The benefit was proved by the Sn/SnSb system (52) (23) (18), the silicon/carbon composite anode materials (53) (54), as well as, by a great variety of systems with the same principle (18) (23).

3.2.3 Spinel Type Transition Metal Oxides

Typically metal oxides are characterized by relatively high potentials (usually between 1.4 V to 1.8 V) and low lithium capacities (23). Within recent years, predominantly the spinel type lithium titanate ($Li_4Ti_5O_{12}$) has attracted great attention because of its excellent, reversible lithium ion insertion and extraction. One drawback is the minor high-rate characteristics of this material, which has to be improved. One of the most effective ways to achieve good rate characteristics is to prepare the electrode material coated with carbon (55). Materials exhibiting good rate characteristics can also be obtained from high surface area modifications, such as in nano-crystalline films made by sol-gel methods (56).

Spinel lithium titanate is especially considered for low voltage applications and described as a zero strain insertion material due to almost negligible changes in the unit cell on insertion of up to one lithium ion (57). An average insertion potential of 1.5 V and capacities close to 150 $mAh \cdot g^{-1}$ are observed for this material (23). According to the average insertion potential no protective layer is formed, due to the fact that the electrolyte is stable at the insertion potential. This results in far less ageing effects as far as the anode electrode is concerned, but the low cell voltage has to be taken into consideration as well.

3.3 Cathode Materials for Lithium Ion Batteries

Transition metal compounds and chalcogenides represent the group of positive host materials with prime importance (13). Within the recent years, the by far largest numbers of positive electrode materials gaining importance, are inorganic transition metal oxides or sulphides and can be divided into one, two and three dimensional host materials. According to the structural build up of these materials (Figure 15) the lithiation/delithiation mechanisms proceed in different dimensions.

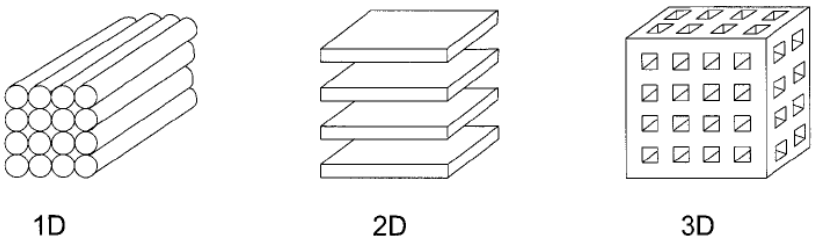

Figure 15: Schematic build-up of one-, two-, and three-dimensional transition-metal oxides and chalcogenides.

All nowadays practically used secondary lithium ion batteries contain positive electrode materials that act as lithium source. According to this, the lithium ion batteries are assembled in the discharged state. Next to above introduced lithiated inorganic transition metal oxides, especially lithium iron phosphate gained enormous importance within the last years.

3.3.1 Layered Metal Oxide Electrodes

Figure 16 shows the crystal structure of two dimensional layered metal oxide electrode materials. The best known and commercial most successful cathode material of this type is represented by lithium cobalt oxide ($LiCoO_2$). Hence this material is lithiated - it fulfils the function of the lithium source within the lithium ion cell. $LiCoO_2$ adapts the α-$NaFeO_2$-type structure, which can be regarded as a distorted rock salt superstructure (see Figure 16) (29). The delithiation / lithiation occurs within the two dimensional layers, build up by CoO_2 (13).

As a matter of fact not all of the lithium stored within the host material is able to be reversible delithiated / lithiated. After the stoichiometry of the host material reaches $Li_{0.5}CoO_2$ the former cubic structure converts to a hexagonal structure. This structure change, corresponding to a potential

value of > 4.2 V vs. Li/Li^+ inhibits the relithiation of the till then delithiated lithium (29) (23). This structure changes also result in the release of oxygen (29) (23).

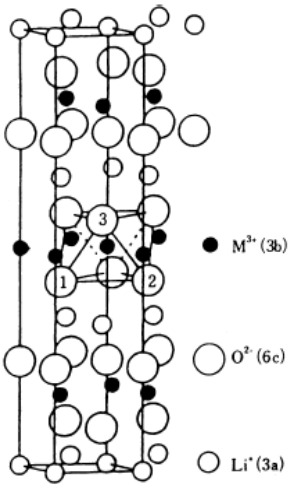

Figure 16: The two-dimensional crystal structure of $LiMO_2$ (M = Ni, Co, V, etc.) of the a-$NaFeO_2$ type. (29)

Securing that the cathode potential does not exceed 4.2 V vs. Li/Li^+, specific capacities of up to 140 $Ah \cdot kg^{-1}$ can be obtained reversibly (13). By coating of the active material particles by e.g. Al_2O_3 better safety, higher cell potentials, rate capability and capacities can be achieved (58) (59).

Limited worldwide reserves of the transition metal cobalt - mainly in politically insecure regions - lead on to price increases, although it has to be mentioned, that cobalt is mainly demanded within steel production. Due to the price increases the demand for a replacement of this positive electrode material rises.

Replacement can be achieved by alternative materials (Chapter 3.3.2 and 3.3.3), or by the reduction of the cobalt amount within the two dimensional host structure of $LiCoO_2$.

Without a change in the α-$NaFeO_2$-type structure it is possible to substitute parts of the Co^{3+} ions by Ni^{2+} ions and Mn^{4+} ions, resulting in $LiNi_xMn_xCo_{1-2x}O_2$ ($0 \leq x \leq 0.5$) (60) (61). Within the last years special attraction is attributed to host material with the stoichiometric formula $LiNi_{1/3}Mn_{1/3}Co_{1/3}O_2$ (62).

3.3.2 Spinel Oxide Compounds

Spinel oxides are classified as three dimensional host materials for secondary lithium ion batteries. The best known and commonly used material of this type is lithium manganese oxide ($LiMn_2O_4$). It provides a working voltage of 4 V and a specific capacity of 130 $Ah \cdot kg^{-1}$ (63) (64). Especially due to its low price the material represents a promising alternative to $LiCoO_2$.

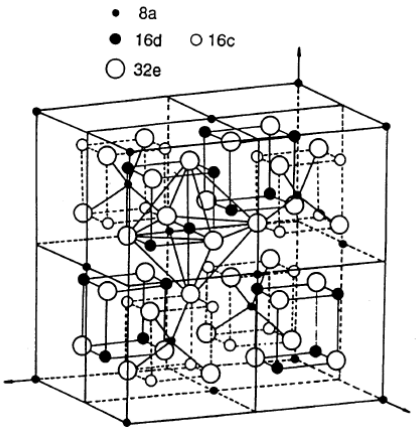

Figure 17: Lattice structure of $LiMn_2O_4$ (29)

Tarascon and *Guyomard* made a decisive step towards to the commercialization of a secondary lithium ion battery system containing $LiMn_2O_4$ cathode material and carbon anode material (65) (66) (67). However, even after optimization of the materials the cells have turned out slight capacity fading on long term cycling. This fading is attributed to two reasons.

During charging the cells reach very high voltages leading to instability of the electrolyte (chapter 3.4). This process results in the slow dissolution of the soluble Mn^{2+} species of the $Li_xMn_2O_4$ host electrode in the electrolyte. The soluble Mn^{2+} species is produced from the Mn^{3+} species by the disproportionation reaction to Mn^{2+} and Mn^{4+} (29) (13).

Furthermore the material provides a poor cycling behaviour in the 3 V regions. This poor cycling behaviour is attributed to an asymmetric lattice expansion / contraction of the lithium manganese oxide electrode material during charge / discharge reactions, which is mainly a result of the Jahn-Teller effect of the Mn^{3+} cation (68). By this effect the cubic crystal symmetry of the spinel electrode framework is changed into tetragonal symmetry (64) (69).

Intensive work has been done in order to stabilize the material in 3 V regions. On the one hand some manganese in $LiMn_2O_4$ was replaced by monovalent or multivalent cations (e.g., Li^+, Mg^{2+}, or Zn^{2+}).

On the other hand the oxide was doped with further oxygen, resulting in an increased average manganese ion oxidation state (slightly above 3.5 V), and in a suppression of the Jahn-Teller effect on deep discharge (70).

Moreover the part wise substitution of the Jahn-Teller ion Mn^{3+} by trivalent cations (e.g., Al^{3+}, Fe^{3+}, Ni^{3+}, Co^{3+}, or Cr^{3+}) was investigated intensely. Unfortunately, all reported doping methods resulted in noticeably decreased values of specific capacity (71).

3.3.3 Phospho Olivine Compounds

Over the past few years olivine structured phosphate based materials $LiMPO_4$ (M = Fe, Mn, Co, Ni) have generated considerable interest as a new class of positive electrode materials for lithium ion batteries (72) (25). Much attention has been focused especially on the $LiFePO_4$ compound, due to its low cost, low toxicity, remarkable theoretical capacity (170 $Ah \cdot kg^{-1}$) and operating voltage of 3.4 V vs. Li/Li^+ (25).

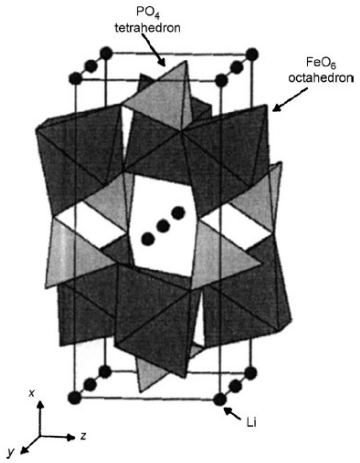

Figure 18: The olivine structure of $LiFePO_4$ (73)

In contrast to layered metal oxide electrodes (see chapter 3.3.1) the olivine structured phosphate based compounds do not decompose at elevated temperatures. Accordingly, the accompanied oxygen evolution of Li_xMO_2 materials does not occur at $LiMPO_4$ compounds. Oxygen evolution is prohibited due to the fact, that $LiMPO_4$ materials have a highly stable three dimensional framework, because of strong covalent P–O bonds within the $(PO_4)^{3-}$ polyanion (72).

The material provides an excellent stability during cycling and storage conditions, which results in special attraction of this material for automotive applications.

Unfortunately, the major drawback of $LiMPO_4$ materials in general and $LiFePO_4$ in particular is the poor rate capability, associated to limited electronic and ionic conductivity. Researchers enabled long term cyclability and accordingly the breakthrough of $LiFePO_4$, by optimized syntheses techniques to minimize the particle size (74). Furthermore researchers were able to increase the performance using different methods for coatings of the active material by carbon. These methods included e.g. incorporating of an organic or polymeric component with precursors before firing, addition of metal particles to the electrode mix, or solid-solution doping by metals supervalent to Li^+ (75) (76) (77).

3.4 Common Electrolytes for Lithium Ion Batteries

Due to the strong negative or positive electrode potentials the use of aqueous electrolyte solutions within lithium ion batteries is excluded (reviewed within the chapters 3.2 and 3.3). Consequently, the application of nonaqueous, nonprotonic electrolyte solutions is unavoidable. Nonprotonic electrolytes must have good ionic conductivity and high chemical stability, while they have to assure safety and must be cost effective (29).

Particular importance is contributed to the inorganic conducting salts contained within electrolyte solutions. The variety of inorganic conducting salts is strongly limited, because of their moderate solubility in nonaqueous solvents. The conducting salts have to ensure a high degree of dissociation and high ion mobility, next to good ionic conductivity, while they should increase viscosity only slightly. Nowadays lithium hexaflurophosphate ($LiPF_6$) has become the conducting salt of choice for most lithium ion batteries. Due to toxicity, explosiveness, corrosive properties or minor ionic conductivity a variety of former considered conducting salts ($LiClO_4$, $LiBF_4$, $LiAsF_5$) are no further issue for commercial lithium ion cells.

In order to establish solvated cations, as well as anions of conducting salts like $LiPF_6$ in nonaqueous solutions, these solutions have to contain solvents with a high dielectric constant (“high dielectric solvent”, HDS) , like ethylene carbonate (EC) and propylene carbonate (PC) (78). Electrolyte solutions containing PC are not favourable, due to the insufficient establishment of appropriate passivation layers with common carbon based negative electrodes (chapter 3.5).

Anyhow, the mentioned polar components, HDS, usually come along with higher viscosity, because of their high dielectric constant. Within lithium ion batteries low viscosity values of the electrolyte solution are desirable because of the easier movement of the lithium ion. For that reason, commonly mixtures of various electrolyte solvencies are used. In order to decrease the viscosity, the HDS electrolyte solvencies are combined with low viscosity components, resulting in less restriction for the movement of the lithium ion.

These solvencies (“low viscosity solvent”, LVS) are for example dimethyl carbonate (DMC), diethyl carbonate (DEC) and 1,2-Dimethoxy ethane (DME) (18) (29).

Figure 19: Structural formula of main organic solvents (29)

Since secondary lithium ion batteries usually operate in temperature ranges from -20°C to 60°C desired properties of electrolyte solvents are low melting points, high boiling points and low vapour pressures. The values of some commonly used electrolyte solvencies are listed within Table 1 (29).

Table 1: Physical properties of commonly used solvents in lithium ion batteries at 25°C (unless otherwise noted) (29)

Solvent	mp (°C, 1 atm)	bp (°C, 1 atm)	Relative permittivity	Viscosity (cP)	Dipole moment (D)	DN[a]	AN[b]
Acetonitrile (AN)	−45.72	81.77	38	0.345	3.94	14.1	18.9
γ-Butyrolactone (BL)	−42	206	39.1	1.751	4.12	–	–
Diethylether (DEE)	−116.2	34.60	4.27	0.224	1.18	19.2	3.9
1,2-Dimethoxyethane (DME)	−58	84.7	7.20	0.455	1.07	24	–
Dimethylsulfoxide (DMSO)	18.42	189	46.45	1.991	3.96	29.8	19.3
1,3-Dioxolane (DOL)	−95	78	6.79[c]	0.58	–	–	–
Ethylene carbonate (EC)	39–40	248	89.6[d]	1.86[c]	4.80	16.4	–
Methylformate (MF)	−99	31.50	8.5[e]	0.330	1.77	–	–
2-Methyltetrahydrofuran (MeTHF)	–	80	6.24	0.457	–	–	–
3-Methyloxazolidin-2-one (MO)	15.9	–	77.5	2.450	–	–	–
Propylene carbonate (PC)	−49.2	241.7	64.6	2.530	5.21	15.1	18.3
Sulfolane (S)	28.86	287.3	42.5[c]	9.87[c]	4.7	14.8	19.3
Tetrahydrofuran (THE)	−108.5	65.0	7.25[c]	0.46[c]	1.71	20.0	8.0

[a] Donicity.
[b] Acceptor number.
[c] At 30°C.
[d] At 40°C.
[e] At 20°C.

According to Figure 20 the molar conductivity passes through a maximum with increasing conductive salt concentration. An optimum between a lack of charge carriers (ions) and a lack of free charge carriers due to ion pair formation has to be found.

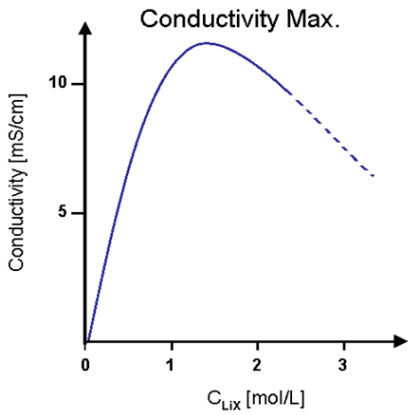

Figure 20: Dependence of the conductive salt concentration on the maximum conductivity (14)

In average, only one third of the charge is carried by the lithium ion, caused by its strong solvation due to the high charge density. This strong solvation leads to a larger hydrodynamic volume than the hydrodynamic volume of the PF_6^- anion, resulting in less mobility of the cations.

Liquid electrolytes are commonly used in combination with porous and inert separator materials. These separators are mainly 10 to 30 µm thick polyolefin foils.

Furthermore it has to be mentioned, that state-of-the-art electrolytes contain one or more electrolyte additives. These additives, added in quantities of about one to five percent, affect the performance of lithium ion batteries in a variety of ways. For example they positively affect the quality of the solid electrolyte interphase (chapter 3.5), they improve the long term cyclability of the cathode material and they are used for overcharge protection (79) (80).

Huge progress in research has been made within the last years, as far as the research on following electrolyte systems next to liquid electrolytes is concerned:

- solid electrolytes
- gel-type polymer electrolytes
- ionic liquids

The advantages of solid electrolytes are their inflammability, the absence of leakage problems and their high temperature resistance. Nevertheless these benefits are strongly relativized by the minor ionic conductivity (81).

Within gel-type polymer electrolytes the organic electrolyte is integrated in a polymeric matrix. Polymers like polyethylene oxide (PEO) and polyvinylidene fluoride (PVdF) are suitable to combine the chemical properties of liquid electrolytes with the mechanical stability of polymers (82).

Ionic Liquids are salts in liquid state at temperatures below 100°C and do not show a measurable vapour pressure. It is by their unique properties that ionic liquids are entering a broad range of new applications. Nevertheless ionic liquids cannot be used in lithium ion batteries containing graphite anodes and their production is very cost intensive.

3.5 Electrode/Electrolyte Interfaces – The Role of Surface Films in Lithium Ion Batteries

Lithium cells, as well as lithium ion cells, typically function far beyond their thermodynamic stability limits of today known electrolyte systems. At most commonly used negative electrode materials in lithium ion cells (compare chapter 3.2) the potentials can reach close to that of metallic lithium in lithium cells (-3 V vs. NHE), leading to electrolyte reduction (13). Thus, oxidation of the electrolyte may occur at commonly used positive electrode materials.

Fortunately, in suitable electrolytes films are formed on negative electrode materials that inhibit further electrolyte reduction. In the case of metallic lithium these films are formed spontaneously after immersion, while in case of other lithium insertion materials, i.e. on lithium alloys and carbon intercalation compounds, the passivation layer is generated during first charging (13).

This, so called solid electrolyte interphase (SEI) layer is electronically insulating and acts as a “sieve” due to its permeability for lithium-ions and its non permeability for other electrolyte components (43).

The SEI is unique for lithium and its compounds and does not exist on the surface of other alkaline metals and their compounds. It is generally accepted that the SEI formed in organic solvent-based electrolytes consist of a thick and porous layer of electrolyte permeable organic decomposition products (polymers and oligomers) as well as of a thin, and compact layer of electrolyte impermeable inorganic (Li_2CO_3, LiF) and combined (lithium alkyl carbonates) decomposition products.

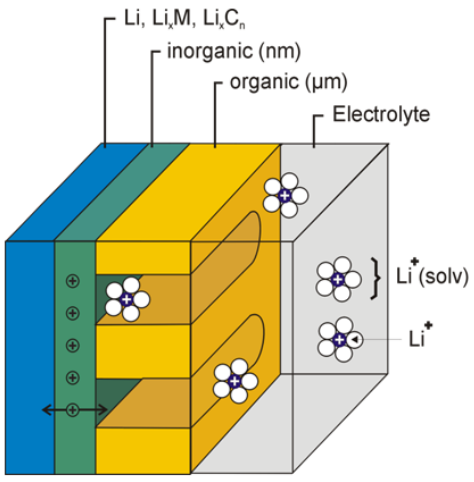

Figure 21: Schematic of the SEI of Li, Li_xM and Li_xC_n in organic electrolytes (14)

With regard to Figure 21 several investigations were carried out in order to investigate the nature of SEI films formed on lithium and graphite. In any case the SEI products were found to be heterogeneous. The accurate composition of the SEI is depending on the electrolyte composition (13) (83) (84).

Certain electrolytes tend to do not establish a suitable protecting layer on carbon electrodes. If no suitable passivation layer is formed, solvated lithium ions intercalate into the graphene layers. This, so called “solvent co-intercalation” is not reversible and leads to the destructive exfoliation of parts of the host material, due to high volume expansions of up to 150% (Figure 22).

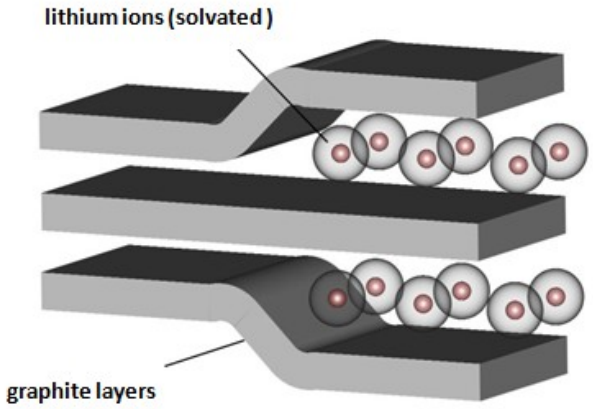

Figure 22: Formation of ternary $Li(_{solv.})_xC_y$ – phase [illustrated by Koller S.] (22)

“Solvent co-intercalation” into carbon anodes occurs because the solvation energy of the lithium ions is larger than the van der Walls forces in between the graphene layers, resulting in ternary phases of solvated lithium ions and the host material (Figure 22) (13).

Reductive decomposition of corresponding solvent molecules is further accompanied with the formation of gaseous compounds. For e.g. propylene carbonate based electrolytes a suitable, efficient passivation layer on carbon electrodes is not established, but a large amount of emerging propene was proved (85).

Desired properties of an “ideal” solid electrolyte interface are:

- permeable for lithium cations
- low resistance for fast Li^+ transport
- impermeable for solvent molecules
- impermeable for anions
- electronically insulating, in order to prevent further electrolyte decomposition
- thin and pin hole free, well adherent and slightly flexible
- little charge capacity consumption during the SEI formation

The tools for the study of the surface chemistry of non aqueous lithium salt solution on metallic lithium and graphite included X-Ray photoelectron spectroscopy (XPS) (86), Auger electron spectroscopy (AES) (87), Fourier transform infrared spectroscopy (FTIR) (88), and Raman spectroscopy (89).

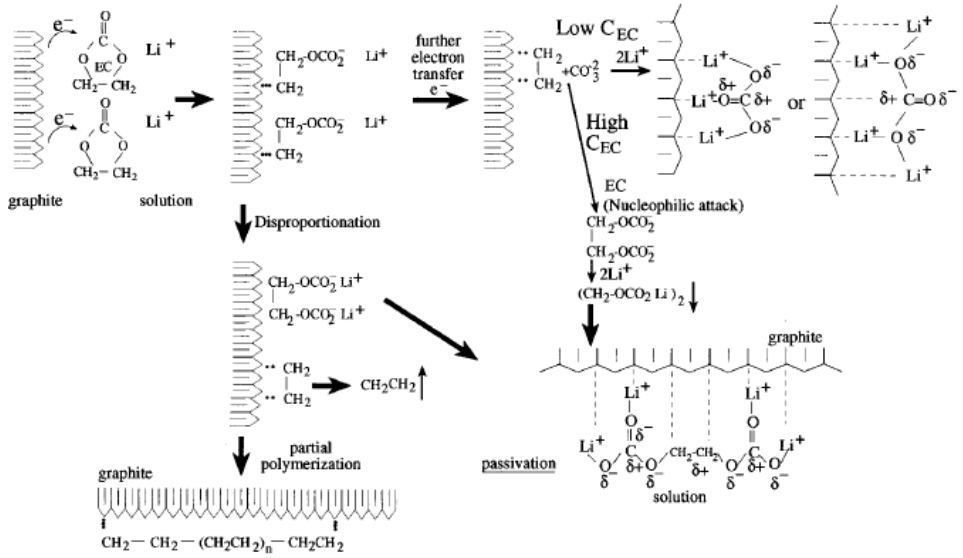

Figure 23: Reduction mechanisms of cyclic alkyl carbonates (ethylene carbonate) on graphite (90)

Aurbach et al. found out, that the SEI layer in carbonate based electrolytes is composed of species like Li_2CO_3, $ROCO_2Li$, lithium alkoxides, Li_2O, LiF, LiCl, as well as other organic and polymeric species. Within Figure 23 *Aurbach* et al. suggested major aspects and reactions of the surface chemistry of graphite electrodes in electrolyte solutions containg ethylene carbonate (EC) as major component.

The reaction pathways are based on FTIR and XPS spectroscopic studies (91) (90). Nowadays most electrolyte solutions contain EC and further considerations on electrolyte solutions are done within chapter 3.4.

Edström et al. identified Li_2CO_3 and solute-related decomposition products (LiCl, LiF) as predominant SEI components (92). This very relevant fact is of particular importance for the present work and has to be discussed in more detail.

All non aqueous electrolyte solutions contain traces of O_2, N_2, CO_2, as well as H_2O, because these traces are simply unavoidable within the processing steps (18). The substances are reactive with lithium and lithiated carbons and lead to surface reactions forming lithium oxides, lithium nitrides, lithium hydroxides and lithium carbonates (93). These surface products have to be expanded by the decomposition products of $LiPF_6$, the most common conducting salt. This salt decomposes to LiF and PF_5, which represents its equilibrium reaction (94). Due to hydrolysis of PF_5 hydrofluoric acid (HF) and PF_3O are formed (18). Hence, $LiPF_6$ solutions contain hydrofluoric acid in any case. The within the electrolyte contained HF reacts with both, electrodes and basic surface species, forming lithium fluoride as the major solid product (18).

Although the film formation on lithium compound surfaces allows lithium ion batteries to operate at today's standards, they are also a major drawback as far as battery ageing is concerned. Unfortunately, the today known electrolyte solvents and conducting salts as well as the crystallinity and micromorphology of the anode material only tend to finish the SEI´s film forming process within the first three cycles. Depending on the quality of the formed film, this film formation occurs in a minor degree also in each following charging step of the battery, specially enhanced by elevated temperatures.

The composition and nature of the SEI plays a critical role for the cycle life as well as for the calendar life of carbon based lithium ion batteries. Therefore the growth of the lithium fluoride film on carbon anodes can be used to determine the ageing of lithium ion batteries.

3.6 Ageing Effects in Lithium Ion Batteries

Because of their high volumetric and gravimetric energy density and their low self discharge rates, lithium ion batteries are extensively used in portable instruments like laptops and mobile phones. In addition they are a very promising candidate as power source in electric vehicles and hybrid vehicles. For these applications the long-term storage behaviour as well as the long-term cycling behaviour becomes of increasing interest.

3.6.1 General Aspects

Ageing of a battery can be defined as the modification of its properties with time and use (18). Unfortunately, especially lithium ion batteries are complex systems and the processes leading to ageing are especially complicated. Ageing effects like capacity fading and power fading do not result from single causes, but are the sum of a number of various processes and their interactions. Most of these processes cannot be studied separately and occur at similar timescales, complicating the investigation of these ageing effects (95).

Furthermore general information upon cell ageing is difficult to evaluate, because each lithium ion cell system has its own chemistry. Many ageing effects are strongly influenced by the cell components nature (e.g., active material, electrode design, electrolyte composition, electrolyte additives, electrolyte/electrode impurities, etc.). According to the overview of the ageing causes described in Table 2, mainly capacity loss and loss of power is observed during battery ageing. Two types of ageing situations have to be distinguished: On the one hand during cycling and on the other hand ageing upon storage.

In any case ageing of lithium ion batteries can be contributed to changes of the electrode / electrolyte interface and in the electrolyte, of the active material, as well as of the composite electrode (current collector, conductive additives, binder, porosity, etc.). It is generally accepted that changes of the electrode / electrolyte interface are mainly responsible for ageing of lithium ion batteries containing carbon as anode material.

3.6.2 Ageing Mechanisms of Anode Materials

Within this chapter mainly ageing effects on carbon anodes are discussed, due to the fact that carbon anode materials represent the most important anode material and the greatest understanding of anode ageing has been accomplished with graphite based batteries (18) (83).

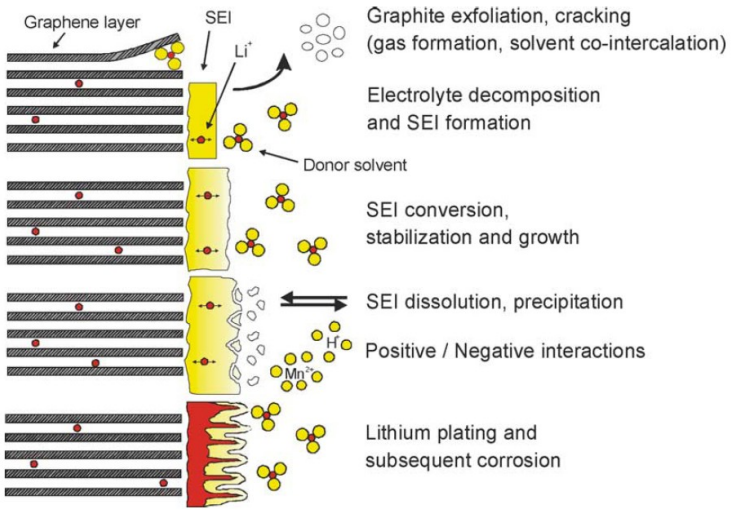

Figure 24: Changes at the interphase of the carbon anode and the electrolyte (95)

Ageing effects during storage can be monitored by the electrochemical values such as capacity loss, impedance rise, potential change, the state of charge and the state of health, although someone has to be aware of the fact, that the electrode potential of anode materials based on graphite do not vary significantly with the state of charge (95) (4).

According to Figure 24 changes at the interphase of the electrode and the electrolyte due to reactions of the anode material with the used electrolyte are considered by many researchers to be the major source for ageing in lithium ion batteries (95) (96). The circumstance that common used anode materials operate at a voltage outside the electrochemical stability window of the electrolyte was already pointed out within chapter 3.5. Hence, during charging and accordingly low polarisation potential of the anode, reductive electrolyte decomposition takes place (95). This decomposition is accompanied by irreversible consumption of the electrolyte and lithium ions. Normally this consumption is stopped by a protective layer, called solid electrolyte interphase. This protective layer is permeable for lithium cations, rather impermeable for electrolyte components and prevents the electrolyte compounds from further reduction (95) (18).

Table 2: Lithium-ion anode ageing—causes, effects, and influences (95)

Cause	*Effect*	*Leads to*	*Reduced by*	*Enhanced by*
Electrolyte decomposition (→SEI) (Continuous side reaction at low rate)	Loss of lithium Impedance rise	Capacity fade Power fade	Stable SEI (additives) Rate decreases with time	High temperatures High SOC[1] (low potential)
Solvent co-intercalation, gas evolution and subsequent cracking formation in particles	Loss of active material (graphite exfoliation) Loss of lithium	Capacity fade	Stable SEI (additives) Carbon pre-treatment	Overcharge
Decrease of accessible surface area due to continuous SEI growth	Impedance rise	Power fade	Stable SEI (additives)	High temperatures High SOC (low potential)
Changes in porosity due to volume changes, SEI formation and growth	Impedance rise Over-potentials	Power fade	External pressure Stable SEI (additives)	High cycling rate High SOC (low potential)
Contact loss of active material particles due to volume changes during cycling	Loss of active material	Capacity fade	External pressure	High cycling rate High DOD[2]
Decomposition of binder	Loss of lithium Loss of mechanical stability	Capacity fade	Proper binder choice	High SOC (low potential) High temperatures
Current collector corrosion	Over-potentials Impedance rise Inhomogeneous distribution of current and potential	Power fade Enhances other Ageing mechanisms	Current collector pre-treatment (?)	Overdischarge Low SOC (high potential)
Metallic lithium plating and subsequent electrolyte decomposition by metallic lithium	Loss of lithium (Loss of electrolyte)	Capacity fade (Power fade)	Narrow potential window	Low temperature High cycling rates Poor cell balance Geometric misfits

[1] SOC ... State of Charge
[2] DOD ... Depth of Discharge

Although the formation of the solid electrolyte is mostly completed within the first cycles, a continuous growth at a lower rate even seems to occur in the later stages of cycling, due to the fact that irreversible charge capacities and self-discharge reactions still can be observed after prolonged cycling. Accordingly a rise of the cells impedance can be measured, which is directly linked to the power fade of the cell (97) (98).

Whereas the formation at the solid electrolyte interphase takes place mainly in the first cycles, processes like conversion, stabilization and growth of this interphase proceeds during further cycling and storage (95). As mentioned in chapter 3.5 the quality of the solid electrolyte interphase is strongly depended on the electrolyte components.

Furthermore especially elevated temperatures definitely enhance ageing effects like the continuous growth of the solid electrolyte interphase (99) (100) (101). During the usage of lithium ion batteries at elevated temperatures the solid electrolyte interphase starts to break down and partly dissolves, followed by reprecipitation of electrolyte components. Thus, during the growth of the interphase electrolyte components as well as lithium ions are consumed, resulting in the release of gaseous products, loss of electrolyte and loss of so called “mobile lithium”. The term mobile lithium actually

sums up all lithium ions used for the charge/discharge reactions in the electrodes and is therefore proportional to the possible practical capacity of the lithium ion battery.

The loss of mobile lithium due to the continuous growth of the solid electrolyte interphase, also enhances further ageing effects, especially on cathode materials that are only able to provide a certain amount of lithium, before the crystal structure of this materials is destroyed irreversible.

3.6.3 Ageing Mechanisms of Cathode Materials

Regarding to ageing effects of lithium ion batteries cycling as well as different storage conditions can also strongly affect cathode materials (83) (18). In general the ageing of cathode materials is dependent on the nature of the cathode material and can be summed up by the ageing of the active material itself, degradation of inactive electrode components, oxidation processes of the electrolyte components and interaction of ageing products with the negative electrode (95). According to ageing mechanisms of anode materials in chapter 3.6.2 these effects do not occur separately and are influencing each other, which makes it difficult or impossible to study them separately.

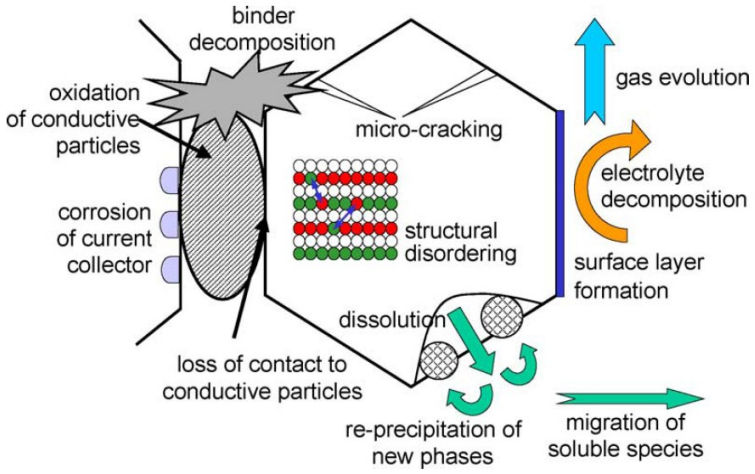

Figure 25: Overview on basic ageing mechanisms of cathode materials according to Vetter et al. (95)

Most lithium ion batteries use lithium cobalt oxide as cathode material. The electrochemical reaction of this positive electrode material proceeds as a deinsertion / insertion reaction of lithium ions from / in the host structure, according to chapter 3.3.1. On the one hand the material has to deal with mechanical stress because of the electrochemical reaction and the changes in the molar volume involved with this reaction (95). When the Li_xCoO_2 cathode material is charged beyond 4.2 V vs. Li/Li^+

the former cubic structure converts to a hexagonal structure. As a matter of fact not all of the lithium stored within $LiCoO_2$ can be reversible delithiated / lithiated.

This fact becomes even more important after focussing on the loss of the, in chapter 3.6.2 described mobile lithium, especially with respect to nowadays common battery charge / discharge proceedings. In the first place these proceedings are based on the supervision of the batteries cell voltage. Typically, these charge / discharge proceedings do not play tribute to the loss of mobile lithium and changes at the electrodes caused by ageing.

Unfortunately, the loss of mobile lithium and the changes at the electrode lead to changes in the electrodes reduction and oxidation potentials. Therefore, for example, the charge potential of $LiCoO_2$ is changed to potentials beyond 4.2 V vs. Li/Li^+. At this time ageing is not only the result of the loss of mobile lithium and changes of the anode´s surface due to growth of the solid electrolyte interphase, but rather also by the irreversible structural changes of the $LiCoO_2$ cathode.

Other cathode materials like $LiMn_2O_4$ host electrodes lead to further ageing mechanisms, like the dissolution of of the soluble Mn^{2+} species in the electrolyte. These ageing effects have been discussed within chapter 3.3.2.

As far as the ageing of cathode materials is concerned, especially $LiFePO_4$ shows minor ageing effects compared to the previously mentioned cathode materials. $LiFePO_4$ is an olivine structured, phosphate based material introduced within chapter 3.3.3. This material enables the deinsertion of all lithium ions up to a boundary structure of $FePO_4$. Consequently, the host structure does not undergo any structural changes and ageing influences caused by a loss of mobile lithium are not observed. Due to that effect, this material represents the material of proper choice within the experimental part of this thesis, when the influence of solid electrolyte interphase growth is studied (see chapter 4.4).

4 Experimental Part

4.1 Introduction

Within chapter 3.6 ageing characteristics of lithium ion batteries were introduced. These ageing characteristics can be monitored by capacity and power fade analysis, as well as by impedance studies.

Unfortunately, these ageing characteristics originate from various ageing mechanisms that are partly dependent on each other. One curtail step in order to gain information about ageing mechanisms of commercial cells is the study of the electrode potentials next to the terminal voltage, also called cell voltage. By the study of electrode potentials the assignment of ageing characteristics caused by electrode defects, misbalancing of the electrodes to each other, loss of anode or cathode active materials, loss of electrolyte and loss of mobile lithium ions can be facilitated.

4.2 Back fitting of Commercial Battery Electrodes in Swagelok© Test Cells

4.2.1 Experimental Setup

Electrode materials were gained from industrial cells in order to back fit these materials in Swagelok© test cells. The scheme of a Swagelok© test cell is shown in Figure 26.

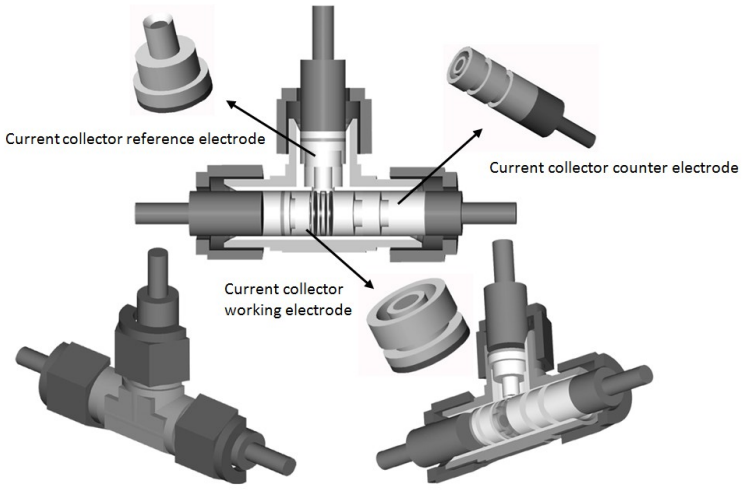

a.) drawing by Koller S.

Figure 26: Scheme of a Swagelok© test cells (22)

Commercial 2.3 Ah A123 cells ($C/LiFePO_4$) were discharged to 2.6 V. Thereupon these cells were opened in an argon filled glove box (< 1 ppm H_2O, < 1 ppm O_2) (see Figure 27). Anode and cathode material was gained from the cells and in addition one side of the double-sided composite electrode layer was removed by the use of acetone. Circular electrodes with a diameter of 12 mm were punched out of the gained electrode material. After that the electrodes were assembled in Swagelok© test cells using:

- separator: Freudenberg-Vlies FS2190 (poly propylene, 23 µm); ø 13 mm,
- electrolyte: EC/DEC = 3:7 (v:v), 1 M $LiPF_6$
- reference electrode: Li/Li^+

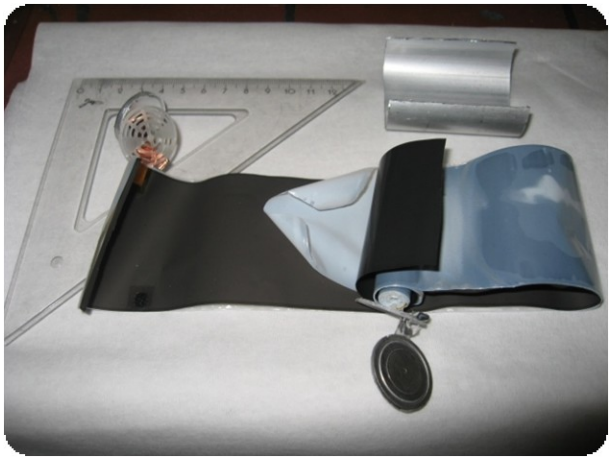

Figure 27: Disassembled 2.3 Ah A123 lithium ion battery

4.2.2 Experimental Results

The cycling performance of the back fitted industrial electrodes in Swagelok© test cells is shown in Figure 28. The theoretically battery capacity could be estimated with 1.57 mAh by the comparison of the electrodes surface in the Swagelok© test cells and the nominal cell capacity of the origin cell and its surface.

The charge / discharge conditions for the measurement on a MACCOR Test Series 4000[1] battery testing device were the following: First the cells were charged / discharged for 3 times using a C rate[2] of 0.2 C from 2.4 V to 3.6 V. Thereupon the cells were charged / discharged at a C rate of 1 C. The charging step was not followed by a constant voltage charging step.

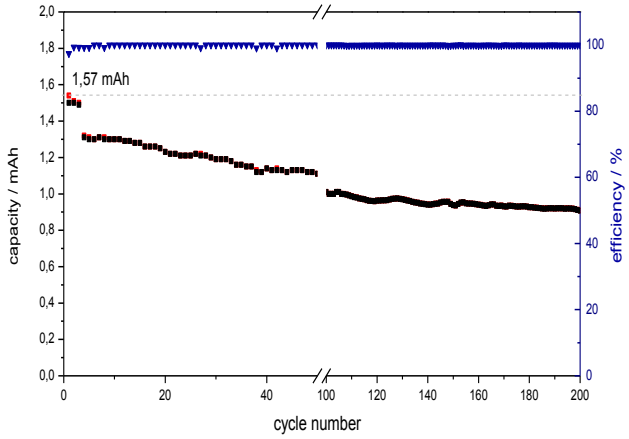

Figure 28: Charge / discharge capacity and efficiency of industrial electrodes in Swagelok© test cells

Within the performed measurements a strong capacity fading was observed, one exemplary measurement is shown within Figure 28. Applicable indication for this phenomenon was given by the progress of the potential curves of these measurements. All measurements showed corresponding potential curves, one exemplary measurement is shown within Figure 29.

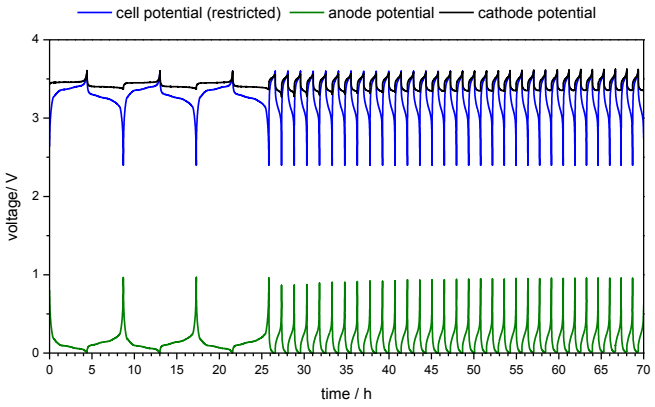

Figure 29: Progress of the potential curves of back fitted electrode materials during the charge /discharge test

[1] all charge / discharge test within this thesis have been measured on this testing device

[2] C rate: current that is needed to charge the battery/electrode within one hour

Within the measurements the cell voltage is mainly controlled by the potential of the anode. The operating potential window of the anode reaches from almost 0 V (close to metallic lithium deposition) to almost 1 V. As might be expected, these data prove that the cathode is obviously not the capacity limiting electrode.

The balancing of the electrodes was studied by further measurements. By these measurements the charge / discharge processes were not controlled by the terminal voltage, but only by a restriction of the cathode potential window (see Figure 30). The operating conditions for the measurements were chosen as follows:

Within the measurement displayed in Figure 30 the potential window of the cathode was restricted in the limits of 3.7 V and 3 V, which represents typical operating values for $LiFePO_4$ cathode materials. Terminal voltage and the anode potential were recorded, but their potentials were not restricted. First the cells were charged with a C rate of 0.2 C, followed by a discharge step at 0.2 C. Subsequent charge / discharge cycles were carried out at a C rate of 1 C.

The previously made assumption that the cell is limited by the capacity of the anode is confirmed by the measurement displayed in Figure 30.

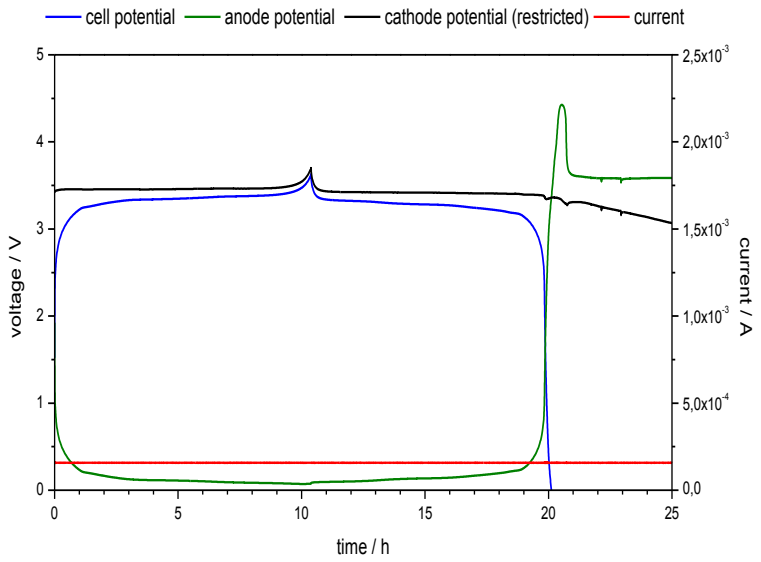

Figure 30: Potential curves of back fitted electrode materials (restricted only by the cathode potential):

During the first charge reaction the anode never reaches critical potentials close to 0 V (deposition of metallic lithium), while the full deintercalation of the cathode is reflected by the values of the cathode potential. Nevertheless, during the discharge reaction obviously not all of the lithium ions are reintercalated into the cathode. The cathode potential does not change significantly during the

discharge reaction, although the anode reaches far higher potentials, because no more lithium ions can be deintercalated of the anode material. In such potential regions copper dissolution of the copper current collector takes place. This process results in a complete destruction of the cell.

The measurement confirms that lithium ions are irreversible lost during the first charge reaction. This effect can be mainly attributed to further filming process at the anode material. In fact a second formation process occurs after the initial formation at the anode surface. This result is contributed to the back fitting process of the electrode materials.

Therefore the electrode balancing cannot represent the original cell balancing by the use of these electrode materials within Swagelok© test cells. Alternative methods for the determination of the electrode potentials had to be found.

4.3 Realizing Reference Electrodes in Commercial Cells

4.3.1 The Benefits of Reference Electrodes in Commercial Cells

Extended cycling leads to capacity fading caused by various mechanisms, introduced within chapter 3.6. According to chapter 4.2 no proper knowledge about the realistic potential values of the electrodes during charging can be generated by back fitting of electrode materials.

Monitoring of anode and cathode potentials, next to the cell voltage, can also be achieved by the insertion of a Li/Li^+ reference electrode into the original cell (see Figure 31). Due to the demands of high specific capacities as well as high volumetric capacities, industrial lithium ion cells do not provide a lot of space, which can be used for the embedment of Li/Li^+ reference electrodes. Special importance has to be contributed to the sealing of the batteries after the embedment process of reference electrodes.

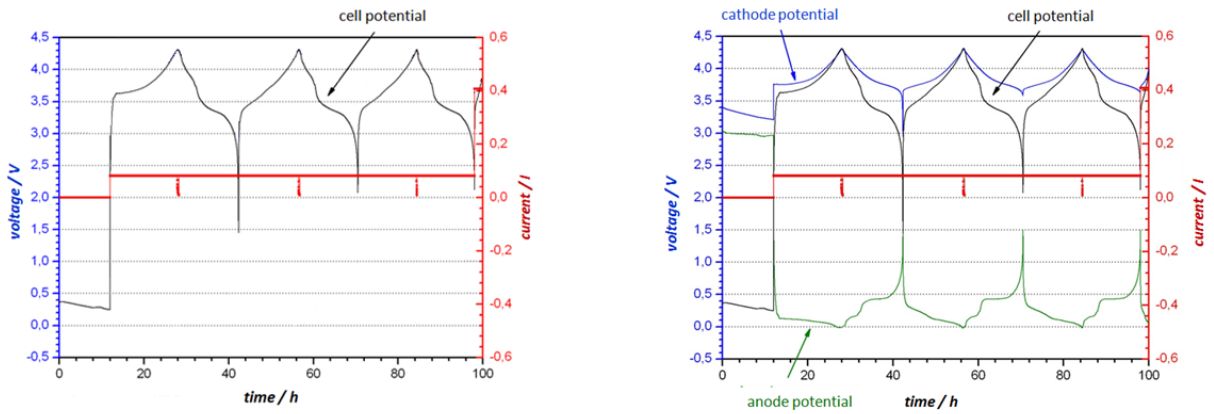

Figure 31: measurable voltage profiles by commercial cells without (left) and with embedded reference electrode (right)

4.3.2 Realizing Reference Electrodes in 26650 Cells ($C/LiFePO_4$)

4.3.2.1 Experimental Setup

In order to investigate 2.3 Ah cells of the manufacturer A123 special adapters were constructed. Therefore printed circuit boards FR4 (epoxide resin and fibre glass reinforcement) were etched with HCl conc. and stacked using adhesives in order to connect the printed circuit board material to each

other. One copper layer on the FR4 material was retained and shaded in a hole, which was filled with metallic lithium. The flexible cathode conducting tap was passed around the reference adapter using an opening. This circular opening segment was closed using a counterpart segment after passing the cathode tab through. So actually a negative shape fitting the cathode pole cap was formed, what enabled the embedment of a reference electrode.

According to Figure 32 various shapes have been designed. As a function of the hole´s geometry the surface of the lithium reference electrode varied. Furthermore reference adapters for two separate reference electrodes have been constructed. Lithium reference electrodes with greater surface areas were used for impedance measurements and the adapter shown in the middle of Figure 32 was used for charge/ discharge tests.

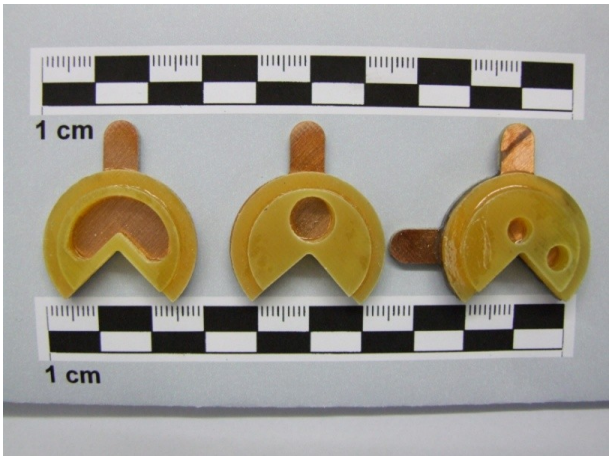

Figure 32: Various shapes of reference electrode adapters (counterpart circle segment not displayed)

The typically operating sequence for the embedment of the reference electrode contained the following steps:

All procedures were done by the use of an argon filled glove box (< 1 ppm H_2O, < 1 ppm O_2). After discharging to 2.6 V, the positive cap contacting the cathode was removed using a casing cutter. Thereupon a Celgard© 2400 separator (PP, 25 µm) was applied on the separators of the electrode stack. The reference adapter, filled with metallic lithium, was applied on the original aluminium case of the battery. In order to change the original cell setup as less as possible no further electrolyte was added.

Special tribute was paid to the sealing of the opened cell. Therefore Parafilm© as well as a hot glue gun have been used.

4.3.2.2 Experimental Results

Li/Li^+ reference electrodes have been embedded in industrial 2.3 Ah A123 cells according to chapter 4.3.2. The embedding of reference electrodes in commercial cells always modifies the original cells as a consequence of the intervention.

Especially the sealing of the opened cells is considered to be a major reason for the slightly declined cycle performance of the cells containing a reference electrode. Great emphasis was put onto the minimization of this effect. Nevertheless, according to Figure 33 the cycling performance differs slightly due to the intervention. The cells were cycled with a C rate of 1 C at 25°C within the potential window of 2.4 V to 3.6 V.

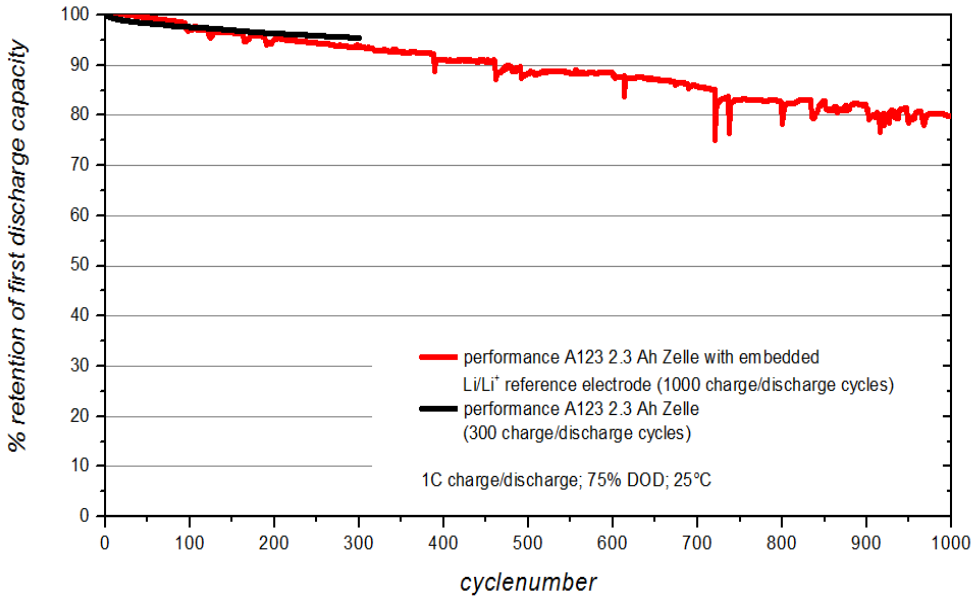

Figure 33: Comparison of the cycling performance of commercial A123 with/ without embedded reference electrode

With regard to the intervention effect caused by the insertion of a reference electrode, the changes in the potentials of anode and cathode during prolonged charging / discharging time is obvious within Figure 34 and Figure 35.

Figure 34 displays the voltage profiles of the anode and the cathode as well as the cell voltage within the first 100 hours.

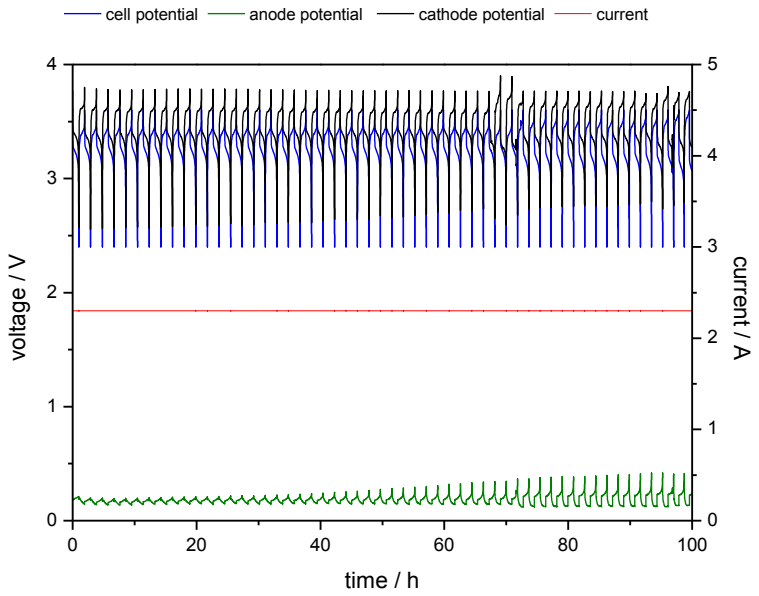

Figure 34: Voltage profiles of a 2.3 Ah A123 cell (C/$LiFePO_4$) during the first 100 hours of charge/discharge reactions

During cycling the anode potential continues to reach higher potentials, while the reduction oxidation reactions at the cathode take place in a continuous smaller potential window. According to Figure 35, which displays the potential profiles between 300 and 400 hours of charging / discharging, this effect is even more considerable.

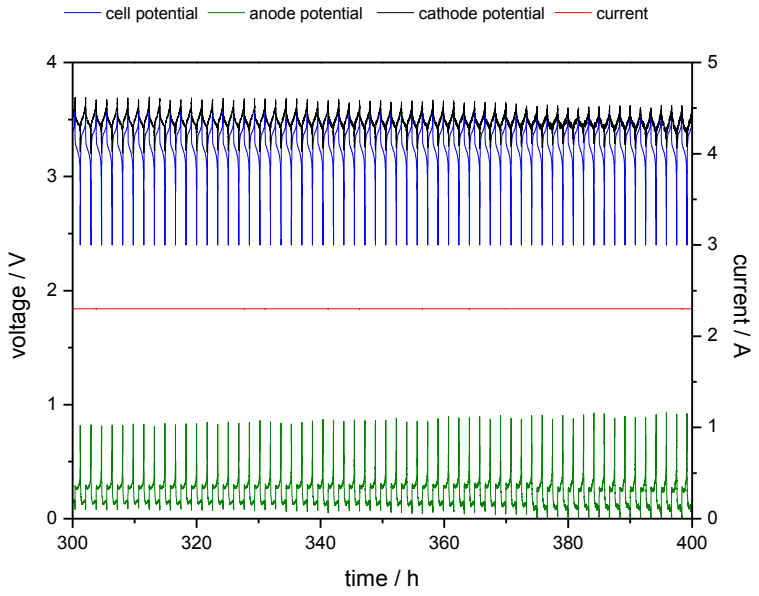

Figure 35: Voltage profiles of a 2.3 Ah A123 cell (C/$LiFePO_4$) between 300 and 400 hours of charge/discharge reactions

The changes in the potential windows of the electrodes have to be assigned to changes in the cell balancing between anode and cathode. These changes represent the result of mobile lithium consumption during the extended cycle life.

Within typical cells the cathode represents the capacity limited electrode, due to the prevention of metallic lithium deposition during charging. At the beginning of cycling (see Figure 34) the anode works in a minor potential window, while the cathode works in a potential range of 2.5 V to 3.8 V. This can be attributed to the reason that the anode is not fully intercalated with mobile lithium ions, while the cathode is fully intercalated. According to Figure 4 this results in a mainly assignment of the terminal or cell voltage by the cathodes potential.

Unfortunately, the irreversible consumption of lithium ions results in a shift of the capacity limiting electrode. With every charge / discharge cycle the cathode is not fully intercalated anymore. Moreover, due to the continuous loss of mobile lithium ions the cathode is even less intercalated, resulting in the fact that the cells switch-off criteria for the charge / discharge gets provided by the anodes reduction / oxidation reaction instead reduction / oxidation reaction of the cathodes.

The potential windows of the negative electrode within Figure 34 and Figure 35 extend on the negative and positive edge, what indicates a rise of the electrodes impedance. This rise of the electrodes impedance can be associated with continually growing of the SEI passivation layer.

Within chapter 3.6.3 it was already mentioned that this capacity fade mechanisms can get gradually outpaced by the loss of cathode active material, due to changes in the crystal lattice. In the case of the presented measurement, $LiFePO_4$ is used as cathode material and this material does not undergo changes in the crystal lattice.

Intensive study and search of literature data resulted in no measurement data of industrial cells in comparable quality and cycle number. The sealing of the cells and the loss of electrolyte and the gaseous phase during the cell opening have to be considered to be responsible for the enhanced loss of initial capacity.

Qi Zhang et al. estimated the potential windows of the anode as well as the cathode by modelling the SOC during cycling (102). Within this publication the authors also contributed the capacity fade mechanisms to the loss of mobile lithium ions in the first stage and to the loss of active cathode material in a second stage (102).

4.3.3 Realizing Reference Electrodes in Coffee Bag Cells (C/LiFePO$_4$)

Within chapter 4.3.2 reference electrodes were embedded in industrial A123 2.3 Ah cells. A major problem caused by the embedment of reference electrodes was contributed to the sealing of these cells. Furthermore the intervention had to be done in already formed cells and the opening of the cells resulted in a loss of electrolyte and the gaseous phase of the cells. In order to prevent these problems reference electrodes were embedded in 50 mAh coffee bag cells[3] before the electrolyte was added to the cell system.

4.3.3.1 Experimental Setup

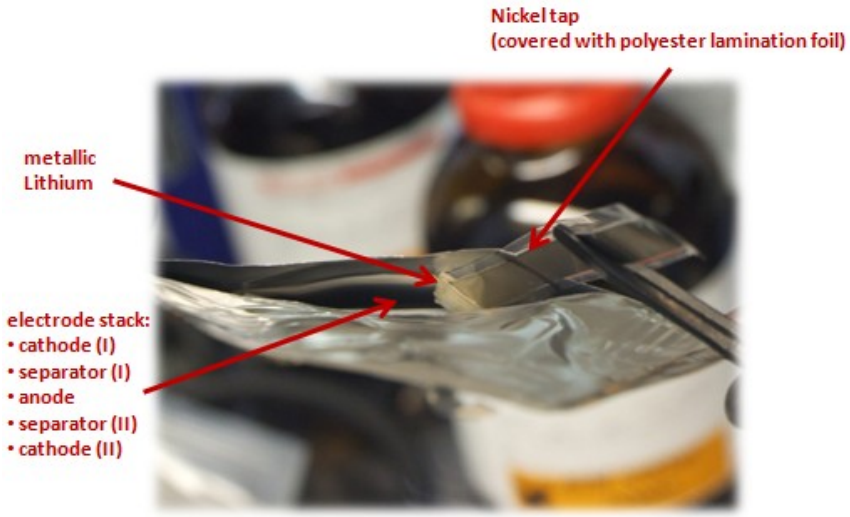

Figure 36: Embedding the reference tab in coffee bag cells

In order to establish a reference electrode in coffee bag cells a nickel tab was used, because nickel does not form intermetallic alloys with lithium like e.g. aluminium. In order to prevent shot circuits this tab was covered with polyester lamination foil sparing the ends out. One end was carefully covered with lithium. Subsequently the reference electrode was embedded between the two separators, according to Figure 36. The reference electrode was embedded as close as possible to the electrodes, without influencing them. In addition weld streams fixed the position of the reference electrode (Figure 37).

[3] Manufacturer not disclosed

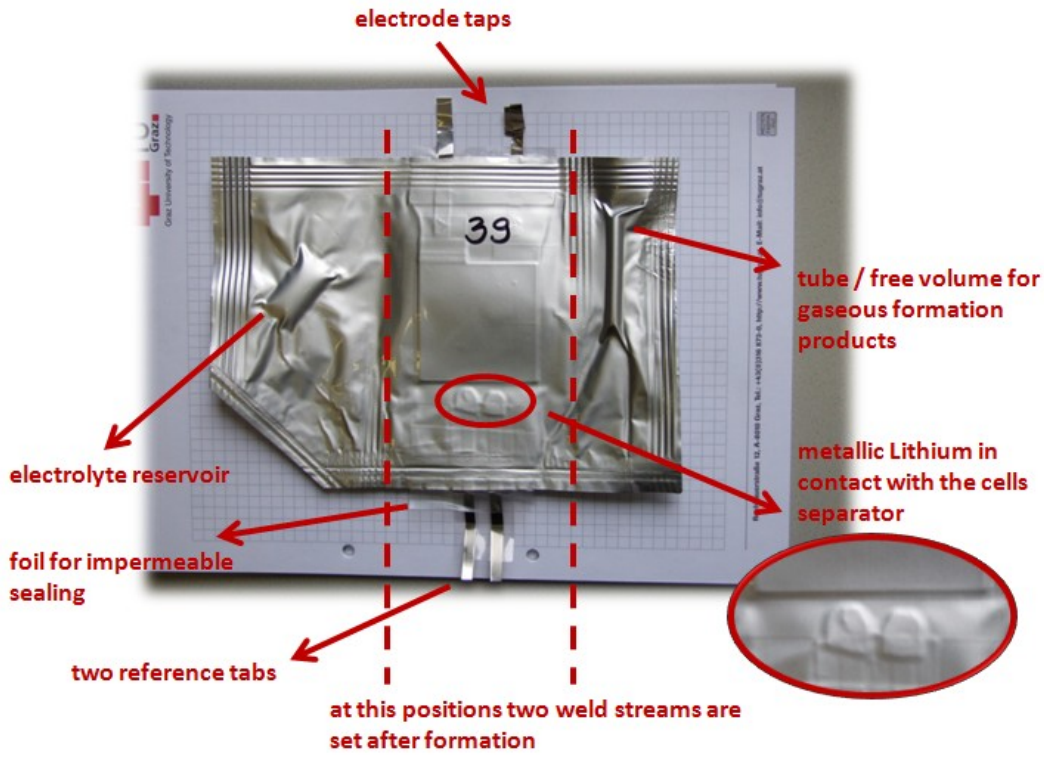

Figure 37: 50 mAh coffee bag cell with embedded reference electrodes (before formation; modification with two separate reference electrodes)

After the reference electrode was embedded carefully, the electrolyte reservoir was opened and the formation cycles were started. The gaseous products, occurring during the formation process were collected within a free volume, displayed within Figure 37. In order to ensure a sealed cell this step was followed by setting of two weld streams.

4.3.3.2 Experimental Results

4.3.3.2.1 Comparison of Cells Cycled with and without Embedded Reference Electrodes

The measurements displayed in Figure 38 and Figure 39, compare a 50 mAh coffee bag cell containing an embedded reference electrode with an original cell. The first three charge and discharge steps were performed at a C rate of 0.1 C in a potential window from 2.4 V to 3.6 V. Thereupon the cells were charged / discharged with a C rate of 1 C. Each charging cycle was expanded by a 5 minutes lasting constant voltage charging step at 3.6 V.

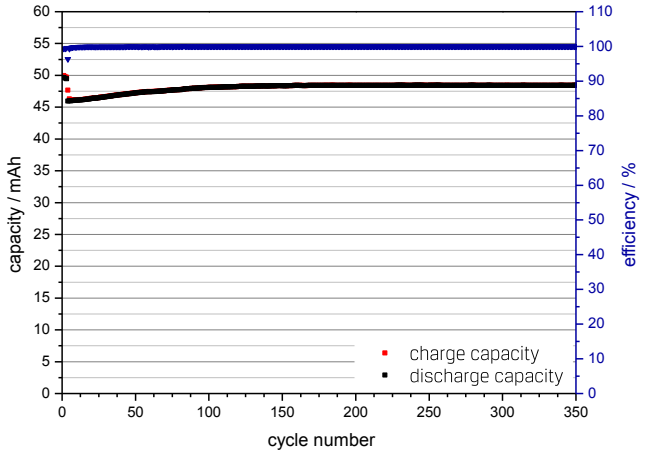

Figure 38: cycle performance of a 50 mAh coffee bag cell with embedded reference electrode

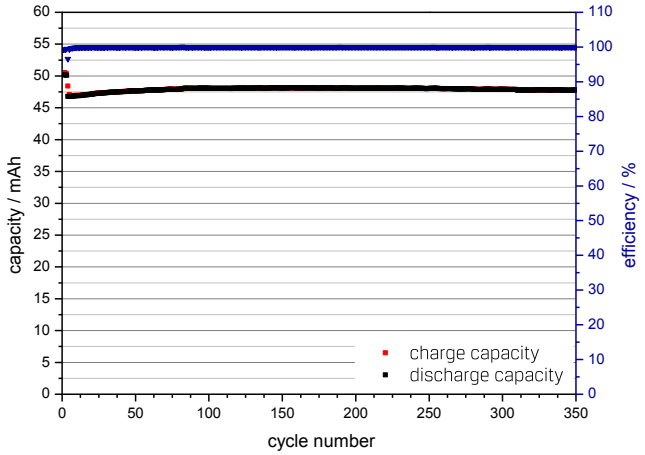

Figure 39: cycle performance of a 50 mAh coffee bag cell without embedded reference electrode

During the performed 350 charging / discharging cycles no influence of the embedded reference electrode on the cycling behavior was recognized.

Noticeable is the increase of the cells capacity during the first 100 cycles, which can be attributed to the manufacture´s $LiFePO_4$ material used. This material undergoes alignments in the crystal lattice within the first 100 cycles and therefore not all lithium ions are able to deintercalate from the first cycles.

The potential curves of the electrodes are shown within Figure 40. The cell is limited by the cathodes capacity and small ageing effects can be observed after about 650 hours (equal to about 300 cycles; see Figure 38), due to the fact that the anodes potential window begins to get larger.

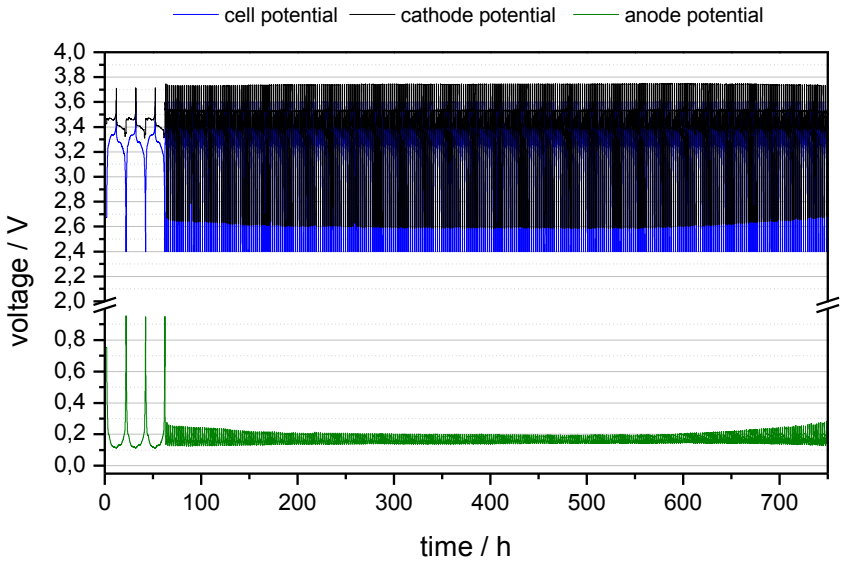

Figure 40: Cell and electrode potentials of a 50 mAh coffee bag cell with embedded reference electrode

Within the first 100 cycles (times up to 250 h) the potential window of the anode declines, which can be attributed to the changes in the cathode material explained before.

By the use of reference electrodes not only the electrode potentials during charging and discharging could be observed, furthermore the influence of different charge and discharge rates on the electrode potentials could be studied.

4.3.3.2.2 Discharge Rate Tests on Coffee Bag Cells with Reference Electrode

According to chapter 4.3.3 coffee bag cells were prepared with reference electrodes. In addition three formation charge / discharge cycles with a C rate of 0.1 C (for 50 mAh cells) were carried out. The capacity value achieved at the third formation cycle was used to estimate the C rate for further measurements.

A discharge rate test was carried out according to the following conditions. In order to ensure less initial changes in the cathode lattice (observed in Figure 38) when the discharge rate test is performed, 50 charge and discharge steps at 1 C were performed. The charge steps were expanded by a 5 minutes lasting constant voltage charging step at 3.6 V. Purposely not more than 50 cycles were chosen, in order to avoid incorrect potential values caused by increasing ageing effects.

During the discharge rate test the charging procedure was carried out at a C rate of 1 C, followed by a constant voltage charging step at 3.6 V for 5 minutes. As shown in Figure 42 and in Figure 43 the discharge rate was increased from 2 C up to 10 C with one monitoring cycle after each increase of the C rate. This monitoring cycle was performed using a charge step at 1 C, an additional constant voltage charging step at 3.6 V (for 5 minutes), as well as a discharge step at 1 C.

In order to gain information about the state of health (SOH) of the lithium ion cell the measurement was concluded with five charge / discharge steps, according to the initial ones.

Figure 41 displays the capacity values of the lithium ion battery during the measurement. The monitoring cycles, as well as the finishing cycles for the estimation of the cells SOH, show no degradation of the electrodes but remarkable achievable capacities at high C rates. The measured data prove the high rate capability of the cell´s electrodes and electrode materials in particular.

Figure 42 and Figure 43 display the potential curves during the rate test. The potential windows of the anode as well as of the cathode seem to be only slightly effected by the rate test.

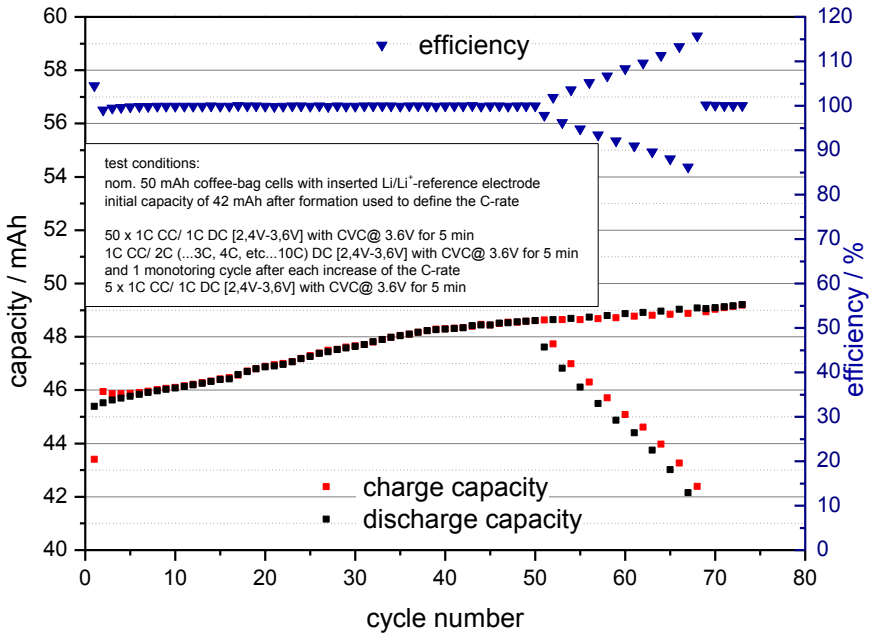

Figure 41: Charge / discharge capacities during discharge rate test

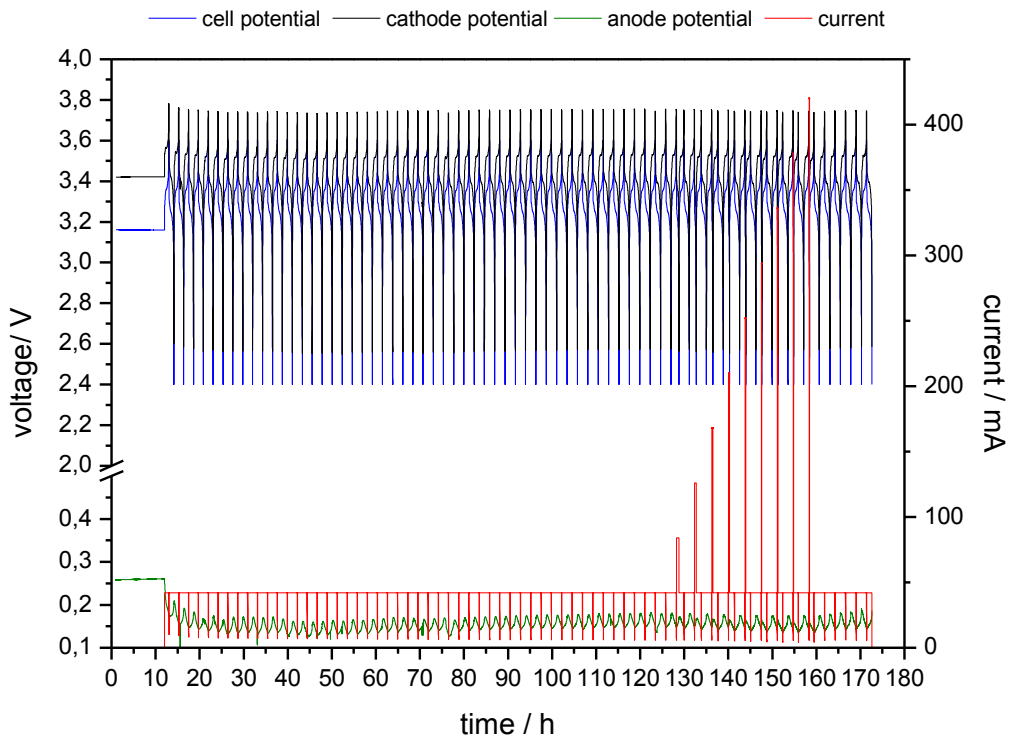

Figure 42: Potential curves of the electrodes before and during the discharge rate test

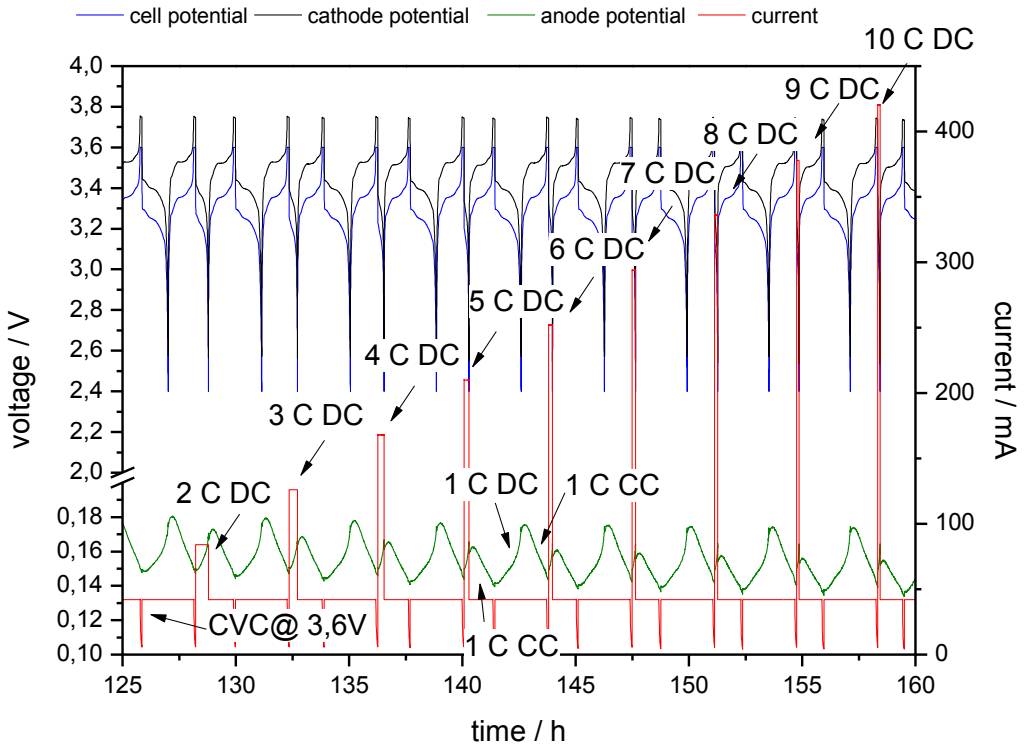

Figure 43: Potential curves of the electrodes during the discharge rate test

The analysis of the potential values for the electrodes against the achieved capacity was of special interest for the modelling project “Modelling, Validation and Test of Lithium-Ion-Batteries for Hybrid Vehicles”. With the help of the measurement data displayed in Figure 44, Figure 45 and Figure 46 the empirical modelling data could be fit to measured values. Obviously the cell potential is mainly characterised by the cathodes potentials. Remarkable is the capacity retention after the discharge rate test. The slightly higher value can be attributed to the changes in the cathode´s lattice structure within the first cycles.

Furthermore, by displaying the potential values vs. the achievable capacity information about the dependence of the cells and electrodes specific over-potentials (see chapter 2.2) on the discharge rate could be gained.

Comparison of the potential differences depending on the discharge rate between Figure 45 and Figure 46 suggest the conclusion that the anode possesses a far higher rate capability than the cathode. These results are confirmed by literature data (18) (4).

Therefore, and according to Figure 44 and Figure 46, the over-potential of the investigated graphite/$LiFePO_4$ batteries during discharge can be mainly attributed to the over-potential caused by the cathodes intercalation.

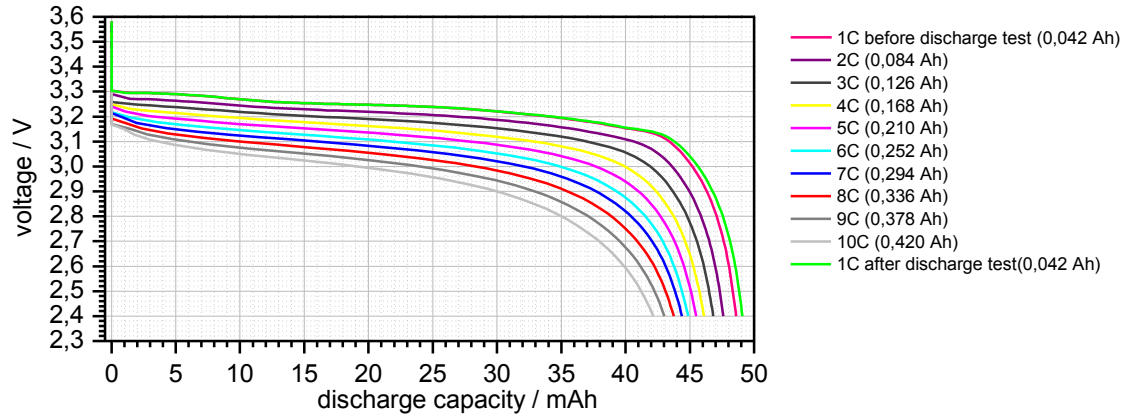

Figure 44: Discharge rate test: rate dependence of the cell potential vs. the achieved discharge capacity

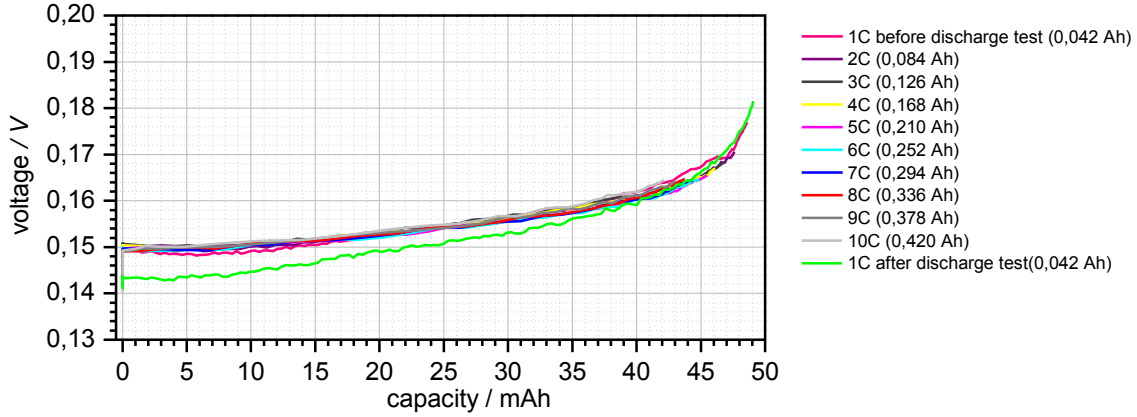

Figure 45: Discharge rate test: rate dependence of the anodes potential vs. the achieved discharge capacity

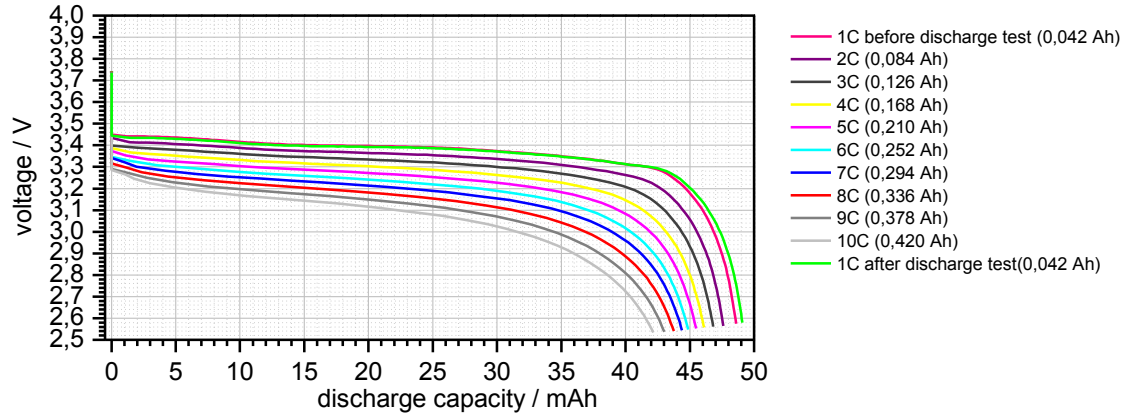

Figure 46: Discharge rate test: rate dependence of the cathode potential vs. the achieved discharge capacity

4.3.3.2.3 Charge Rate Tests on Coffee Bag Cells with Reference Electrode

In order to develop further data for the modeling of lithium ion batteries a charge rate test was carried out additionally. The charge / discharge steps before and after the charge rate test were chosen according to chapter 4.3.3.2.2, but no constant voltage charging steps were added.

During the charge rate test the discharging procedure was carried out at a C rate of 1 C. The charge C rate was increased from 2 C up to 10 C with one monitoring cycle after each increase of the C rate. No constant voltage charging steps were added.

Figure 47 displays the capacity values of the lithium ion battery during the measurement. The decision to carry out no constant voltage cycling resulted in strong capacity fading. But monitoring and finishing cycles display no enhancement of the capacity fading by the charge rate test. The value at the charge C rate of 10 C represents a measurement artifact.

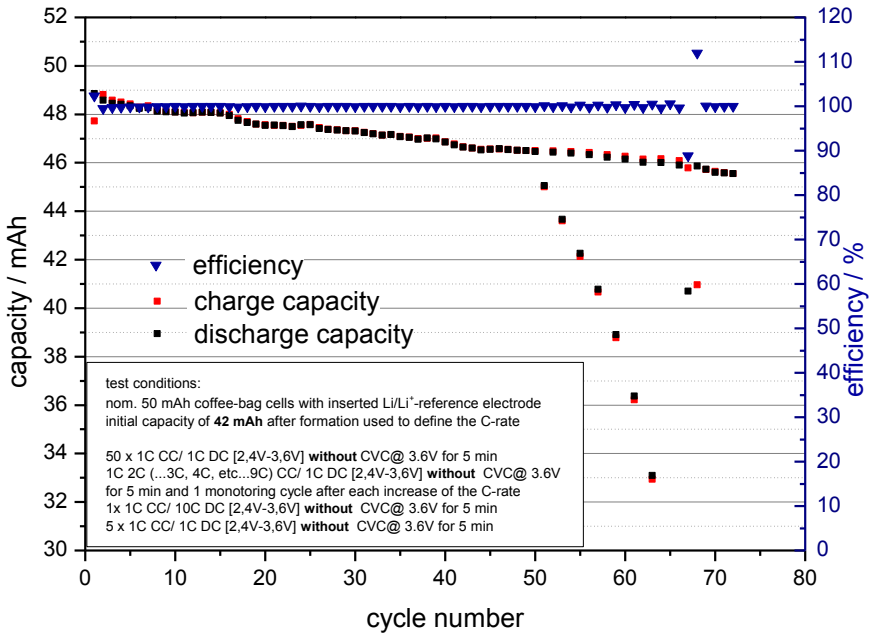

Figure 47: Charge / discharge capacities during charge rate test

By the comparison of the potential differences depending on the discharge rate (see Figure 49 and Figure 50) the potential curve values of both electrodes are strongly influenced at higher charge rates. The over-potentials of the terminal voltage (see Figure 48) originate from over-potentials at both electrodes.

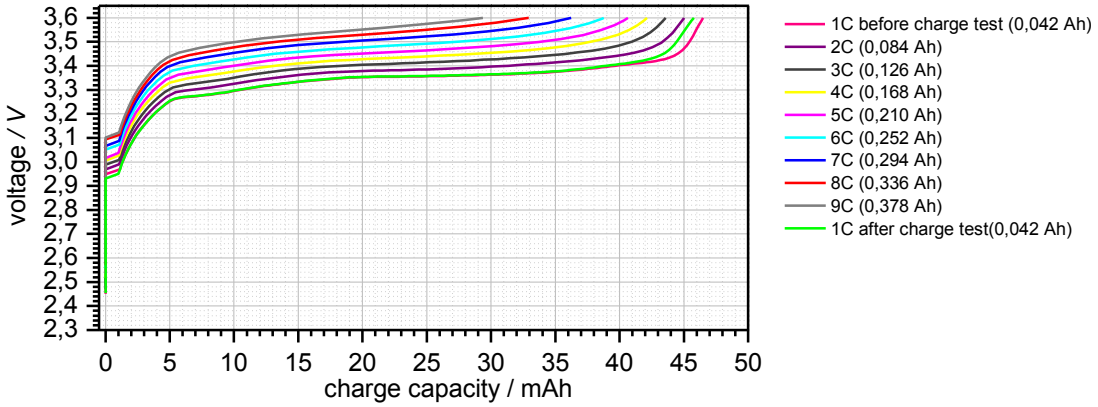

Figure 48: Charge rate test: rate dependence of the cell potential vs. the achieved charge capacity

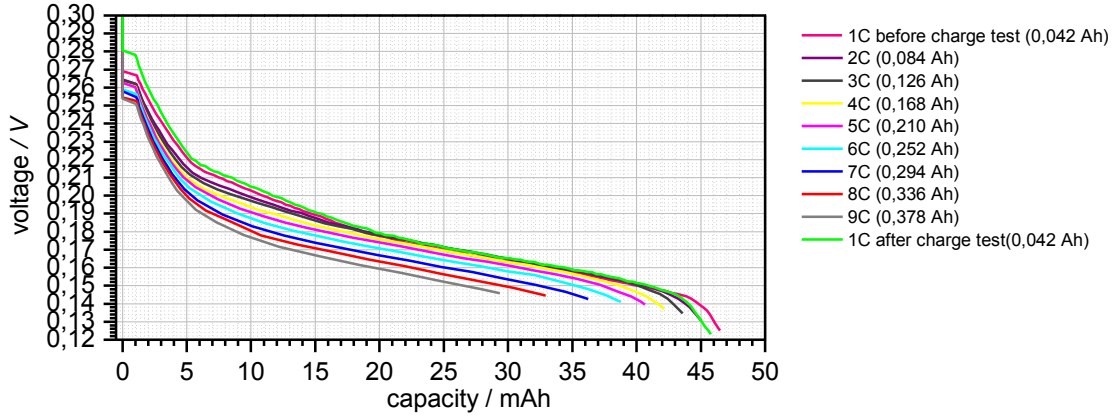

Figure 49: Charge rate test: rate dependence of the anode potential vs. the achieved charge capacity

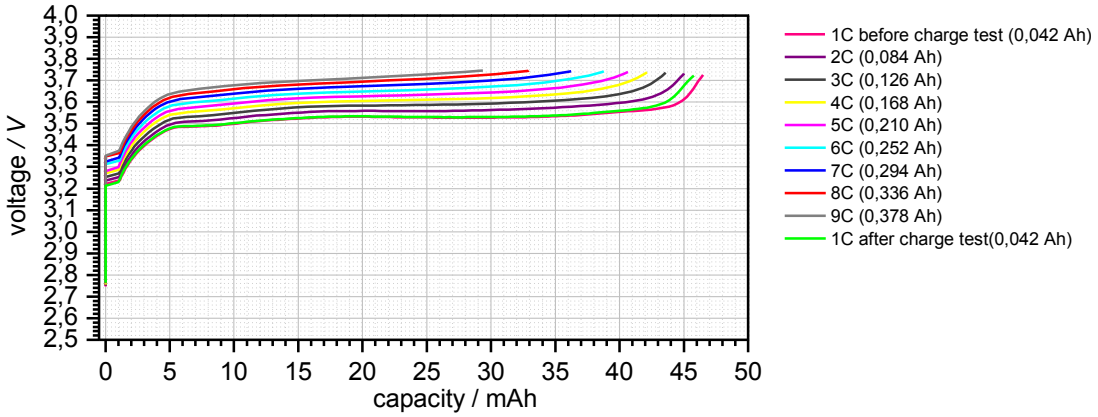

Figure 50: Charge rate test: rate dependence of the cathode potential vs. the achieved charge capacity

4.3.3.2.4 GITT Measurements on Coffee Bag Cells with Embedded Reference Electrode

With regard to the validation of modeling data acquired in the "Modelling, Validation and Test of Lithium-Ion-Batteries for Hybrid Vehicles"-project, measurements at very low C rates had to be realized. These measurement setups allowed the determination of the electrodes and cell potentials unaffected by over-potentials. A measurement method able to use for these kinds of investigations is called galvanostatic intermittent titration technique (GITT). The measurements were first proposed by *Webbner and Huggins* (103) (52). In fact the method was established to evaluate chemical diffusion coefficients of lithium ions in electrode materials, according to Figure 51.

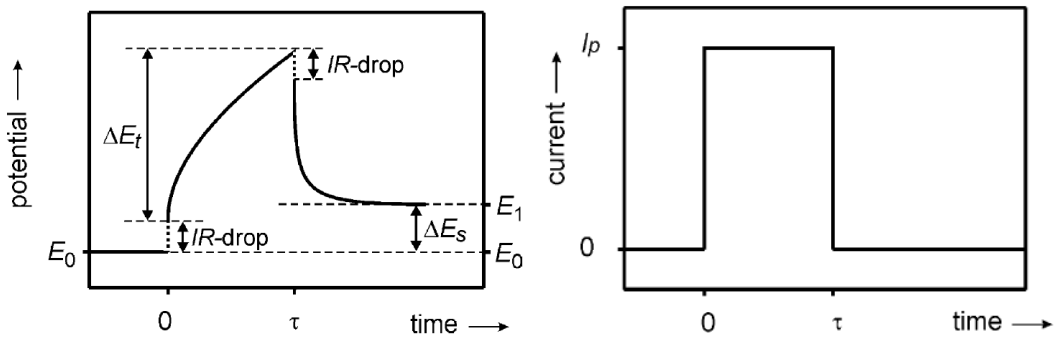

Figure 51: schematic drawing of a current pulse in a GITT measurement (14)

The chemical diffusion coefficient can be obtained by potential responses on small current pulses according to Eq. 28.

$$D^{GITT} = \frac{4}{\pi * \tau}\left(\frac{m_B\, V_M}{M_B\, S}\right)^2 * \left(\frac{\Delta E_s}{\Delta E_t}\right)^2$$

D^{GITT} ... chemical diffusion coefficient
τ ... constant current pulse time
m_B ... mass of host material
V_M ... molar volume of host material
M_B ... molar mass of host material
S ... area of electrode/electrolyte interphase
ΔE_s ... change of steady state voltage during GITT step
ΔE_t ... total change of cell voltage during constant current pulse τ

Eq. 28

Due to the fact that GITT measurements neglect changes in basic parameters like the area of the electrode / electrolyte interphase and the capacity of the electrochemical double layer during the charge / discharge reactions, the calculation of absolute values for the chemical diffusion coefficients is quite defective. Anyhow, by the use of this method basic information on the chemical diffusion of the lithium ions within the battery can be obtained. Especially for the estimation of the electrode

potentials at different state of charges, these measurements represent a useful tool for the verification of the electrochemical battery model, developed by the Virtual Vehicle program.

Therefore various GITT measurements were performed based on different charge / discharge pulse currents in combination with different pulse times and pulse counts.

One exemplary measurement is presented within Figure 52, Figure 53 and Figure 54. This measurement was performed with comparatively high current pulses in order to gain information about the over-potentials of the electrodes during current load. The conditions for the experiment were the following:

After the formation of the coffee bag cell with embedded reference electrode three cycles with charge and discharge steps at 1 C were done. No constant voltage charging step was included during the charge / discharge cycles.

For the GITT experiment a charge / discharge pulse current of 25 mA (corresponding to C/2) was chosen. The constant current pulse time was chosen by 4 minutes, followed by a load free relaxing time of 4 hours. For the charging, as well as for the discharging step, the current pulse and the relaxation were repeated for 35 times, limited in the potential window of 2.4 V to 3.6 V.

The galvanostatic intermittent titration charge / discharge steps were always followed by 50 charging / discharging cycles at a C rate of 1 C.

Alternately, this procedure was continued for 10 times. Unfortunately, the cells were not able to fulfil the whole measurement procedure. Coffee bag cells of this type are actually designed to allow studies on the electrode materials and the balancing of these to each other. Most of these measurements take about 500 hours. That represents a time value such coffee bag cells, produced with laboratory quality standards, can fulfil with ease.

Within the measurement displayed in Figure 52 cycle times of up to 5500 h were obtained. Difficulties with the sealing of these cells, as well as the quality of the embedded reference electrode result in inaccuracies of the measurement after a duration of about 4000 hours.

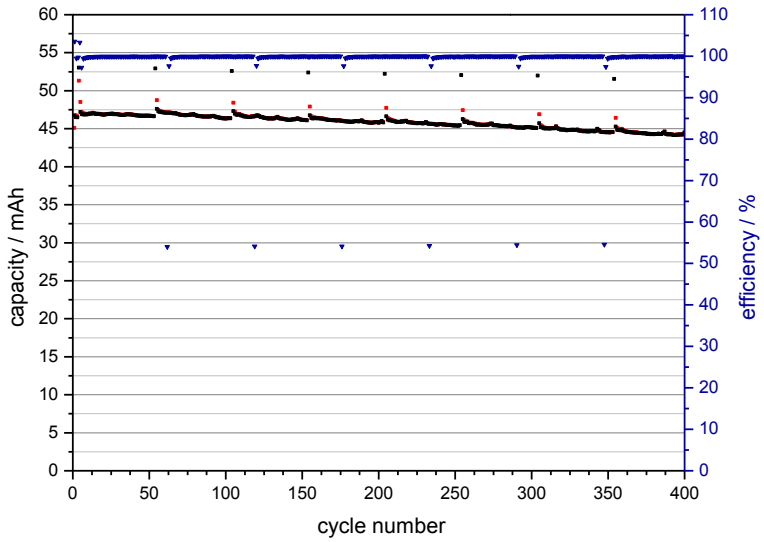

Figure 52: cycle performance of a 50 mAh coffee bag cell with reference electrode during GITT experiment

Figure 52 displays the cycle performance of the 50 mAh cell during the GITT testing procedure. A small decrease in the capacity can be observed with continual charge / discharge cycles. Due to the fact that no constant voltage charging steps were added during the 1 C charge / discharge cycles the amount of capacity fading fits Figure 47.

The capacity fading is partly suppressed by the galvanostatic intermittent titration charge /discharge step. Within this step the electrochemical system gains the needed time to completely finish the deintercalation of lithium ions from the cathode during charging. Within the following 1 C charge/discharge cycles significantly higher capacities can be observed again.

This effect results in a saw-tooth shaped progress of the capacity during the measurement.

Figure 53 and Figure 54 display the potential curves of the first galvanostatic intermittent titration charge / discharge step as well as the potential curves of the 7th GITT charge / discharge step. According to results obtained within chapter 4.3.3.2.2 the cell over-potential mainly results due to over-potentials of the $LiFePO_4$ cathode during intercalation / deintercalation reactions of lithium ions. This is indicated by the potential responses to the current pulses during the relaxing period of the single galvanostatic intermittent titration charge / discharge steps.

According to previous results within this work, the potential windows of the anode expends, while the potential window of the cathode declines. This effect is contributed to the loss of mobile lithium ions with increasing cycle number.

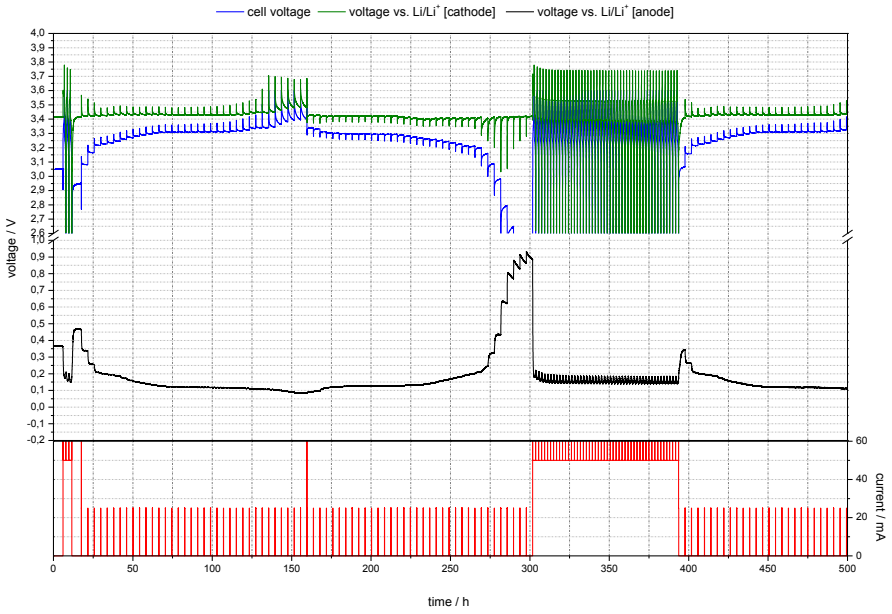

Figure 53: Cell and electrode potentials during the GITT experiment (0-500h)

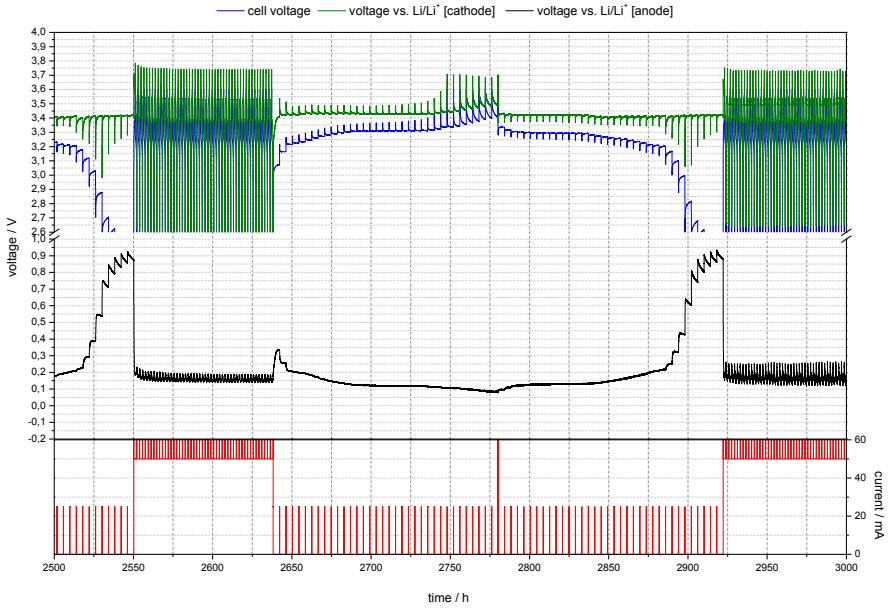

Figure 54: Cell and electrode potentials during the GITT experiment (2500-3000h; 7th GITT charge/discharge cycle)

4.3.4 Conclusion on the Insertion of Reference Electrodes in Lithium Ion Batteries

The development of advanced lithium ion batteries for electric vehicle and hybrid electric vehicle applications requires basic and applied research on both, positive and negative electrodes in order to achieve experience on ageing mechanisms taking place during extended cycling.

By the use of back fitting technique for electrode materials from the origin cell to laboratory test cells, no proper information on the potential curves of the electrodes could be obtained (chapter 4.2). This can mainly be attributed to the loss of lithium, due to decomposition reactions on the anode and accordingly a second formation process on the anodes surface.

Embedding of reference electrodes in commercial 2.3 Ah cells (C/ $LiFePO_4$) allowed the study of the anode and cathode potential next to the cell voltage (chapter 4.3.2). Unfortunately, the insertion of reference electrodes resulted in slightly increased cell ageing contributed to the difficulties related to the sealing of the cells. Furthermore the intervention had to be done in formed cells resulting in a loss of electrolyte and the gaseous phase when the cells were opened for the insertion of the reference electrode.

In order to prevent these problems reference electrodes were embedded in 50 mAh coffee bag cells (C/ $LiFePO_4$) before the electrolyte was added to the cell system (chapter 4.3.3). By the use of this technique remarkable long term stability and outstanding comparability of the measured cells could be achieved.

The measured data proved the high rate capability of the electrodes and the active material. The cells over-potentials, measured by rate tests as well as by GITT experiments, can be mainly attributed to the over-potentials caused by the cathodes intercalation / deintercalation reaction.

With increasing cycle number the anode potential window expends continuously. Especially during the discharging reaction the anodes potential slides to higher values, an effect that can be attributed to the loss of mobile lithium ions with increasing cycle number. Within a publication of the main ageing phenomena in lithium ion batteries by *Vetter* et al. capacity and power fading is mainly caused by electrolyte decomposition due to continuous growth of the solid electrolyte interphase at minor rates (see Table 2) (95).

4.4 Post Mortem Analysis of SEI Components for Determination of Ageing Effects

Within chapter 4.3 of this thesis a slide in the anodes operating potential was observed during continuous cycling. The measurement in Figure 55 displays the capacity and power fading of an industrial manufactured 2.3 Ah A123 cell (C/$LiFePO_4$). Especially the potential difference of the characteristic hysteresis curve during the charging and discharging reaction at the beginning of cycling and at proceeded cycle time is remarkable.

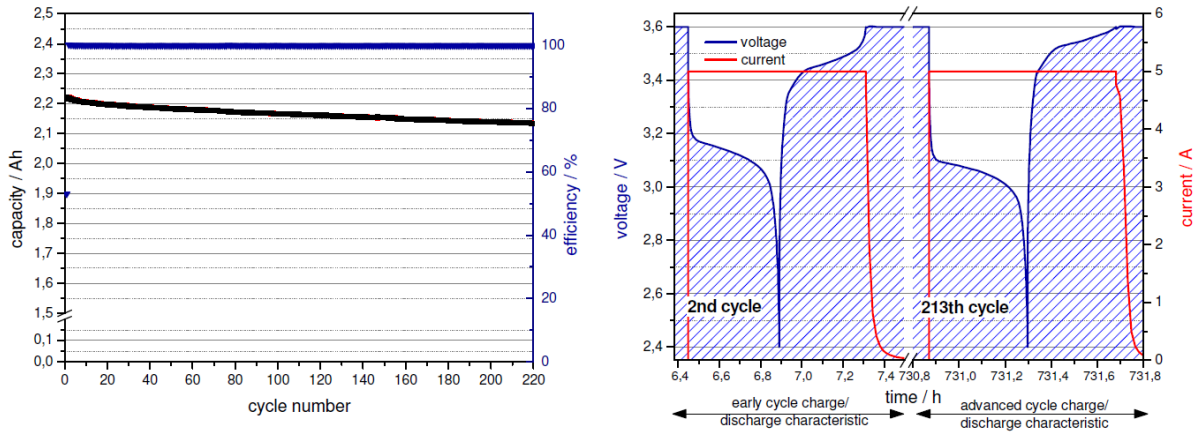

Figure 55: Capacity fading (left) and power fading (right) of industrial manufactured lithium ion cycled between 3.6 V and 2.4 V; C rate 2 C charge/discharge, 20°C

The analysis presented within this chapter puts focus on the quantitative analysis of the ageing mechanism caused by the growth of the solid electrolyte interphase. Although the solid electrolyte interphase is mainly established within the first three charge / discharge cycles minor continuous corrosion of the electrolyte at the anodes surface is assumed to be the major cause for cell ageing. This corrosion rate is promoted by enhanced temperatures during battery use (95) (104).

To the knowledge of the author of this thesis, no publications are reported until now, that prove this ageing effect by experimental values. The rise of the cells impedance, capacity fading and power fading are parameters authors use to describe this ageing phenomena (105) (106) (107).

Unfortunately, these parameters sum up various ageing mechanisms (see Table 2) (95). According to this, the determination and quantitative analysis of single ageing mechanism is not possible by the analysis of these parameters. Within this chapter a new method to determine the continuous growth of the SEI is presented, discussed and validated.

4.4.1 Theoretical Background on the Analysis of the Solid Electrolyte Surface Growth

In order to determine the influence of the solid electrolyte interphase growth on capacity fading separately, the increase of the Lithium and Fluoride concentration on the surface of the anode has been analysed after cycling of the cells.

Within the theoretical part of this work the properties and composition of the solid electrolyte interphase was discussed (see chapter 3.5). The SEI consist of a thick and porous layer of electrolyte permeable organic decomposition products (polymers and oligomers) and a compact layer of electrolyte impermeable inorganic (Li_2CO_3, LiF) and combined (lithium alkyl carbonates) decomposition products (see Figure 21).

According to *Aurbach et al.* the SEI layer in carbonate based electrolytes is composed of species like Li_2CO_3, $ROCO_2Li$, lithium alkoxides, Li_2O, LiF, LiCl, as well as other organic and polymeric species, while *Edström et al.* identified Li_2CO_3 and LiCl, LiF as predominant SEI components (90) (92).

The influence of SEI growth and the resulting loss of mobile lithium on the capacity fading are displayed within Figure 56. Untypically the full-cell study was carried out using a $LiNi_{1/3}Mn_{1/3}Co_{1/3}O_2$ (NMC) with the doubled anode capacity. A silicon/graphite composite electrode was used for the negative electrode.

For the cycling study the potential window of the anode was set to be between 0.005 V and 1.5 V. During the charging process the cut off voltage of the cathode was set to 4.3 V. Within this unconventional balancing the additional lithium can be stored in the cathode material and creates a reserve of lithium that is able to compensate the irreversible loss caused by refilming process at the negative electrode during cycling.

The cycling behaviour of the full cell is controlled by the cycling stability of the anode up to the 210^{th} cycle. After this cycle a sharp bend indicates that the cycling behaviour becomes controlled by the cathode, respectively it's cut off voltage limit. Actually the cycling behaviour becomes controlled by the amount of mobile lithium at this point. All the additional lithium stored within the high capacity anode was lost due to reactions at the anodes surface.

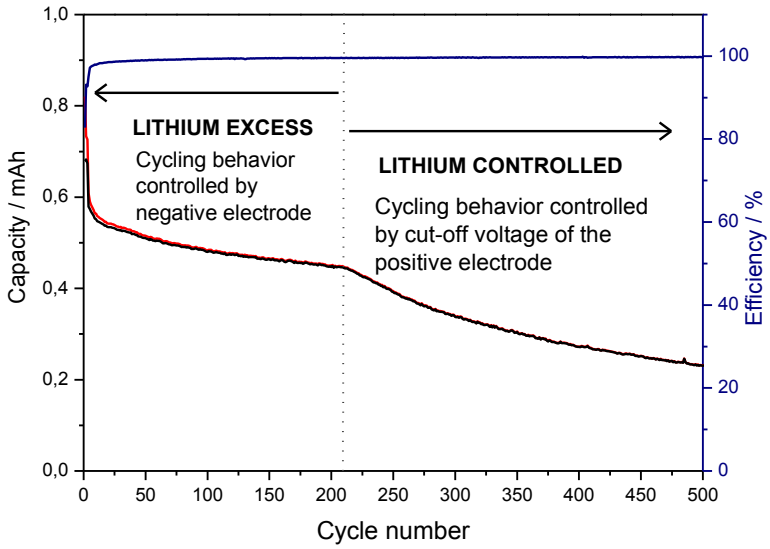

Figure 56: Full-cell cycling study of silicon/carbon composite vs. NMC

In industrial cells the working ranges of the two electrodes cannot be controlled by a reference electrode. Therefore the loss of mobile lithium results in a shift of the two electrodes to higher potential ranges. These shifts were already observed within chapters 4.3.2 and 4.3.3.

Shifts to higher potentials of overcharge sensitive cathode materials result in irreversible changes of the crystal lattice and accelerated cell ageing. Furthermore potentials above 4.2 V result in oxidative electrolyte decomposition of commonly used electrolytes. At this point the loss of mobile lithium furthermore affects the stability of the cathode material, resulting in enhanced ageing of the cell.

4.4.2 Purpose of the Analysis

The purpose of the analysis is to estimate the amount of lithium and fluoride on the anodes surface, in order to gain relative information on the growth of the solid electrolyte surface. In addition the increase of the lithium concentration on the anodes surface is going to be compared to the loss of mobile lithium ions during the charge / discharge cycles.

Unfortunately, the analysis of the lithium and fluoride concentration on the anodes surface is destructive, because the cells have to be disassembled and representative parts of the electrode had to be taken for the analytical measurement.

4.4.3 Description of the Experimental Setup

4.4.3.1 Cycling Conditions and Electrode Probe Sampling

In order to estimate the growth of the SEI depending on the number of charge / discharge cycles the destructive ex situ analysis rendered the use of the same cell impossible. Therefore every analytical measurement had to be done in another cell, cycled for a certain cycle number before.

1 Ah A123 cells (18650) were chosen for the analysis of the lithium and fluoride concentration on the anodes surface. The batteries consisted of a carbonaceous anode material, lithium hexaflurophosphate conducting salt and a $LiFePO_4$ cathode.

Special importance has to be contributed to the $LiFePO_4$ cathode, due to the fact that this cathode material is reversibly capable to delithiate totally. According to chapter 3.3.1 and chapter 4.4.1 layered metal oxide electrodes like $LiCoO_2$ are not able to delithiate all of the lithium stored within the host material reversibly. By the use of these cathode materials the capacity fading of the battery would be strongly affected by cathode ageing due to irreversible crystal disorders caused by the loss of mobile lithium ions.

According to Table 3 the 1 Ah A123 cells were cycled at two different temperatures for cycle numbers in the range of 50 to 3000 full charge/discharge steps. The cells were charged with a current of 5 A (C rate of 5 C) and discharged with a current of 5A in a voltage window of 3.6 V to 2.4 V. No constant voltage charging was performed in addition to the charging procedure.

Table 3: Cycling program of the investigated 1 Ah A123 cells

	description	temperature	storage	50 cycles	100 cycles	250 cycles	500 cycles	1000 cycles	2000 cycles	3000 cycles
Cells cycled	5A charge / 5A discharge	30	2	2	2	2	2	3	2	2
	5A charge / 5A discharge	60	2	2	2	2	2	2	2	2

After each cell had completed the defined amount of cycles the cell was discharged at low rate to a potential of 2.4 V, following an equal slow discharge procedure. This step was followed by the opening of the steel cell case using a Proxxon Precision Rotary Tool with a diamond plate. The procedure was performed accurately but quickly, in order to suppress strong heating of the electrode stack. Special attention was paid to the prevention of short circuits during the opening process. Thereupon the current taps were cut and the electrode stack was unrolled. Afterwards prestigious parts of the anode were cut using a brass cutter.

The electrolyte and especially the conducting salt ($LiPF_6$) were carefully removed by the use of diethylene carbonate (3x 10ml). A possible corruption of the determined lithium and fluoride values was avoided by this cleaning step. The cleaning step was followed by the addition of 20 ml pure water to the samples. By heat treatment of the samples at 70°C the copper conducting foil could be easily separated and removed from the electrodes. Thereafter the samples were filled up to exactly 50 ml, using pure water. In addition the sealed samples were heated to 70°C for 24 hours. Each sample was filtered using an injection filter with a 0.1 µm mesh size.

Further anode materials were cleaned by the use of diethylene carbonate (3x 10ml) for investigation using scanning electron microscopy (SEM) and measurements for the imaging of the elemental distribution using microtome cuts and energy-dispersive X-ray spectroscopy (EDX).

4.4.3.2 Ion-Exchange Chromatography

Subsequently the lithium- and fluoride concentration of the samples was determined by the use of ion exchange chromatography. The setup for the Dionex DX 500 Ion Exchange Chromatography[4] contained:

- Dionex LC 20 Ion-Chromatography system
- Dionex CD 20 conductivity detectors (2x)
- Ionpac AS 14 column (anions)
- Ionpac KS 12A column (cations)
- ASRS Ultra II - suppressor (anions)
- CSRS Ultra II - suppressor (cations)

[4] all from Dionex Corp., Sunnyvale, CA, USA; performed at laboratory of Prof. Dipl.-Ing. Dr. Bruno Sternad

4.4.4 Cycling Study on 1 Ah A123 Cells at Different Temperatures

According to Figure 57 the difference in the operating temperatures resulted in different capacity fading. The cycle number of 3000 charge discharge steps is equal to a cycle time of about 2000 hours. After 3000 times of charging and discharging 1 Ah A123 cells operated at 30°C lose about 25 percent of the initial discharge capacity. Equal cells operated at 60°C even lose about 40 percent of the initial discharge capacity.

For the first 1000 charging / discharging cycles the degree of capacity fading tends to be nearly equal. After 1000 cycles the cell operated at a temperature of 60°C suffers a higher degree of capacity fading.

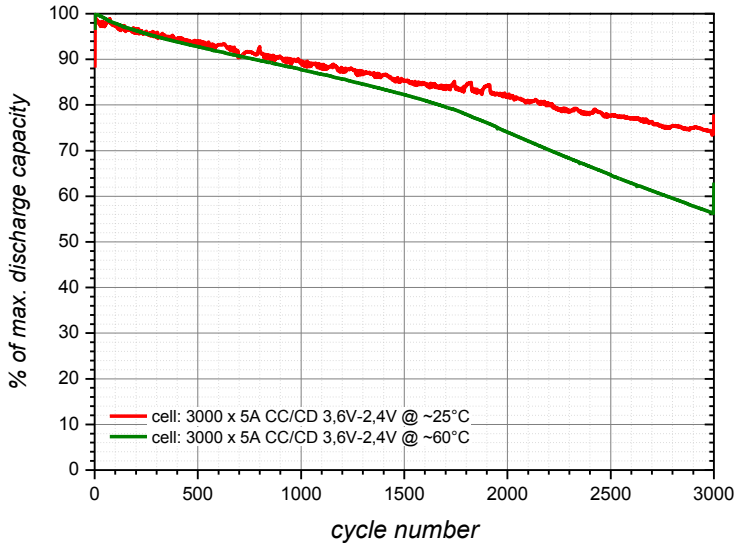

Figure 57: Discharge capacity loss of two exemplary industrial cells cycled at different temperatures

Figure 58 and Figure 59 display the potential curves of the terminal voltage during the discharging step against the achievable capacity at 30°C and respectively at 60°C. The potential curves were gained by a cell cycled for 3000 times. Remarkable is the higher achievable capacity at 60°C, what can be explained by faster reaction kinetics due to the higher operating temperature. The higher operating temperature also results in different terminal voltage values during the displayed discharge cycles in Figure 58 and Figure 59.

Table 4 and Table 5 compare the capacity fading of the batteries at different cycle numbers. After 3000 charging / discharging steps 32 percent of the cells discharge capacity is lost at an operating temperature of 30°C and respectively, a loss of 41 percent is observed for cells cycled at 60°C.

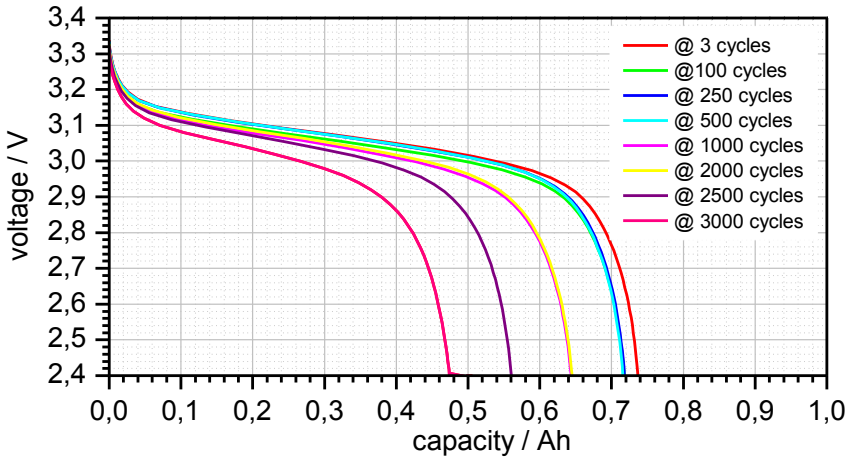

Figure 58: cell potential during discharge vs. capacity of 1 Ah A123 cells cycled at 30°C

Table 4: Comparison of the capacity loss of 1 Ah A123 cells dependent on cycle number at 30°C

Carried out cycle number	Capacity [Ah]	Percentage of capacity-fade
3	0.737	0.0
100	0.718	2.5
250	0.716	2.8
500	0.643	12.6
1000	0.645	12.4
2000	0.584	20.8
2500	0.561	23.9
3000	0.501	32.1

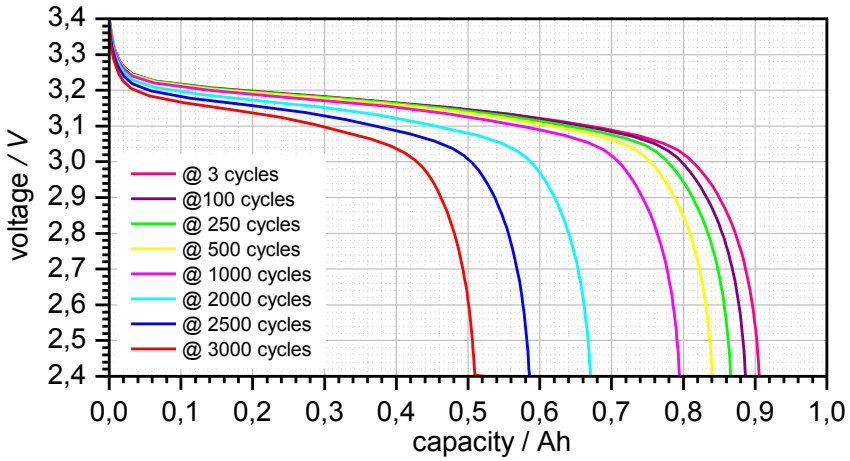

Figure 59: cell potential during discharge vs. capacity of 1 Ah A123 cells cycled at 60°C

Table 5: Comparison of the capacity loss of 1 Ah A123 cells dependent on cycle number at 60°C

Carried out cycle number	Capacity [Ah]	Percentage of capacity-fade
3	0,906	0,0
100	0,887	2,1
250	0,866	4,4
500	0,840	7,2
1000	0,795	12,3
2000	0,671	25,9
2500	0,586	35,4
3000	0,532	41,3

4.4.5 Scanning Electron Microscopy Measurements of the Anodes Surface

After the cells fulfilled the cycling program according to Table 3, the anode surface was investigated by the use of scanning electron microscopy (SEM). The investigation should display eventual defects caused by the cycling procedure. Within this chapter an overview on the results of the SEM investigations will be given.

Figure 60 displays the comparison of the anodes surface before cycling (but formed by manufacture) and after 3000 charge / discharge steps with a C rate of 5 C at an operating temperature of 60°C. Obviously, the electrode had to suffer crack formation during the cycling process at the elevated temperature. This structural damage of the electrode is caused by the volume increases and decreases during the charging / discharging process.

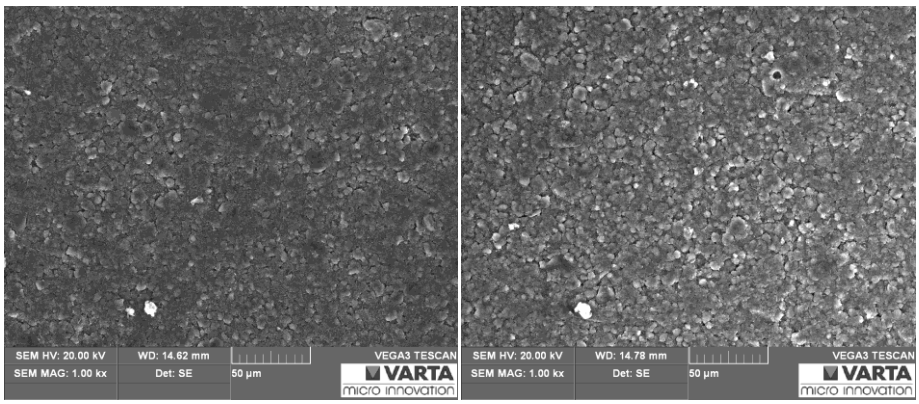

Figure 60: Comparison of the anodes surface left: 0 cycles; right: 3000 cycles at 60°C[5]

During the lithiation process of lithium ions the distance in between the graphene layers widens for about 10 % from 335 pm to 370 pm (see Figure 10 and Figure 12) (33) (34). This volume change due to a change of the stacking order by the graphene layers results in the mechanical stress for the electrode. Within Figure 60 a slight indication on a higher concentration of insulating decomposition products like LiF, Li_2CO_3 caused by the cycling procedure may be given. The electron beam seems to produce a stronger electron cloud at the right picture, though this effect might also be attributed to brightness and contrast settings.

[5] SEM measurement performed at VARTA MICRO INNOVATION GmbH using a TESCAN VEGA3 SBU system with tungsten hair pin cathode

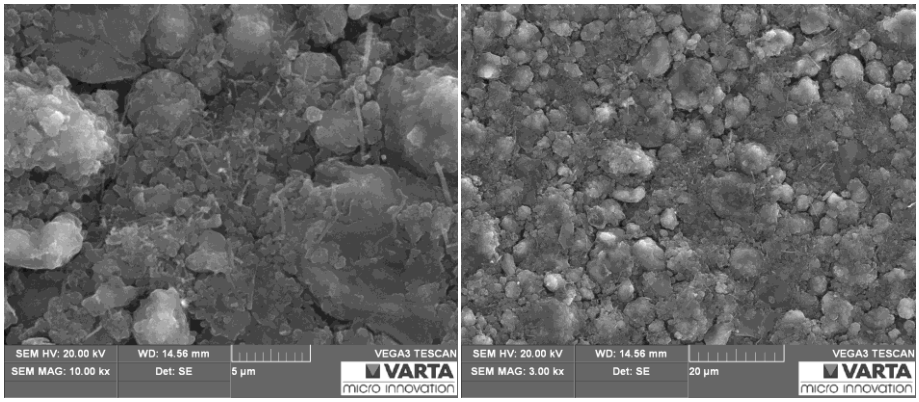

Figure 61: Surface of the anode (before cycling); left: SEM magnification 10kx; right: SEM magnification 3kx[5]

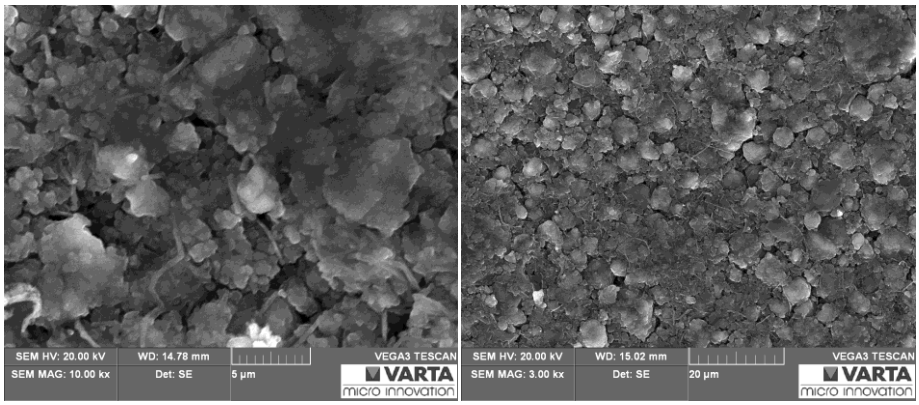

Figure 62: Surface of the anode (3000 cycles at 30°C); left: SEM magnification 10kx; right: SEM magnification 3kx[5]

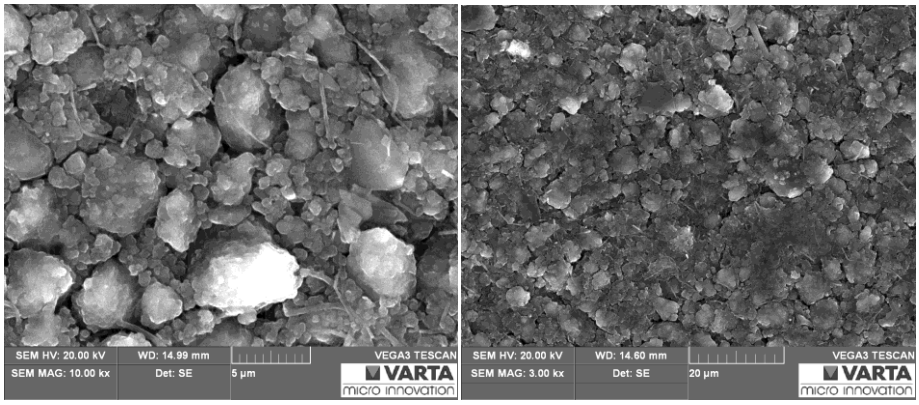

Figure 63: Surface of the anode (3000 cycles at 60°C); left: SEM magnification 10kx; right: SEM magnification 3kx[5]

Within Figure 61, Figure 62 and Figure 63 the influence of the cycle number as well as of the operating temperature is displayed. The anode surface only formed by the manufacturer displays minor cracking (see Figure 61). Figure 62 shows the anodes surface after 3000 charging / discharging steps at an operating temperature of 30°C. The anodes surface after 3000 cycle steps at an operating temperature of 60°C is displayed within Figure 63.

4.4.6 Estimation of the Anodes Lithium and Fluoride Concentration depending on Cycle Number and Operating Temperature

4.4.6.1 Results of the Analysis

Within chapter 4.4.3 the analysis of the lithium and fluoride concentration was already explained to be a destructive, ex-situ method to display the SEI growth of anodes during cycle procedure. Therefore each lithium and fluoride concentration value represents the measured value of one single cell. Unfortunately, even within industrial manufactured cells, the achievable capacities differ.

At the top of Figure 64 and Figure 65 the discharge capacity of the investigated cells is displayed. Structural damages, or moreover, the loss of parts of the electrode material or electrolyte can be observed for the cell cycled for 3000 times at 30°C (see top of Figure 64). This damage of the cell is indicated by the reversible loss of about 10 percent of the cells discharge capacity within one cycle.

The cells cycled at 30°C were not temperature controlled, resulting in slightly differing values for the discharge capacity between the discharge steps, caused by the heating up and cooling down of the cells during the charging / discharging reaction. This effect was avoided for the cells cycled at 60°C by the use of a temperature controlled box.

At the bottom of Figure 64 and Figure 65 the lithium and fluoride concentration values of each sample, according to the investigated cell, is displayed. The values fit to the achieved cycle number of the respective cell, resulting in an increase of the lithium and fluoride concentration on the anode with prolonged cycle number.

Remarkable is the strong increase of the lithium and fluoride concentration at the anodes cycled at an operating temperature of 60°C. This increase will be discussed intensively within this chapter, but suggest the assumption that the rise of the found lithium and fluoride concentration comes along with the higher decrease in discharge capacity with prolonged cycling.

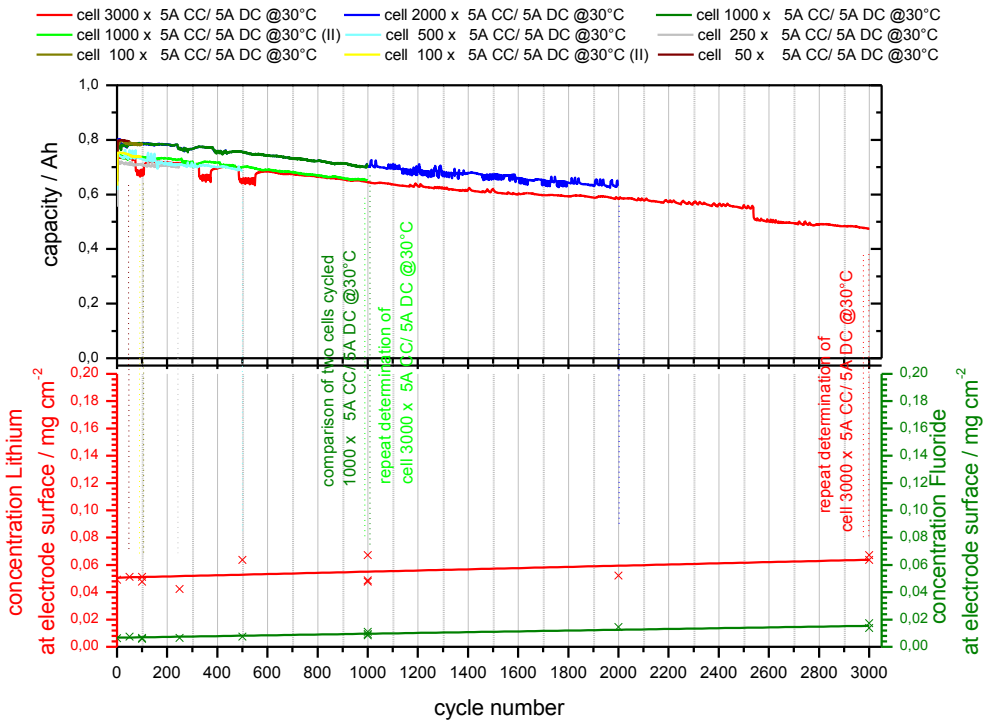

Figure 64: top: cycling performance of 1 Ah A123 cells bottom: corresponding lithium and fluoride concentrations of the anodes for cells cycled 5 A CC / 5 A DC at 30°C

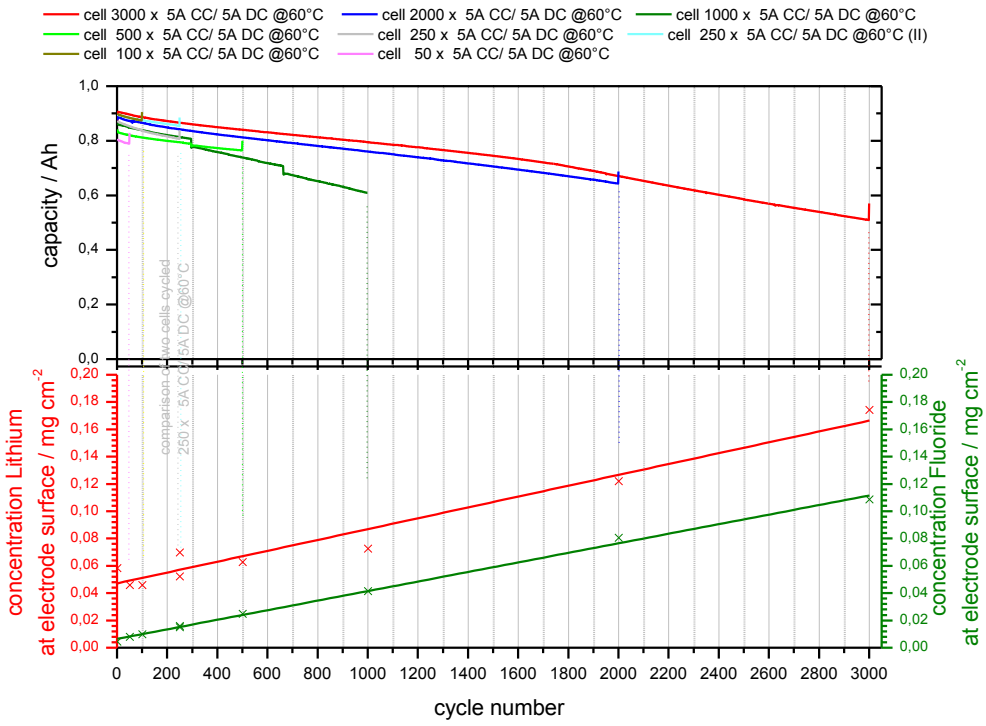

Figure 65: top: cycling performance of 1 Ah A123 cells bottom: corresponding lithium and fluoride concentrations of the anodes for cells cycled 5 A CC / 5 A DC at 60°C

The analysis of the lithium and fluoride concentration on the anode was controlled by comparison measurements of two cells cycled with the same cycling procedure under equal cycling conditions, as well as by repeat measurements of two samples gained from one cycled cell.

The comparison measurement of two cells (cycle number 1000) at an operating temperature of 30°C, results in higher values of the lithium and fluoride concentration for the cell achieving a higher discharge capacity. The found higher values can be explained, because more lithium ions were transported according to the higher discharge capacity.

Unfortunately, not all cycled cells were able to fulfill the expected cycle numbers according to the test matrix given in Table 3. The lithium and fluoride values of these cells were accordingly lower, because the cells transported less lithium ions due to the minor charge / discharge processes after the cell failure. The corresponding measurement is shown in Figure 66.

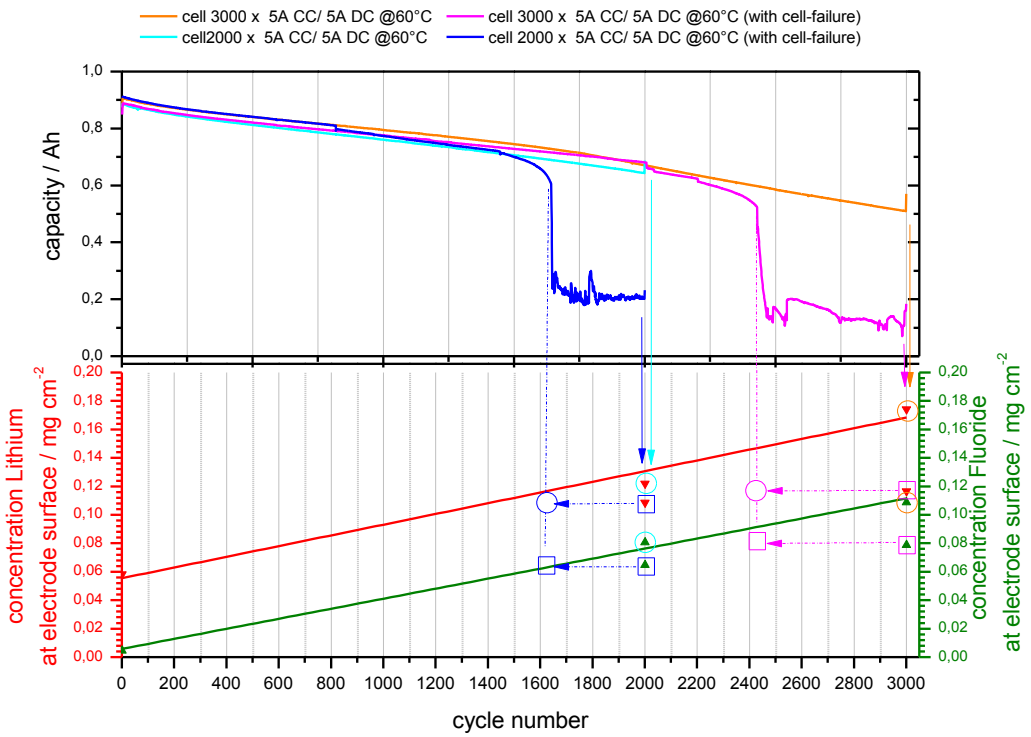

Figure 66: Lithium and fluoride concentrations on the anode of cells suffering cell failures. Fit of the lithium and fluoride concentrations taken by Figure 65

The determined values for the lithium and fluoride concentration are equivalent to a growth of the SEI. Within Figure 64 it becomes obvious that the SEI mounts by degrees with increasing cycle number.

The lithium as well as fluoride values found by ion exchange chromatography increase strongly during charging / discharging at enhanced operating temperatures (see Figure 65). These facts conclude that indeed the growth of the SEI is strongly affected by the operating temperatures of the cell.

Scientists reported on the enhancement of ageing effects at elevated temperatures in general and the continuous growth of the solid electrolyte interphase especially (99) (100) (101). The performed ion exchange chromatography measurements prove this literature data.

4.4.6.2 Calculation of the Lithium and Fluoride Loss on Cell Level and Comparison of the Found Values to the Ampere hours of Charge Reaction

Due to different cycle temperatures, obtained capacities for the cells investigated within chapter 4.4.6.1 were different. In order to be able to compare the measurement results in a better way, the total amount of charge capacity depending on the cycle number was calculated. Furthermore, after measuring the total anode surface area of the investigated cells, the comparison to the surface area of the analytically investigated samples was possible. Therefore the estimation of the total lithium and fluoride was achievable.

The total amount of mobile lithium in the cell could be estimated according to Calculation 1. A nominal cell capacity of 1.1 Ah (before formation) means a total amount of mobile lithium of 259 mg in the cell. At the beginning of cycling 44 mg lithium and 5 mg fluoride were found at the anode (0 cycles performed; except formation by the manufacturer). The found concentrations of lithium and fluoride match to a loss of about 10% of the charge capacity by the formation of graphite based anodes (13).

Figure 67 displays the calculated amount of lithium and fluoride on the total surface of the anode against the total overall charge capacity for the cells operated at 30°C. Additionally, the percentage of charge capacity loss in comparison to the achieved charge capacity is displayed against the overall charge capacity. Figure 68 displays the according values for the cells operated at 60°C.

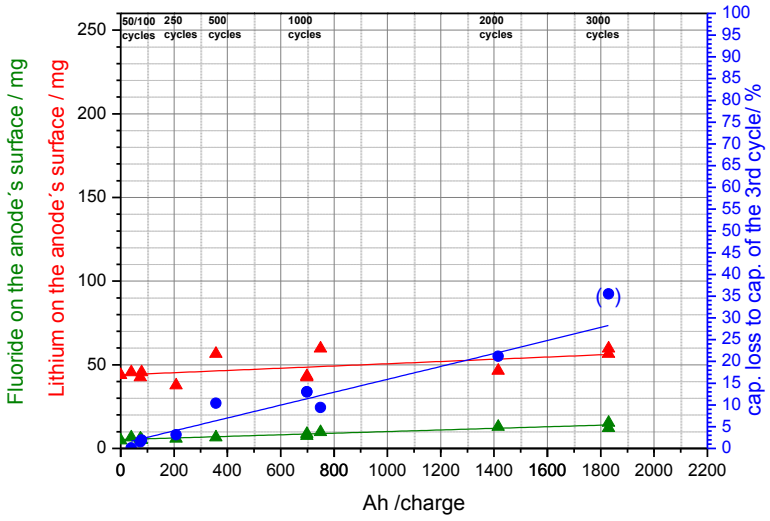

Figure 67: Comparison of the lithium and fluoride concentrations on the anodes surface vs. Ah of charging at 30°C[6]

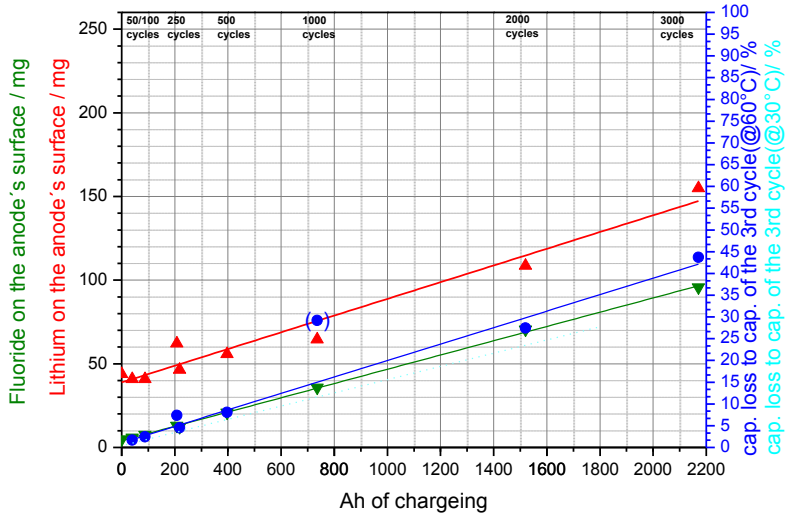

Figure 68: Comparison of the lithium and fluoride concentrations on the anodes surface vs. Ah of charging at 60°C[6]

Figure 67 displays, that the percentages of capacity loss at an operating temperature of 30°C do not follow the loss of lithium and fluoride at the anode of the cell. The effect is not predominant, because the small increase of the lithium and fluoride concentration is covered by strong, different capacity loss. Further studies in order to explain these results will be done within chapter 4.4.7.

[6] analytical values set in braces were not used for line fitting

Corresponding increase of the lithium concentration at the anode and charge capacity loss is observed for the cells operated at 60°C (see Figure 68). The analytical measurements show that 2000 charge/ discharge cycles at 60°C result in the loss of 25 % of the initial cells capacity by SEI growth.

For the measurements displayed in Figure 67 and Figure 68 the loss of the charge capacity can be calculated with the help of the amount lithium found at the anode. In the following, an exemplary calculation will be done for the found values after 2000 charge / discharge steps at 60°C:

Calculation 1: Calculated capacity loss of a cell cycled 2000 times at 60°C based on analytically measured data

Measured amounts of lithium and fluoride at the anode surface of the investigated cells before cycling (after formation):

lithium: 43.9 mg fluoride: 4.9 mg

Mobile lithium content in cell system (following Eq. 2; Q= 1.1 Ah; before formation):

$$m = \frac{M \cdot Q}{z \cdot F}$$

mobile lithium content in cell system ≈ 303 mg
mobile lithium left in the cell after SEI Formation: ≈259 mg

Lithium amount measured after cycle 2000 (60°C):

108.6 mg

Initially found lithium value:

43.9 mg

Additional lithium at the anode caused by 2000 cycles (60°C):

64.7 mg

Mobile lithium left in the cell after cycle 2000 (60°C): [259 mg- 64.7 mg]

=194.3 mg

---

259 mg of mobile lithium = 1 Ah

194.3 mg of mobile lithium = 0.75 Ah [loss of 0.25 Ah due to SEI growth]

Table 6: Calculated loss of capacity according to the analysed amounts of lithium at the anode (30°C)

cycle number	calculated mobile lithium left [mg]	calculated loss of capacity [%]
	less initially analyzed lithium value (0 cycles) and lithium value analysed at the anodes surface (X cycles)	
0	259	0
50	257	1
100	257	1
250[7]	265	(-)
500	264	(-)
1000	258	0
2000	256	1
3000	243	6

Table 7: Calculated loss of capacity according to the analysed amounts of lithium at the anode (60°C)

cycle number	calculated mobile lithium left [mg]	calculated loss of capacity [%]
	less initially analyzed lithium value (0 cycles) and lithium value analysed at the anodes surface (X cycles)	
0	259	0
50	262	(-)
100	262	(-)
250	256	1
500	247	5
1000	238	8
2000	194	25
3000	148	43

To sum up, the analytical measurements point to the conclusion that the capacity loss of cells operated at 30°C and 60°C origin of different effects. The capacity loss of the cells cycled at 60°C predominantly origins from the loss of lithium at the anodes surface. The capacity loss of cells cycled at 30°C results of other ageing effects and will be discussed within chapter 4.4.7.

[7] analysed value low because of minor overall cell capacity (see Figure 64)

4.4.7 Approaches to Validate the Values Generated by the Use of Ion Exchange Chromatography

To the authors knowledge the analysis of the anode by the use of ion exchange chromatography presented within chapter 4.4.6 was done for the first time and cannot be compared to literature data. Within this analysis it becomes obvious that the growing of the solid electrolyte interphase is enhanced by high temperatures during cycling.

The question at this point is the validation of the found values. Cross sections of anodes were characterized by the use of energy-dispersive X-ray spectroscopy (EDX). Although lithium cannot be detected by the use of EDX, the increase of fluoride concentration according to the analytical measurements should be obvious (see Figure 65 and Figure 68).

The electrodes cross sections were cut using microtome technique (measurements performed at Austrian Centre for Electron Microscopy and Nanoanalysis; FELMI-ZFE; TU Graz)

Additionally, further electrochemical techniques were used in order to validate the loss of Lithium at the anode material. These measurements explained the different ageing effects at different operating temperatures observed within chapter 4.4.6.

The use of elemental mapping techniques and electrochemical techniques enabled the validation of the analytically found data.

4.4.7.1 Evidence for the Growth of the Solid Electrolyte Interphase at Elevated Temperatures Using Microtome Cuts and EDX Measurements of the Anodes Cross Section

In order to validate the increasing concentration of lithium at the anode of 1 Ah A123 cells during the charge / discharge process at elevated temperatures microtome cuts were performed on two electrodes. The one electrode completed 50 charge / discharge cycles at 60°C, while the second electrode passed 3000 cycles at 60°C.

Thereafter the cross sections of the two electrodes were analysed by energy-dispersive X-ray spectroscopy (EDX) using mapping technique.

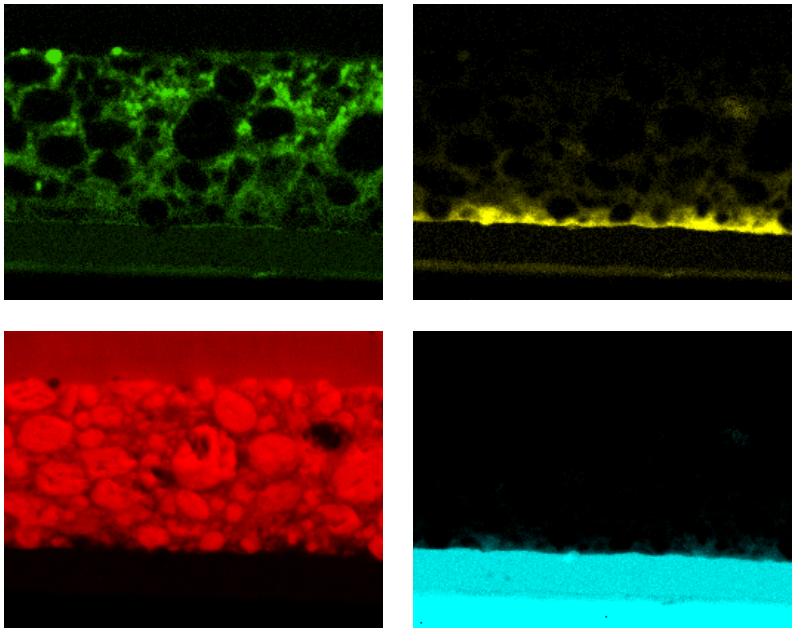

Figure 69: Element distribution images on a cross section cut of an anode (50 charge discharge cycles at 60°C) up/left: fluoride distribution; up/right: phosphor distribution; down/left: carbon distribution; down/right: copper distribution[8]

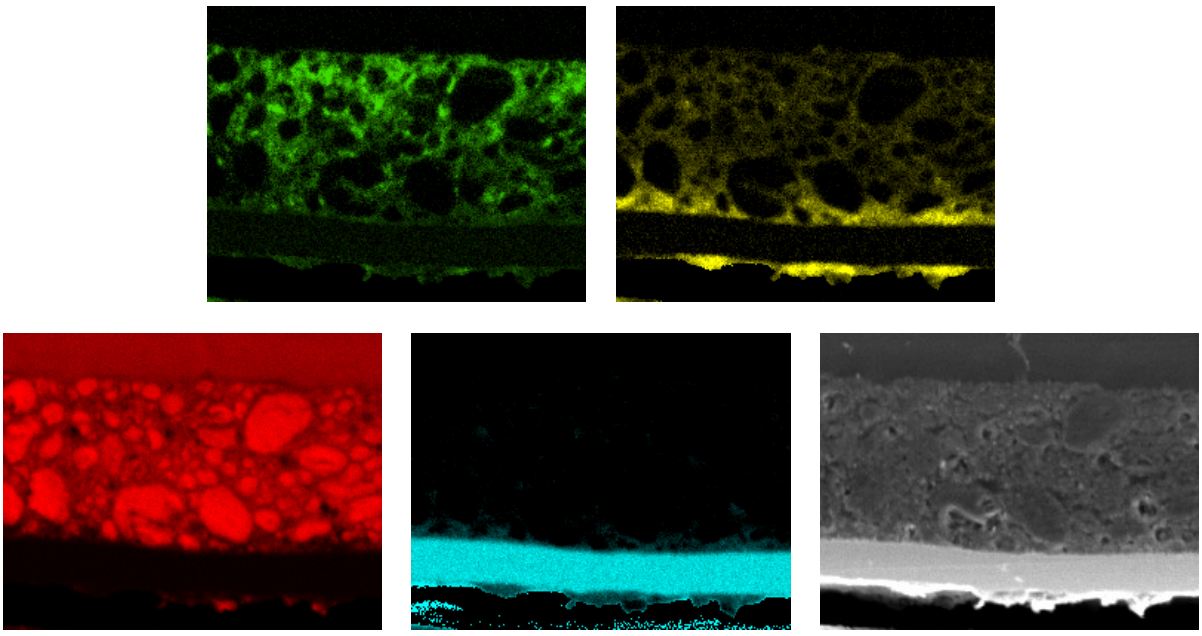

Figure 70: Element distribution images on a cross section cut of an anode (3000 charge discharge cycles at 60°C) up/left: fluoride distribution; up/right: phosphor distribution; down/left: carbon distribution; down/middle: copper distribution; down/right: SEM image[8]

Figure 69 shows the cross section of the electrode after 50 charge / discharge cycles at 60°C. The elemental distribution of the electrode cycled for 3000 times at 60°C is displayed within Figure 70.

[8] Microtome cuts and EDX mapping performed at Austrian Centre for Electron Microscopy and Nanoanalysis; FELMI-ZFE; TU Graz

The comparison of the elemental mapping images representing fluoride confirms the analytical data acquired by ion exchange chromatography. An explicit increase of the fluoride concentration can be observed within Figure 70.

Furthermore the amount of phosphor increases strongly as well. This fact can also be attributed to the decomposition of the $LiPF_6$ conducting salt during the charge / discharge reactions at elevated temperatures.

According to the carbon distribution images, the particle size of the graphite particles seem to decline, resulting in cracks within the electrode. This can be attributed to the influence of volume changes during the intercalation and deintercalation of lithium ions already observed by SEM images in chapter 4.4.5.

Another interesting result is shown by the copper distribution images. Copper foil is used as the current collector for anode materials. The copper distribution image within Figure 70 indicates the slight corrosion of the copper current collector, due to the sliding of the anode to high potentials. Some copper seems to have infiltrated the composite electrode.

Shu et al. described that the copper current collector can be gradually etched by the used organic electrolyte (108). Especially within $LiPF_6$ based electrolyte, the existence of HF also can etch the surface oxides of current collector (109).

4.4.7.2 Electrochemical Evidence for the estimated Lithium and Fluoride Concentration at the Anode

Within this chapter the investigation of the growth of the solid electrolyte interphase by the increase of the lithium and fluoride concentration at the anode is validated by electrochemical measurements.

The amount of lithium detected at the anode matches to the loss of cell capacity for measurements operated at higher temperatures. At temperatures of 30°C the capacity decrease during prolonged cycling is significantly larger than the analyzed loss of mobile lithium by ion exchange chromatography. This effect was displayed within Figure 67 and Figure 68 in chapter 4.4.6.1 and discussed within chapter 4.4.6.2.

Changes of the used cycling procedure can explain this effect and furthermore, the changes enable the proof of the analytically analyzed data and their interpretation.

4.4.7.2.1 Theoretical Background – The Importance of the Rate Capability on Achievable Capacity

The term rate capability describes the differences in the achievable capacity, if cells are operated at different currents. In fact, the rate capability is a result of the over-potentials in a cell occurring at certain currents. If no constant voltage charging steps are performed at the end of the charging process, the capacity of the cell is limited by occurring over-potentials.

Furthermore the over-potentials are influenced by the operating temperature during cycling, according to Butler-Volmer equation (see Eq. 15; Eq. 16), Tafel equation (see Eq. 18Eq. 19), as well as by diffusion over-potentials (see Eq. 20).

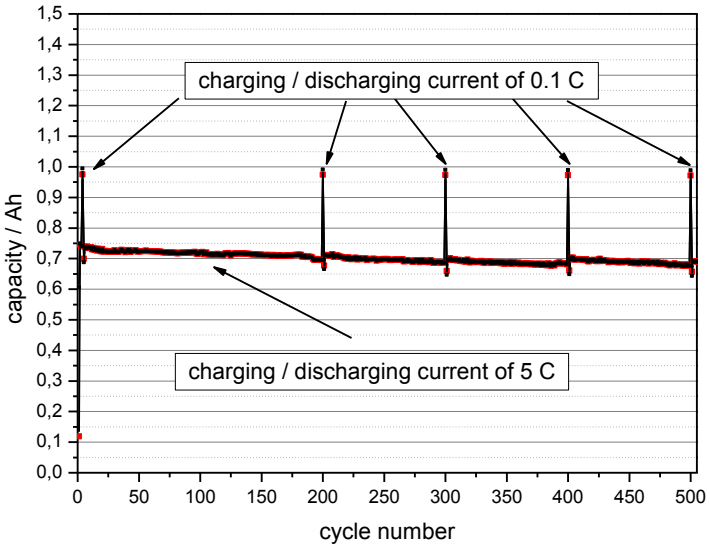

Figure 71: influence of the charging / discharging rate on the achievable capacity

Figure 71 describes the importance of the rate capability on the achieved capacity of 1 Ah A123 cells. The cells were cycled using the procedure described within chapter 4.4.3.1. Additionally, at the beginning, as well as at every 100th cycle, a special charging and discharging step was embedded in the test procedure. These charging steps and discharging steps were performed using a small current of 0.1 A (equal to 0.1 C).

Within the cycles operated at a current of 5 A (equal to 5 C), not all mobile lithium is intercalated into the carbon anode during the charge reaction, leading to smaller capacity values. Cycles operated by a small current of for example 0.1 A (equal to 0.1 C) ensure that all available mobile lithium is intercalated in the anode during the charge reaction. This actually results in the maximum achievable capacity.

By the use of this cycling procedure, the validation of the analytically determined values within chapter 4.4.6 and chapter 4.4.7 is possible.

The method ensures the electrochemical determination of the maximum available mobile lithium concentration, due to the separation of the lithium loss and the capacity fade caused by the rate capability. Therefore these values have to fit to the amount of lithium lost at the anode due to SEI growth.

4.4.7.2.2 Study on the Rate Capability of 1 Ah A123 Cells operated at 30°C

The influences of the charging / discharging rate next to the cells operating temperature on the capacity of 1 Ah A123 cells were shown within chapter 4.4.4. Especially, the differences in the achievable capacity at different operating temperatures are obvious by comparing Figure 58 and Figure 59. In order to estimate the loss of mobile lithium, two cells were cycled according to the cycling procedure described within chapter 4.4.7.2.1. In order to allow the comparison to previously generated data, one cell was operated at 30°C, while the second cell was operated at 60°C.

Figure 72 displays the capacity study of 1 Ah A123 cells operated at 30°C. By the use of the above described operating procedure the maximum available mobile lithium amount can be detected.

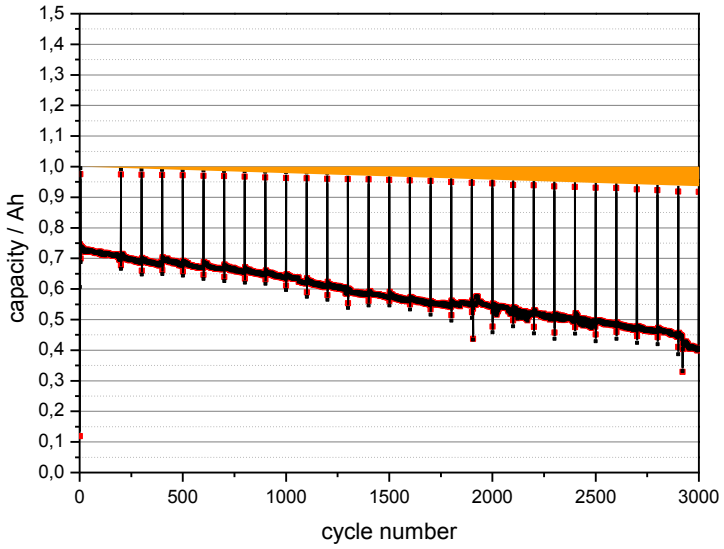

Figure 72: Cycling study of 1 Ah A123 cells at 30°C (including low current cycling steps)

Obviously the decrease of the available mobile lithium is significantly lower, than the capacity fading. For this reason the ageing behavior of the cells cycled at 30°C cannot be attributed to the loss of mobile lithium. Predominantly, minor losses of lithium already have a great impact on the cells kinetic at temperatures of about 30°C.

According to this, the measurement data of Figure 67 can be explained. The discrepancies between the analytically detected lithium values at the anode and the significantly higher capacity fading are clarified. The calculated values for the capacity fading based on the analytically detected amounts of

lithium (see Table 6) are indicated by an orange area within Figure 72. The area fits to the loss of mobile lithium, what actually proves the data generated by the analytical analysis in chapter 4.4.

4.4.7.2.3 Study on the Rate Capability of 1 Ah A123 Cells operated at 60°C

Figure 73 displays the measured data of 1 Ah A123 cells operated at 60°C according to the cycling conditions introduced within chapter 4.4.7.2.1. Remarkable is the enhancement of the capacity fading after about 1000 charging / discharging cycles. This phenomenon was already observed within Figure 65.

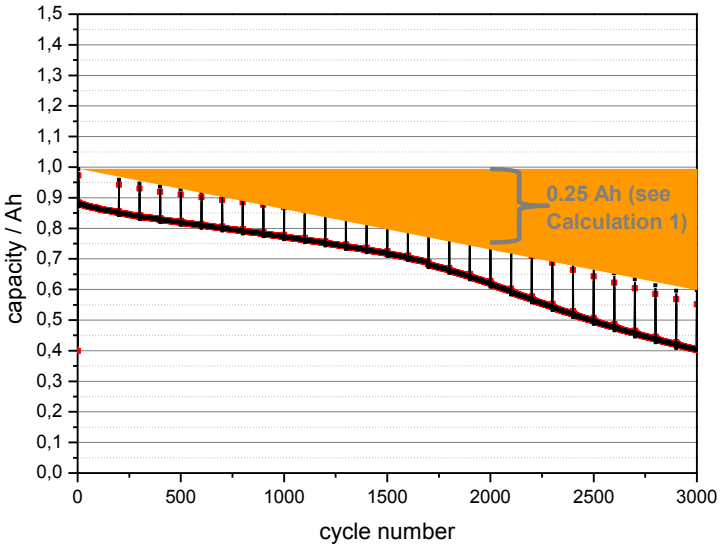

Figure 73: Cycling study of 1 Ah A123 cells at 60°C (including low current cycling steps)

Due to the enhanced capacity fading of the charge / discharge cycles operated at a current of 0.1 C as well, this ageing effect can be attributed to the loss of mobile lithium as well.

The calculated values for the capacity fading based on the analytically detected amounts of lithium (see Table 7) are indicated by an orange area within Figure 73. Obviously, the area fits to the loss of mobile Lithium.

4.4.8 Concluding Remarks on the Post Mortem Analysis of SEI Components for Determination of Ageing Effects

Summing up, it can be said that the analytical analysis in chapter 4.4 was proved by electrochemical measurements. All of the lithium found at the anode by ion exchange chromatography and EDX measurements is no longer available for the intercalation / deintercalation reaction. This amount of lithium is consumed by the growth of the solid electrolyte interphase. This effect is strongly enhanced by elevated temperatures.

Ramadass et al. studied the capacity fading of Sony 18650 cells (C / layered metal oxide cathode), cycled at elevated temperatures in a very interesting publication (101). The authors considered the rate capability, the loss of secondary active material ($LiCoO_2$/carbon) and the loss of primary active material (Li^+) to be the three most significant parameters to cause capacity loss. Unfortunately they were not able to estimate the loss of primary active material (Li^+). Therefore they calculated its value by subtraction of the measured secondary active material loss and rate capability loss from the total capacity loss.

Within this thesis, the author was able to prove the importance of primary active material loss (Li^+) as the major cause for cell ageing at enhanced temperatures by independent analytical, electrochemical and imaging analysis. Due to the fact that $LiFePO_4$ represented the positive electrode material, secondary active material loss was reduced as far as possible, in order to allow an independent analysis.

While the loss of mobile lithium causes capacity fading in the investigated cells, the growth of the SEI – based on these losses of mobile lithium – represents the predominant reason for power fading within the cells. Within cells containing carbon anodes and $LiFePO_4$ cathodes other ageing effects like the degradation of active material is of minor importance.

4.5 Approach to Suppress Cell Ageing caused by the Loss of Mobile Lithium[9]

4.5.1 Introduction

Lithium ion cells function far beyond their thermodynamic stability limits of the common electrolyte systems. On the one hand – fortunately – the SEI prevents the electrolytes mainly from further decomposition but on the other hand – unfortunately – common electrodes and electrolytes suffer from continuous decomposition at a minor rate. This effect sums up, resulting in a loss of mobile lithium within the cell system.

At the present time no electrolytes are known that operate in their thermodynamic stability limits in combination with carbon electrodes or carbon/metal alloy electrodes. Furthermore the state of the art balancing of electrodes within lithium ion cells is almost of 1:1 ratio, resulting in no possibility to equalize losses of mobile lithium.

If high capacity anode materials are combined with state of the art cathode materials, balancing in a ratio of 1:1 is practically impossible, due to the thickness of the positive electrode. But the according free capacity of the anode can be used to generate a pool of lithium. This pool of lithium would counteract to the loss of mobile lithium and accordingly slow down capacity losses.

Unfortunately, high capacity anode materials like silicon or silicon/graphite composites suffer from enhanced electrolyte decomposition due to the great volume changes during the charging / discharging reaction (see chapter 3.2.2).

Normally the lithiation of these stages is avoided, resulting in utilization of only about 70% of the theoretically possible capacity. The unused capacity can be applied for the generation of the lithium pool, described above.

[9] Patent pending: VARTA Micro Innovation GmbH; P 50961 DE

At the present time the following possibilities for the addition of an extra amount of lithium are thinkable:

- One method is represented by the usage of so called stabilized lithium powder (110). In fact, the surface of these lithium particles is stabilized by a thin layer of lithium phosphate. They can easily be incorporated during electrode fabrication either in the cathode material or in the anode material.

- An alternative represents the usage of transition meal nitrides ($Li_{3-x}M_xN$; M=Co, Cu) in composite anode materials (111) (112). These materials are able to delithiate more lithium than it can reversible lithiate. Although the material provides high, stable and reversible capacity the processability of the material is difficult, because it tends to quick hydrolysis.

- Over lithiated cathode materials like $LiNi_{0.425}Mn_{0.425}Co_{0.15}O_{2,}$ represent a group of positive electrode materials that are capable to delithiate more lithium ions than they are able to lithiate reversibly (113).

- The usage of lithium salts is thinkable. This salts would be dissolved in the electrolyte and decomposed during discharging, resulting in gassing and intercalation of lithium ions in the anode.

- Furthermore anode materials can be charged to a certain degree. Thereafter they get disassembled carefully and reconstructed in the desired electrode stack.

4.5.2 Cell Balancing and Cell Reactions

Figure 74 displays the balancing of a high capacitive anode to a cathode, as well as the additionally added amount of lithium. The columns within the figure corresponded to the amounts of lithium, which can be stored within the electrodes. Respectively they correspond to the specific capacities of the electrodes. Because the high capacitive anode exceeds the capacity of the cathode by values in between 20 to 100 percent, no total anode capacity was displayed within the Figure 74. According to the legend at the bottom of Figure 74, the striped area represents the additionally added amount of lithium. Before the first charging cycle this amount can either be located within the cathode, the anode or the electrolyte. Within Figure 74 the additional lithium is stored in the cathode material.

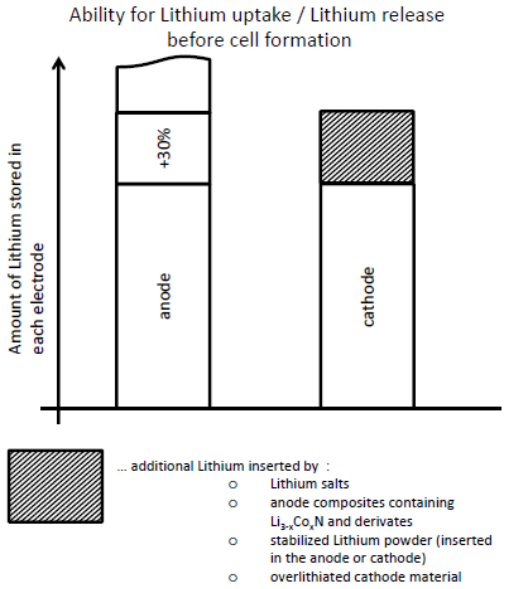

Figure 74: Schema of the cell balancing before the first charging step

The first charging procedure is described by Figure 75. The maximum possible amount of lithium ions is delithiated from the cathode material and inserted into the anode material. The height of the pictured arrows corresponds to the amount of lithium transported between the electrodes. Parts of the lithium ions are irreversible lost due to the SEI formation at the anodes surface. In the sense of the invention the lithium loss due to SEI formation is smaller than the amount of lithium additional added to the cell.

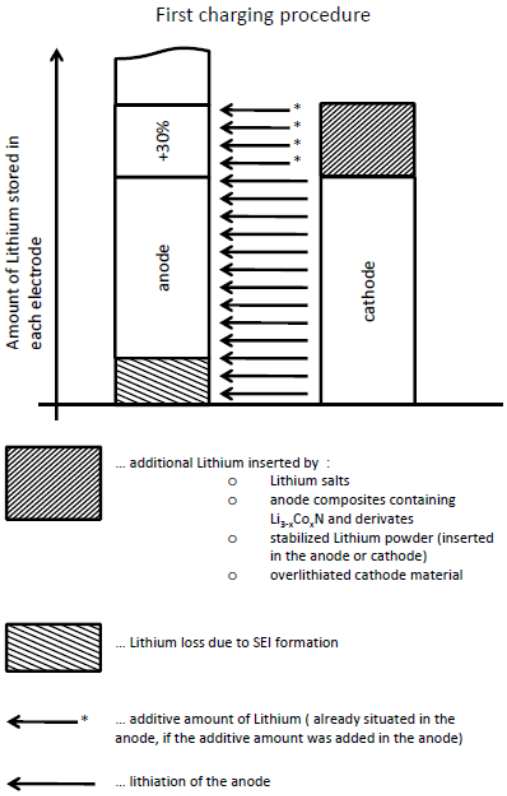

Figure 75: Schema of the first charging step

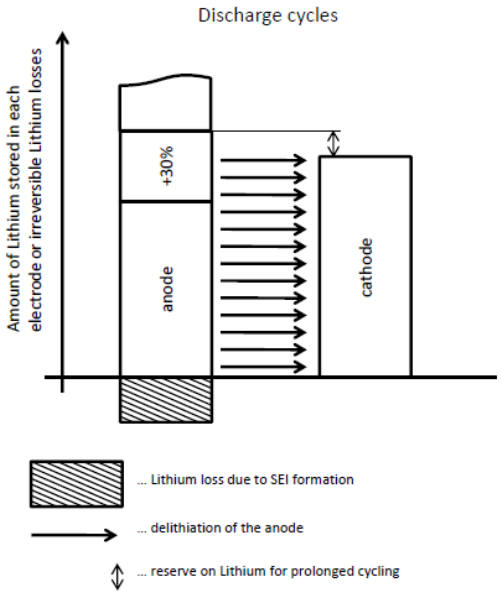

Figure 76: Discharge reaction

Within Figure 76 the amount of lithium lost due to SEI formation is displayed below the x-axis, because this amount of lithium is irreversible lost for charge / discharge reactions. At this point it has to be noted that the specific capacity of the anode – symbolized by the height of the column – was

not changed by the formation of the SEI. The amount of lithium being incorporated back into the cathode is displayed by the height of the arrows.

The difference between the amounts of lithium additionally added to the cell to the amounts of lithium lost due to SEI formation represents the pool of additional lithium. This pool remains in the anode material. If further lithium is lost in the cell because of e. g. SEI growth, the lithium pool acts as a reverse and replaces the lost lithium until it is spent.

The further charging processes are displayed within Figure 77.

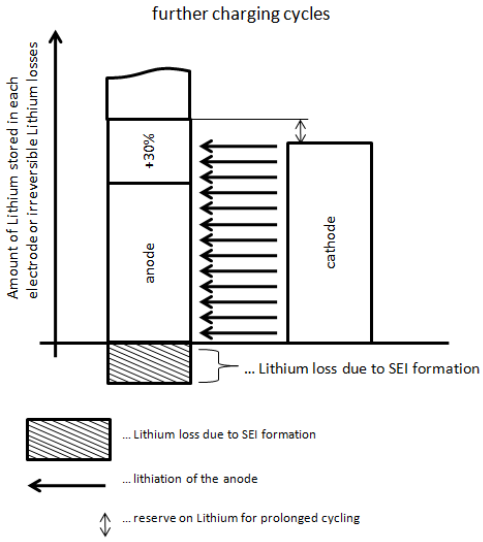

Figure 77: further charging steps

4.5.3 Benefits of the introduced Balancing Setup

The introduced balancing method of lithium ion cells containing high capacitive anode materials provides further benefits next to the described suppression of cell ageing.

The great volume changes of high capacitive anode materials lead to strong mechanical stress. Repeated full lithiation of these materials would result in cracking of the active material particles and irreversible inactivation of these particles. By the use of the introduced balancing method these materials would be charged to a high lithiation grade only once. Within the following cycles the anode is not fully delithiated anymore, remaining an amount of lithium within the anode.

By the use of the introduced balancing method a higher discharging voltage of the cell is ensured. Due to the generated lithium pool the anode is not fully delithiated during discharging. The potential window of the anode gets lower during the discharging step, resulting in a higher discharging voltage of the cell.

According to the state of the art, many cathode materials combined with high capacity anode materials do not permit fully delithiation. Cut off criteria for the charging reactions are controlled by the nominal voltage of the cell. If the cell suffers a lack of mobile lithium, cathode materials are delithiated above their maximal delithiation grade. This over delithiation is followed by irreversible changes in the lattice structure, gassing and accelerated ageing. By the use of the introduced balancing method the lithium pool is able to delay the delithiation of the cathode material above their maximal delithiation grade.

4.5.4 Experimental Results

The comparison of Figure 78 and Figure 79 displays the benefits of the introduced balancing technique. For the generation of the lithium pool according to chapter 4.5.1 and chapter 4.5.2 anode materials were charged to a certain degree. Thereafter they were disassembled carefully and reconstructed in an electrode stack.

4.5.4.1 Electrode Preparation

The charge / discharge capacities and efficiencies of a full cell are shown within Figure 78.

The anode material was prepared by slurry technique, out of an aqueous solution. The slurry contained 8 percent by weight Sodium-Carboxymethylcelluloses (Na-CMC; Sigma Aldrich) binder material, 20 percent by weight nano-silicon (n-Si; 30 – 50 nm; Nanostructured and Amorphous Materials Inc.), 60 percent by weight graphitic carbon (Quingdao) and 12 percent by weight conducting agent (carbon black/carbon nano-fiber). Water and additional a surfactant was added to enable homogenized slurry dispersion. The slurry was applied on a current collector (copper-foil; 12 µm, Fa. Schlenk), using an automated doctor blade. In a dry oven the solvent was removed at 120°C afterwards, followed by punching out electrodes (12 mm diameter). At least the electrodes were died at 120°C for 24 hours under vacuum (< 10^{-2} mbar).

The cathode material was prepared using slurry technique, out of organic solution. The slurry contained 5 percent by weight polyvinylidenedifluoride hexafluoropropylene based binder, 88 percent per weight $LiCoO_2$ cathode active material (Fa. Varta Microbattery) and 7 percent by weight conducting agent (carbon black/carbon nano-fiber). For the slurry preparation N-Methyl-2-pyrrolidone (NMP, 98%) was used. The aluminum current collector was roughened by 5% KOH, in order to improve adhesion properties. The application of the slurry on the current collector was done using an automated doctor blade. Thereupon the solvent was removed at 70°C, followed by electrode punching and a further drying process at (70°C; 24 hours; $< 10^{-2}$ mbar).

4.5.4.2 Measurement Conditions

The capacity of the anode measured within Figure 78 was 0.393 mAh (max. theoretical capacity of 1250 $mAh \cdot g^{-1}$).This anode was combined with a cathode achieving a capacity of 0.240 mAh. According to this, the anode used only about 763 $mAh \cdot g^{-1}$ of its specific capacity.

The cell was controlled by the cut off criteria of the terminal voltage in the values from 3 V to 4.2 V. The nominal cell capacity was 0.240 mAh, according to the cathodes capacity. The cathode was restricted to avoid higher potentials than 4.2 V, while the anode was controlled to avoid potential higher than 1.5 V.

Two cycles were performed at a C rate of 0.1 C, followed by cycles at currents of 0.5 C. For the measurement the C rate of 1 C was equal to 0.240 mAh.

The charge / discharge capacities and efficiencies of a full cell with prelithiated anode are shown within Figure 79. In the anode a lithium pool was generated by lithiation against metallic lithium. The anode was prelithiated to 70 percent of the maximum capacity. The capacity of the anode in Figure 79 was 0.404 mAh (max. theoretical capacity of 1250 $mAh \cdot g^{-1}$) .This anode was combined with a cathode achieving a capacity of 0.253 mAh. According to this, the anode used only about 783 $mAh \cdot g^{-1}$ of its specific capacity.

Cycling procedure as well as the C rate was chosen according to the previous measurement.

The measurements were performed in Swagelok© test cells: The used electrolyte and separator are listed below:

- separator: Freudenberg-Vlies FS2190 (poly propylene, 23 µm); ø 13 mm,
- electrolyte: EC/DEC = 3:7 (v:v), 1 M $LiPF_6$ + 2% VC
- reference electrode: Li/Li^+

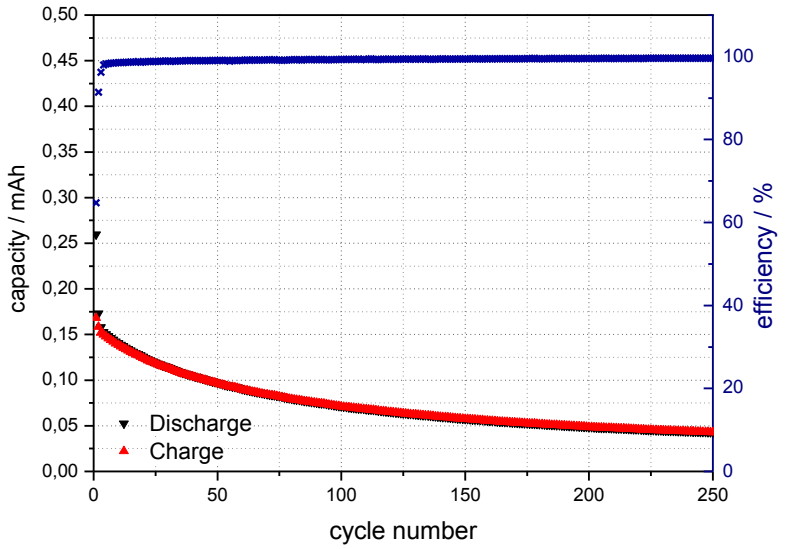

Figure 78: Full cell study (Si/C composite vs. $LiCoO_2$)

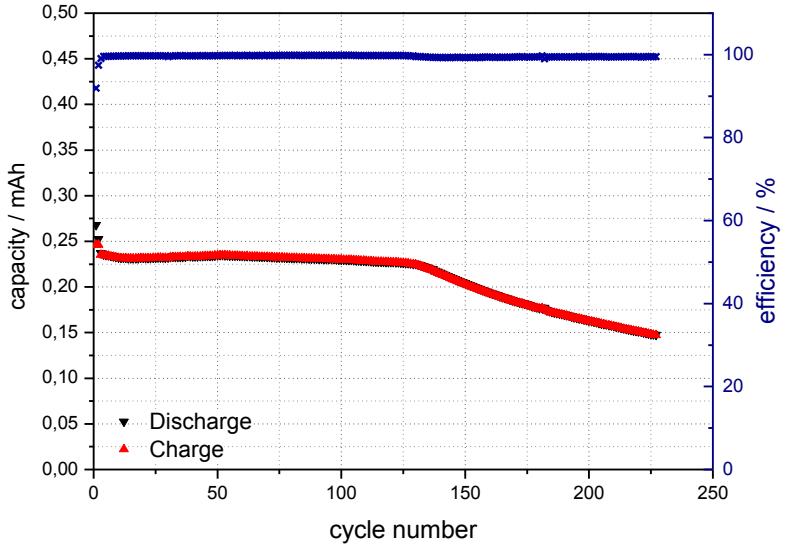

Figure 79: Full cell study of a prelithiated anode (Si/C composite [70% prelithiation] vs. $LiCoO_2$)

By the comparison of Figure 78 and Figure 79 the strong difference in cycling behavior is evident. The generation of a lithium pool in the anode enabled the suppression of the ageing phenomena, caused by the loss of mobile lithium.

By the use of the presented cell balancing method for cells containing high capacitive anodes, noticeable higher capacity values for a higher cycle number can be established.

5 Conclusion

The 2002 published discussion paper “Future Needs and Challenges for Non-Nuclear Energy Research in the European Union” summarises the outcome of eight workshops organized by the European Commission in Brussels, 2001 (114). Within this report the lithium ion battery is set to play a key role in the area of novel concepts and systems for electricity storage, transport and distribution networks. The report points out that further improvement on lithium ion batteries has to be achieved within the key issues of the small temperature operating window, the specific energy and energy density and the limited cycle and calendar life.

The FreedomCAR and Vehicle Technologies (FCVT) is a U.S. national Office of Energy Efficiency and Renewable Energy program developing more energy efficient and environmentally friendly highway transportation technologies that will enable the U.S to use less petroleum. Within this program the study of ageing processes in lithium ion batteries is also set to play a key role in research activities.

The present work focuses on the estimation of cell parameters, in order to enable the validation of modelling data developed within the “COMET K2 Forschungsförderungsprogramm” of the Virtual Vehicle.

By the use of back fitting technique for electrode materials from the origin cell to laboratory test cells no proper information on the potential curves of the electrodes could be obtained (chapter 4.2). This was mainly attributed to the loss of lithium, due to decomposition reactions on the anode. As a consequence of that, reference electrodes were embedded in commercial 2.3 Ah cells (C / $LiFePO_4$) and 50 mAh coffee bag cells (C / $LiFePO_4$). These reference electrodes allowed the study of the anode and cathode potential next to the cell voltage (chapter 4.3.2 and chapter 4.3.3).

By the use of this technique remarkable long term stability and outstanding comparability of the measured cells could be achieved.

To the authors knowledge no data of similar quality was reported within literature up to this date.

The measured values for the anode and cathode potential next to the cell voltage in dependence of charging / discharging conditions and pulse relaxations tests enabled the validation of modeling data. Moreover, the investigation displayed a major ageing mechanism of lithium ion batteries. The large influence of the loss of “mobile lithium” on the capacity fading of the cell could be observed.

This loss of mobile lithium can be contributed to a continuous growth of the solid electrolyte interphase. In order to estimated values for this continuous electrolyte reduction a novel analysis method was developed within chapter 4.4.

This technique used ion exchange chromatography and enabled to estimate the growth of the solid electrolyte interphase by the determination of the lithium and fluoride concentration at the anodes surface.

Independent from the analytically measured values of the SEI growth, electrochemical measurements and EDX techniques investigating cross-sections of anode materials enabled a validation of this novel analysis method (see chapter 4.4.7).

All measurements displayed a continuous growth of the SEI and a strong dependence of the operating temperatures during cycling.

Within chapter 4.5 approaches to overcome ageing effects caused by this growth of the SEI and the connected loss of mobile lithium are introduced. Furthermore measurements performed within this chapter could display the desired suppression of this ageing effect.

6 Register

6.1 Figures

6.2 Tables

7 References

1. **Varta Micro Innovation GmbH.** http://www.vartamicroinnovation.at. [Online] [Cited: 03 08 2011.] http://www.vartamicroinnovation.at/main/DE/VARTA/Ihre_Beteiligung/Unterlagen/index,method=main.html.

2. **Linden, David.** *Handbook of Batteries, 2nd ed.* New York : McGraw-Hill Inc., 1995.

3. **Atkins, P. W.** *Physical Chemistry. 5th edition.* s.l. : W.H. Freeman & Company, 1994.

4. **Besenhard, Jürgen O.** *Handbook of Battery Materials.* Weinheim : Wiley-VCH, 1999.

5. *upload.wikimedia.org.* [Online] [Cited: 03 01 2011.] http://upload.wikimedia.org/wikipedia/commons/2/20/Daniell-Element.jpg.

6. *labspace.open.ac.uk.* [Online] [Cited: 04 01 2011.] http://labspace.open.ac.uk/file.php/5259/T357_1_ie001i.jpg.

7. **Alberty, R.A. and Silbey, R.J.** *Physical Chemistry.* New York : John Wiley, 1996.

8. **Bard, A.J. and Faulkner, L.R.** *Electrochemical Methods.* London : John Wiley, 1980.

9. **Bockris, J.O'M. and Reddy, A.K.N.** *Modern Electrochemistry, vols. 1-2.* New York : John Wiley, 1970.

10. **Southampton Electrochemistry Group (Ed.).** *Instrumental Methods in Electrochemistry.* Chichester : E. Horwood, 1985.

11. **Bard, A.J. and Faulkner, L.R.** *Electrochemical Methods. Fundamentals and Applications, 2nd edition.* s.l. : John Wiley and Sons, 2001.

12. **A123 Systems.** a123systems.com. [Online] [Cited: 11 01 2011.] http://www.a123systems.com/a123/products.

13. **Winter, M., et al.** *Advanced Materials.* 1998, Vol. 10, 725.

14. **Koller, S. and Schmuck, M.** lecture. *Batteries and Supercapacitors.* TU Graz : s.n., 2010.

15. *„Elektrische Energiespeicher in Hybrid- und Elektrofahrzeugen“, Seminar für Kraftfahrzeug- und Motorentechnik.* **Sauer, D. U.** Berlin : s.n., 2009.

16. **Galvani, L.** *De viribus electricitatis in motu musculari commentarius.* Bologna : Accademia delle Scienze, 1791.

17. http://batteryuniversity.com. [Online] [Cited: 17 01 2011.] http://batteryuniversity.com/learn/article/the_nickel_based_battery_its_dominance_and_the_future.

18. **Walter A. van SChalkwijk, Bruno Scrosati.** *Advances in Lithium-Ion Batteries.* New York : Kluwer Academic/ Plenum Publishers, 2002.

19. **Goodenough, J.B. and Mizushima, K.** *Patent GB 11953/79* United Kingdom, April 1979.

20. **Nagaura, T. and Tozawa, K.** *Prog. Batteries Sol. Cells.* 9, 1990, 209.

21. *http://picasaweb.google.com.* [Online] [Cited: 18 01 2011.] http://picasaweb.google.com/lh/photo/Uka2IieahCx9sykaSGvBig.

22. **S., Koller.** Doctoral Thesis. *About the Nature of the Electrochemical Formation of Binary Lithium-Silicon Intermetallic Phases from Nonaqueous Electrolytes.* TU Graz : s.n., 2009.

23. **Gholam-Abbas Nazri, Gianfranco Pistoia.** *Lithium Batteries, Science and Technology.* s.l. : Kluwer Academic Publishers, 2004.

24. **Tanaka, K. et al.** New Orleans, Louisiana : 184th ECS Fall Meeting, 1993.

25. **Ozawa, Kazunori.** *Lithium Ion Rechargeable Batteries; Materials, Technology and New Applications.* Weinheim : WILEY-VCH Verlag GmbH & Co. KGaA, 2009.

26. **Fauteux, D. and Koksbang, R.** *J. Appl. Chem.* 23, 1993, Vol. 1.

27. **Sawai, K., Iwakoshi, K. and Ohzuku, T.** *Solid State Ionics.* 69, 1994, 273.

28. **Kinoshita, K.** *Carbon: Electrochemical and Physicochemical Properties.* New York : Wiley , 1987.

29. **Wakihara, M.** *Materials Science & Engineering.* R33, Reports 2001, 109.

30. **Hérold, A.** *Bull. Soc. Chim. Fr.* 187, 1955, 999.

31. **Legrand, A. P. and Flandrois, S.** *Chemical Physics of Intercalation.* s.l. : NATO ASI Series B, 1987. Vol. 172, p. 3.

32. **Tran, T. D. and Kinoshita, K.** *J. Electroanal. Chem.* 386, 1995, 221.

33. **Billaud, D., McRae, E. and Hérold, A.** *Mater. Res. Bull.* 14, 1979, 857.

34. **Song, X. Y., Kinoshita, K. and Tran, T. D.** *J. Electrochem. Soc.* 143, 1996.

35. **Besenhard, J.O. and Fritz, H.P.** *Angew. Chem. Int. Engl.* 95, 1983, 950.

36. **Rüdorff W., Hofmann U.** *Z. Anorg. Allg. Chem. .* 238, 1938, 1.

37. *Proc. of the 2. Ulmer Elektrochemische Tage, Ladungsspeicherung in der Doppelschicht.* **Besenhard, J.O. and Winter, M.** [ed.] Schmickler W. Germany : Universitätsverlag Ulm, 1995. p. 13.

38. **Fisher, J.E.** [book auth.] A. P. Legrand and S. Flandrois. *Chemical Physics of Intercalation.* s.l. : NATO ASI Series B, 1987, Vol. 172. p. 59.

39. **Dahn, J.R.** *Phys. Rev. B.* 44, 1991, 9170.

40. **Inaba, M., et al.** J. Electrochem. Soc. 142, 1995, 20.

41. **Dahn, J. R., et al.** [book auth.] G. Pistoia. *Lithium Batteries: New Materials, Developments and Perspectives.* Amstadam : Elsevier, 1994. p.1.

42. **Winter, M., Novák, P. and Monnier, A.** *J. Electrochem. Soc.* 145, 1998, 428.

43. **Peled, E.** *J. Electrochem. Soc.* 126, 1979, 2047.

44. **Goldenfield, N.** *J. of Power Sources.* 26, 1989, 121.

45. **Faul, I. and Knight, J.** *Chem. Ind.* 1989, 820.

46. **Peled, E.** [book auth.] J.-P. Gabano. *Lithium Batteries.* London : Academic, 1983, 03.

47. **Dey, A. N.** *J. Electrochem. Soc.* 118, 1971, 1547.

48. **Fauteux, D. and Koksbang, R.** *J. Appl. Chem.* 23, 1993, 1.

49. **Yang, J., Winter, M. and Besenhard, J.O.** *Solid State Ionics.* 90, 1996, 281.

50. **Besenhard, J.O., Yang, J. and Winter, M.** *J. of Power Sources.* 68, 1997, 87.

51. **Chan, C. K., et al.** *J. of Power Sources.* 189, 2009, 34.

52. **Huggins, R.A.** [book auth.] J.O. Besenhard. *Handbook of Battery Materials.* Weinheim : Wiley-VCH, 1999.

53. **Zhou, Z., et al.** *J. of Alloys and Compounds.* 507, 2010, 309.

54. **Fuchsbichler, B., et al.** *J. of Power Sources.* 196, 2011, 2889.

55. **Yu, H., et al.** *Electrochimica Acta.* 53, 2008, 4200.

56. **Kavan, L. and Grätzel, M.** *Electrochem. Solid-State Lett.* 5, 2002, A39.

57. **Ohzuku, T., Ueda, A. and Yamamoto, N.** *J. Electrochem. Soc.* 142, 1995, 1431.

58. **Kim, Y.J., et al.** *J. Electrochem. Soc.* 149, 2002, A1337.

59. **Chen, Z. and Dahn, J.R.** *Electrochem. Solid-State Lett.* 6, 2003, A221.

60. **Jiang, J., et al.** *J. Electrochem. Soc.* 152, 2005, A556.

61. **MacNeil, D.D., Lu, Z. and Dahn, J.R.** *J. Electrochem. Soc.* 149, 2002, A1332.

62. **Cho, T.H., et al.** *J. of Power Sources.* 142, 2005, 306.

63. **Ohzuku, T., Kitagawa, M. and Hirai, T.** *J. Electrochem. Soc.* 137, 1990, 769.

64. **Goodenough, J. B., et al.** *Rev. Chim. Miner.* 21, 1984, 435.

65. **Guyomard, D. and Tarascon, J. M.** *J. of Power Sources.* 54, 1995, 92.

66. **Tarascon, J. M. and Guyomard, D.** *Solid State Ionics.* 69, 1994, 293.

67. **Guyomard, D. and Tarascon, J. M.** *US Patent 5 192 629,* 1193.

68. **Thackeray, M. M., et al.** *Mater.Res. Bull.* 18, 1983, 461.

69. **Thackeray, M. M., et al.** *J. of Power Sources.* 21, 1987, 1.

70. **Gummow, R. J., de Kock, A. and Thackeray, M. M.** *Solid State Ionics.* 69, 1994, 59.

71. **Tarascon, J. M., et al.** *J. Electrochem. Soc.* 138, 1991, 2859.

72. **Padhi, A.K., Nanjundaswamy, K.S. and Goodenough, J.B.** *J. Electrochem. Soc.* 144, 1997, 1188.

73. **Goodenough, J.B.** *J. of Power Sources.* 174, 2007, 996.

74. **Prosini, P.P., et al.** *Electrochim. Acta.* 48, 2003, 4205.

75. **Doeff, M.M., et al.** *Electrochem. Solid-State Lett.* 6, 2003, A207.

76. **Croce, F., et al.** *Electrochem. Solid-State Lett.* 5, 2002, A47.

77. **Chung, S.Y., Bloking, J.T. and Chiang, Y.M.** *Nat. Mater.* 2, 2002, 123.

78. **Sasaki, T., et al.** *J. of Power Sources.* 150, 2005, 208.

79. **Abe, K., et al.** *J. of Power Sources.* 153, 2006, 328.

80. **Chen, J., Buhrmester, C. and Dahn, J.R.** *Electrochem. Solid-State Lett.* 8, 2005, A59.

81. **Owens, B. B.** *J. of Power Sources.* 90, 2000, 2.

82. **Kim, K. M., et al.** *Solid State Ionics.* 161, 2003, 121.

83. **Arora, P., White, R.E. and Doyle, M.** *J. Electrochem. Soc.* 145, 1998, 3647.

84. **Aurbach, D. and Ein-Eli, Y.** *J. Electrochem. Soc.* 142, 1995, 2882.

85. *Advanced electrochemical mass spectrometry.* **Raimann, P., et al.** Biarritz,France : International Meeting on Lithium Batteries, 2006.

86. **Kanamura, K., et al.** *J. Electroanal. Chem.* 394, 1993, 49.

87. **Aurbach, D., et al.** *J. Electroanal. Chem.* 145, 1998, 1421.

88. **Goren, E., Chusid, O. and Aurbach, D.** *J. Electrochem. Soc.* 138, 1991, L6.

89. **Panitz, J.-C., Novák, P. and Haas, O.** *Appl. Spectrosc.* 55, 2001, 1131.

90. **Aurbach, D., et al.** *Electrochimica Acta.* 45, 1999, 67.

91. **Aurbach, D., et al.** *J. Electrochem. Soc.* 143, 1996, 3809.

92. **Andersson, M., et al.** *Electrochimica Acta.* 47, 2002, 1885-1898.

93. **Aurbach, D.** *J. Electrochem. Soc.* 136, 1989, 1610.

94. **Sloop, S.E., et al.** *Electrochem. Solid-State Lett.* 4, 2001, A42.

95. **Vetter, J., et al.** *J. of Power Sources.* 147, 2005, 269.

96. **Aurbach, D., et al.** *Solid State Ionics.* 148, 2002, 405-416.

97. **Amine, K., et al.** *J. of Power Sources.* 2001, 684-687.

98. **Zaban, A. and Aurbach, D.** *J. of Power Sources.* 1995, 289-295.

99. **Ramadass, P., et al.** *J. of Power Sources.* 2002, 606-613.

100. **Andersson, A.M., Edström, K. and Thomas, J.O.** *J. of Power Sources.* 1999, 8-12.

101. **Ramadass, P., et al.** *J. of Power Sources.* 112, 2002, 614-620.

102. **Zhang, Q. and White, R.-E.** *J. of Power Sources.* 179, 2008, 793-798.

103. **Weppner, W. and Huggins, R.A.** *J. Electrochem. Soc.* 124, 1977, 1569.

104. **Wohlfahrt-Mehrens, M., Vogler, C. and Garche, J.** *J. of Power Sources.* 127, 2004, 58-64.

105. **Tröltzsch, U., Kanoun, O. and H.-R., Tränkler.** *Electrochimica Acta.* 51, 2006, 1664-1672.

106. **Sarre, G., Blanchard, P. and Broussely, M.** *J. of Power Sources.* 127, 2004, 65-71.

107. **Lee, S., et al.** *J. of Power Sources.* 185, 2008, 1367-1373.

108. **Shu, J., et al.** *Electrochimica Acta.* 56, 2011, 3006-3014.

109. **S.T. Myunga, S.T., et al.** *Electrochim. Acta.* 55, 2009, 288.

110. **Lithium, FMC.** *WO 2008/143854* 2008.

111. **Liu, Y., et al.** *Electrochemical Acta.* 49, 2004, 3487-3496.

112. **Takeda, Y., et al.** *Solid State Ionics.* 130, 1999, 61-69.

113. **Trana, N., et al.** *Solid State Ionics.* 176, 2005, 1539-1547.

114. **European Commision.** www.solarpaces.org. [Online] 2002. [Cited: 02 03 2011.] http://www.solarpaces.org/Library/docs/Report_NNE_Expert_Workshops.pdf.

115. **Denis, S., et al.** *J. Power Sources.* 79, 1999, 81.